Hedgehog Signaling Strength Is Orchestrated by the *mir-310* Cluster of MicroRNAs in Response to Diet

Ibrahim Ömer Çiçek,* Samir Karaca,† Marko Brankatschk,‡ Suzanne Eaton,‡ Henning Urlaub,† and Halyna R. Shcherbata*,[1]

*Max Planck Research Group of Gene Expression and Signaling, and †Bioanalytical Mass Spectrometry Research Group, Max Planck Institute for Biophysical Chemistry, 37077 Göttingen, Germany, and ‡Max Planck Institute of Molecular Cell Biology and Genetics, 01307 Dresden, Germany

ORCID ID: 0000-0002-3855-0345 (H.R.S.)

ABSTRACT Since the discovery of microRNAs (miRNAs) only two decades ago, they have emerged as an essential component of the gene regulatory machinery. miRNAs have seemingly paradoxical features: a single miRNA is able to simultaneously target hundreds of genes, while its presence is mostly dispensable for animal viability under normal conditions. It is known that miRNAs act as stress response factors; however, it remains challenging to determine their relevant targets and the conditions under which they function. To address this challenge, we propose a new workflow for miRNA function analysis, by which we found that the evolutionarily young miRNA family, the *mir-310*s (*mir-310*/*mir-311*/*mir-312*/*mir-313*), are important regulators of *Drosophila* metabolic status. *mir-310*s-deficient animals have an abnormal diet-dependent expression profile for numerous diet-sensitive components, accumulate fats, and show various physiological defects. We found that the *mir-310*s simultaneously repress the production of several regulatory factors (Rab23, DHR96, and Ttk) of the evolutionarily conserved Hedgehog (Hh) pathway to sharpen dietary response. As the *mir-310*s expression is highly dynamic and nutrition sensitive, this signal relay model helps to explain the molecular mechanism governing quick and robust Hh signaling responses to nutritional changes. Additionally, we discovered a new component of the Hh signaling pathway in *Drosophila*, Rab23, which cell autonomously regulates Hh ligand trafficking in the germline stem cell niche. How organisms adjust to dietary fluctuations to sustain healthy homeostasis is an intriguing research topic. These data are the first to report that miRNAs can act as executives that transduce nutritional signals to an essential signaling pathway. This suggests miRNAs as plausible therapeutic agents that can be used in combination with low calorie and cholesterol diets to manage quick and precise tissue-specific responses to nutritional changes.

KEYWORDS *Drosophila*; oogenesis; follicle stem cell; Hedgehog signaling; miRNA; the *mir-310*s; *Rab23*; dietary restriction; metabolic stress; Hh ligand

ORGANISMS are constantly subjected to changes in nutrient availability and composition, which depend on quantity and quality of consumed food. Currently, there is a considerable amount of data regarding the cellular metabolic processes and signaling pathways involved in metabolism regulation; however, we know little about the mechanisms that efficiently readjust these pathways in response to ever-changing dietary fluctuations. MicroRNAs (miRNAs) are great candidates for such regulation due to their unique features: miRNA expression is extremely dynamic; one miRNA can regulate hundreds of different targets; and more than one miRNA may coordinately regulate a single target. This presents a great number of combinatorial possibilities, which allows for greater precision in regulation of gene expression.

miRNAs have been shown to be involved in virtually all studied biological processes, including regulation of cellular metabolism and organismal homeostasis (Xu *et al.* 2003; Teleman *et al.* 2006; Barrio *et al.* 2014), development of metabolic disorders, and the highly energy-demanding process of carcinogenesis (Bhattacharyya *et al.* 2006; Leung and Sharp 2010; Ross and Davis 2011). However, it remains extremely difficult to decipher specific *in vivo* requirements for each miRNA due to the facts that their mutant phenotypes are very subtle (Lai 2015), and most miRNA mutants are

doi: 10.1534/genetics.115.185371
Manuscript received November 26, 2015; accepted for publication January 18, 2016; published Early Online January 22, 2016.
Available freely online through the author-supported open access option.
Supporting information is available online at www.genetics.org/lookup/suppl/doi:10.1534/genetics.115.185371/-/DC1.
[1]Corresponding author: Max Planck Institute for Biophysical Chemistry, Am Fassberg 11, 37077 Göttingen, Germany. E-mail:halyna.shcherbata@mpibpc.mpg.de

viable, fertile, and apparently normal in well-controlled lab conditions. Furthermore, correlating causal targets to miRNA phenotypes remains the key challenge. Even though multiple algorithms and databases predicting miRNA–messenger RNA (mRNA) interactions based on sequence and physical-chemistry properties exist, they have large numbers of false positives and currently only very few interactions have been experimentally validated. It has been shown that dietary modulations modify miRNA expression profiles, but to date there is a paucity of *in vivo* functional studies that aim to decipher the complex networks involving nutrition-dependent miRNAs and their targets. Such studies may offer new concepts for preventive and therapeutic strategies for metabolic disorders, including obesity and diabetes.

Since the dietary requirements for major nutrients (sugars, fats, and amino acids) appear to be universal and the signaling pathways involved in the basic logic of nutrient signaling are conserved, studies in model organisms have proven to be beneficial for the understanding of metabolic stress. In *Drosophila*, similarly to vertebrates, steroids, insulin, and TOR signaling play a critical role in regulation of nutritional responses, suggesting that *Drosophila* can be used as a relevant model to study nutritional stress (Drummond-Barbosa and Spradling 2001; Konig *et al.* 2011; Wei and Lilly 2014). Particularly, the *Drosophila* ovarian germline stem cell community is a very attractive model to study how adult stem cell self-renewal and differentiation is coordinated with organismal metabolism. In the *Drosophila* germarium, there are two stem cell types of extremely different origin: the germline stem cells (GSCs) and the somatic follicle stem cells (FSCs). These stem cells also have very distinctive stem cell niche types: the stationary, cell–cell adhesion-dependent GSC niche and the dynamic, cell–matrix adhesion-dependent FSC niche (Song and Xie 2002; Nystul and Spradling 2007; Morrison and Spradling 2008). Interestingly, the GSC niche not only controls GSC maintenance, but also has a distant influence on FSC division and differentiation. The FSC gives rise to somatic ovarian cells that come in different types: the follicular epithelium, stalk, polar, and border cells, all of which protect and assist the germline, ensuring sufficient egg differentiation. Therefore, for proper oogenesis progression, it is extremely important that GSC and FSC divisions and the differentiation of their progeny are synchronized (Gilboa and Lehmann 2006; Chang *et al.* 2013; Konig and Shcherbata 2015). Dependent on nutrient availability, insulin ligands are produced in the brain to activate insulin signaling in the GSCs to cell-autonomously control their division rate; in contrast, the Hh ligand is locally produced by the GSC niche, it travels three to five cell diameters to the posteriorly located FSCs to stimulate their proliferation (Forbes *et al.* 1996a; Drummond-Barbosa and Spradling 2001; Zhang and Kalderon 2001; O'Reilly *et al.* 2008; Rojas-Rios *et al.* 2012)

Importantly, Hh signaling is highly dependent on the diet, because its multiple components are regulated by cholesterol and lipid levels (Panakova *et al.* 2005; Sieber and Thummel 2012; Hartman *et al.* 2013). Upon dietary restriction, an organism has to quickly change its cellular metabolism and adapt to unfavorable conditions; however, it is very unlikely that levels of cholesterols and lipids would drop instantly (Efeyan *et al.* 2015), resulting in sufficient downregulation of Hh signaling. This highlights the importance of the existence of other levels of regulation to ensure the quick and robust response of Hh to dietary changes. While downstream Hh effectors have been well studied in different systems, the upstream regulators of Hh signaling and their roles in energy homeostasis are yet to be revealed. Our data for the first time demonstrate that Hh signaling strength upon nutritional fluctuations can be modulated by miRNAs.

Here we used a new workflow allowing for effective identification of miRNA-regulated processes and relevant targets. First, we applied quantitative proteomic analysis of miRNA mutants to identify the major biological processes affected by miRNA loss. Second, tissue-specific dissection of miRNA mutants was performed to identify the most prominent phenotypes caused by miRNA insufficiency. Third, based on the vast amount of previously published data, we compared these phenotypes to the key phenotypes associated with major signaling pathways. Fourth, we used several databases (Enright *et al.* 2003; Kheradpour *et al.* 2007; Betel *et al.* 2008) to predict potential miRNA targets, among which several genes relevant to the identified signaling pathway were selected and further confirmed using *in vitro* and *in vivo* assays. Finally, genetic analyses and rescue experiments under normal and defined stress conditions were performed to validate miRNA roles in certain biological processes.

Using this paradigm, we found that in *Drosophila* during adulthood, the *mir-310*s orchestrate Hh signaling strength in accordance with nutritional status. We identified three new *mir-310*s targets, *Rab23*, *DHR96*, and *ttk*, all of which are involved in Hh pathway regulation. By simultaneous targeting of multiple regulators of the pathway, the *mir-310*s safeguard a quick and robust response of Hh signaling to dietary fluctuations. Additionally, we discovered a molecular function for the membrane trafficking protein Rab23 in the process of Hh ligand intracellular transport and secretion in the stem cell niche. Plausibly, Hh signaling management by the *mir-310*s is just one example of many diet-dependent processes regulated by these miRNAs. Our proteomic data, generated by SILAC labeling accompanied by mass spectrometry analysis, revealed that multiple critical metabolism-related genes are deregulated due to the *mir-310*s deficiency under normal and dietary restrictive conditions, suggesting that in general, the molecular function of these miRNAs is management of organismal homeostasis upon dietary fluctuations.

Materials and Methods

Fly stocks

All fly stocks were maintained and crosses were set up on standard food with yeast, cornmeal, and agar at 25°, constant humidity, and a 12-hr light–dark cycle. The nutrient restriction experiments were done using 2% agar-agar (Serva), 25% apple

juice, and 2.5% sugar medium. The nutrient-starved flies were fed this medium plain, whereas the well-fed flies were given additional fresh yeast paste made of dry yeast and 5% propionic acid (~50% w/v). Food vials of both conditions were refreshed every 2 days. The following fly stocks were used: *Oregon-R-C* and *w*^{1118} as controls; *mir-310*s deletion lines *KT40* (Tsurudome *et al.* 2010), *w**; *Df(2R)mir-310-311-312-313 P(neoFRT)42D/CyO*, *P(GAL4-twi.G)2.2*, *P(UAS-2xEGFP)AH2.2* (no. 58923 Bloomington *Drosophila* Stock Center, BDSC), and the deficiency line *w[1118]*; *Df(2R)Exel6070*, *P(w[+mC]=XP-U)Exel6070/CyO* (no. 7552 BDSC) as mutant alleles; *mir-310*s-*Gal4* (P(GawB)NP4255 from Drosophila Genomics and Genetic Resources, Kyoto) (Yatsenko *et al.* 2014), *UAS-mCD8*::*GFP*, *UAS-nLacZ* line (gift from Frank Hirth) for expression analyses; *tub-Gal80*^{ts}; *bab1-Gal4/TM6* and *w*; +; *bab1-Gal4/TM6* (no. 6803 BDSC), *UAS-hh* (gift from Christian Bökel), *UAS-Rab23 RNAi* (*y[1] v[1]*; *P(y[+t7.7] v[+t1.8]=TRiP.JF02859)attP2* (no. 28025 BDSC), *UAS-hh RNAi* (Sahai-Hernandez and Nystul 2013), and a *mir-310*s rescue line (*w*-; *Sco/CyO*; *attB2 mir-310*s *res long 2/TM6B*) carrying a large genomic region encompassing the *mir-310*s as a transgene in the 3rd chromosome (gift from Eric Lai) for rescue experiments. To generate the *UAS-Rab23* line, we cloned *Rab23* cDNA into the *UASt* vector (gift from Alf Herzig). Cloning was performed by standard cloning techniques, digesting the *Rab23* cDNA vector (RH23273 clone from Drosophila Genomics Resource Center) and the *UASt* vector with *Eco*RI and *Kpn*I restriction enzymes. The microinjection and recovery of the transgenic flies was done by Bestgene. The site-specific integration on the 3rd chromosome (76A2 site) was achieved by the *att* sites in the *UASt-Rab23* plasmid and *PhiC31* into the *PBac[yellow[+]-attP-9A]VK00013* strain. *Rab23*::*YFP*::*4xmyc* line (also referred as *Rab23*::*YFP* in the text) was generated by ends-in homologous recombination, and the initial genomic duplication was resolved using the I-Cre system. The size of the homologous sequence 5′ from the YFP start codon is 4045 bp, and the size of the homologous sequence 3′ from *Myc tag DNA* fragment is 3601 bp. The donor construct was verified by sequencing. Recombination events were verified by PCR. In our analyses, homozygous flies bearing endogenously tagged *Rab23* copies were used.

For SILAC analysis, qRT-PCR (list of primers, Table S11), immunohistochemistry, luciferase assay, coupled colorimetric assay (CCA), and coimmunoprecipitation, refer to File S1.

Results

mir-310s loss of function causes defects in energy metabolism and deregulation of nutritional homeostasis-associated genes

In our previously performed screen for stress-dependent miRNAs (Marrone *et al.* 2012), we found that the miRNAs from the newly evolved *mir-310*s family are differentially expressed under stress and disease conditions. Therefore, we aimed to decipher the potential role for these miRNAs in maintenance of a healthy physiological state. To begin with, we studied global changes in protein expression caused by *mir-310*s deficiency. The quantitative SILAC proteomics data of miRNA mutant flies were generated for the first time using previously described (Sury *et al.* 2010) mass spectrometry of heavy isotope-labeled *Drosophila*. This analysis resulted in a sizeable list of proteins with altered expression levels caused by *mir-310*s deficiency. Since miRNAs are generally identified as fine tuners of gene expression, we considered proteins with a moderate (≥30%) relative increase or decrease with a *P*-value of 0.1 for filtering for the significant data (Supporting Information, Table S1), which resulted in the identification of 264 proteins that were up- or downregulated in *mir-310*s mutants, among which 24 are predicted *mir-310*s direct targets (Table S1, bold boxes).

Next, using the STRING database (Franceschini *et al.* 2013), we created functional association networks of deregulated genes; then, we grouped these genes into functional groups according to their gene ontology (GO) terms from the UniProt database (UniProt Consortium 2014). This analysis revealed distinct functional groups: lipid and energy metabolism, protein homeostasis, nucleotide synthesis, mitochondria, muscle and neural development/function, cuticle formation, and others (Figure 1A). Furthermore, 20% of the altered genes were reported to be lipid droplet associated (Kuhnlein 2011). Importantly, the common denominator of these affected gene functions was their involvement in energy metabolism and homeostasis, suggesting that the *mir-310*s are involved in regulation of these processes, which can be achieved directly by the *mir-310*s regulation of their target genes and indirectly by secondary effects of their targets. It is important to stress that due to the current limitations of quantitative mass spectrometry analyses, only 30% of all predicted *Drosophila* proteins could be identified in this study, which is comparable to previously described SILAC proteomic data (Sury *et al.* 2010). Detected proteins mainly represent the most highly expressed, but not regulatory proteins or transcription factors that are known to efficiently operate even in very low quantities. Despite the limitations of this analysis in identifying direct miRNA targets that belong to these functional groups, it allowed for meaningful identification of the processes regulated by the miRNAs.

Since our proteomics data indicated that the *mir-310*s could be associated with maintenance of metabolism and energy homeostasis, we compared this dataset with genes previously reported to be starvation-sensitive by transcriptome analysis (Farhadian *et al.* 2012) and found 31 genes in common. Next, we measured mRNA expression levels of these genes by qRT-PCR in wild-type and *mir-310*s mutant animals under well-fed and nutrient-restricted conditions (Figure 1B; Table S2). We used two diets: well-fed (sugars + yeast paste) and starved/protein restricted (just sugars, no yeast paste). As has been reported by pioneering studies and recent efforts, the *Drosophila* life cycle (development and adult homeostasis) greatly depends on the nutritional input from the yeast source, which can be reconstituted by addition of amino acids, cholesterol, nucleic acids, folic acid, inositol, biotin, riboflavin, nicotinic acid, pyridoxine hydrochloride, calcium

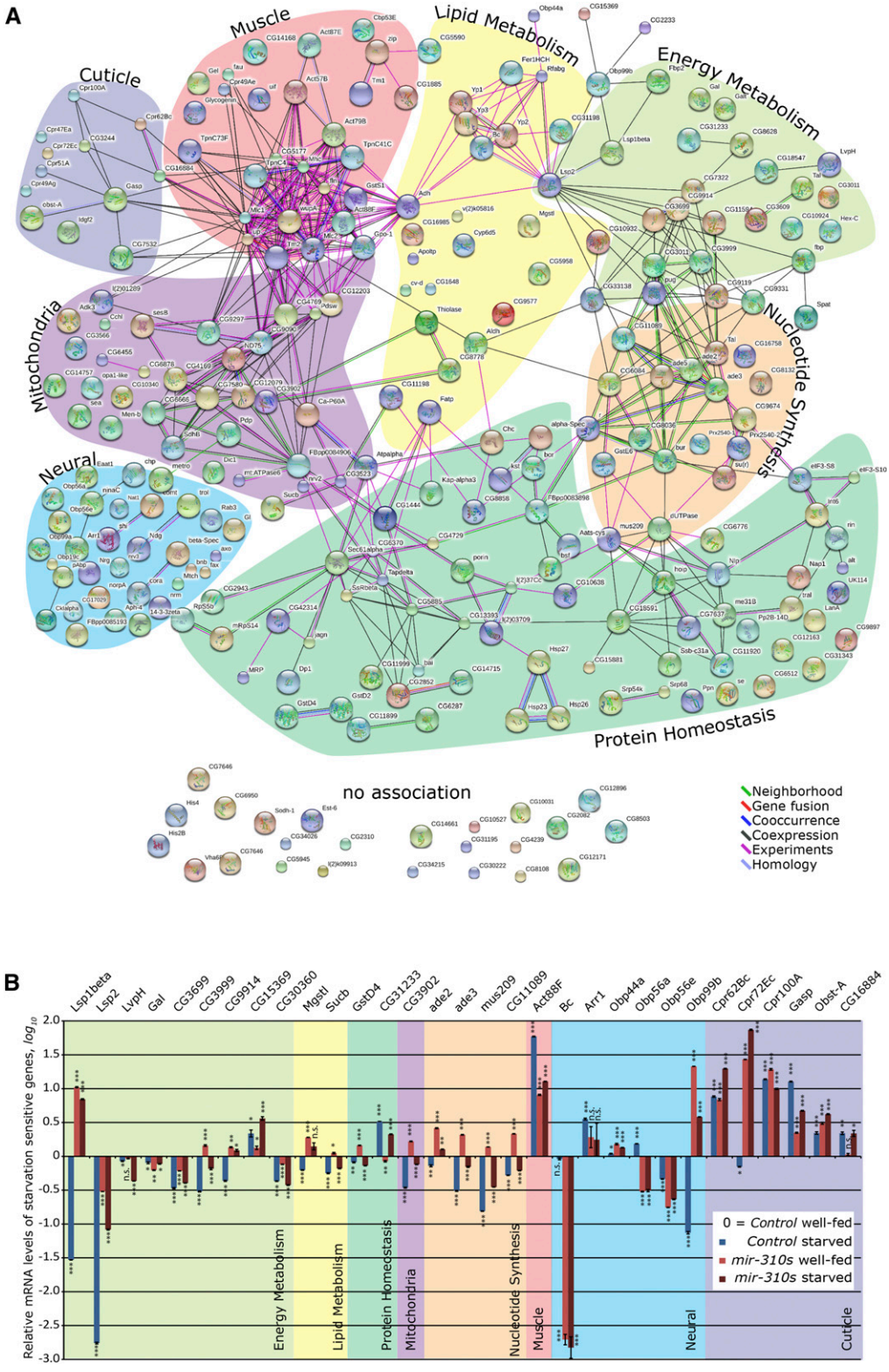

Figure 1 The *mir-310*s-affected genes suggest energy metabolism-related defects. (A) Interaction network of globally up- or down-regulated genes in *mir-310*s loss-of-function (*KT40*/*KT40*) mutant females compared to control (w^{1118}) females exhibits eight interconnected gene ontology groups: energy metabolism, lipid metabolism, protein homeostasis, muscle and neural development and function, mitochondrial, nucleotide synthesis, and cuticle related (Table S1). Large node size indicates the availability of protein structure information. Node colors have no particular meaning. Line colors indicate different evidence types used to generate node interactions (see key). (B) Starvation-sensitive genes have altered mRNA expression levels in *mir-310*s mutant females compared to controls under well-fed and/or nutritionally restricted conditions (10 days), demonstrating the role of the *mir-310*s in the response to changes in nutritional status (Table S2). Functional groups are color coded as in A. In B the bar graph indicates the arithmetic mean (AVE) ± the standard error of the mean (SEM). Significances were calculated using two-tailed Student's *t*-test. $*P < 0.05$, $**P < 0.005$, $***P < 0.0005$.

pantothenate, thiamine, choline chloride, ergosterol, and metal ions (Piper *et al.* 2014). Our starvation conditions supply only simple sugars and lack these essential components needed for optimal homeostasis. In agreement with the proteomic data, most of these genes were aberrantly expressed in *mir-310*s mutants. In addition, starvation induced uncoordinated alterations in the gene expression profiles, consistent with a suggested role for *mir-310*s in dietary response (Figure 1, A and B). For instance, one of the genes, *Larval serum protein 1 β* (*Lsp1beta*), was found to be 10-fold

higher in *mir-310*s mutants under well-fed conditions in comparison to controls. Nutrient restriction caused a sharp decrease (>30-fold) of the *Lsp1beta* transcript levels in control flies, while almost no change was detected in *mir-310*s mutant flies (only a one third-fold decrease). The transcript levels of another gene, *Larval serum protein 2* (*Lsp2*) were downregulated close to zero upon nutrient restriction in control flies; however, in *mir-310*s mutants, *Lsp2* levels were only slightly decreased. As a result, *Lsp2* mRNA levels in nutrient-restricted *mir-310*s mutants were ~40-fold higher in comparison to those in controls. In general, most of the nutrition-dependent genes that were analyzed showed atypical alterations in their expression levels in *mir-310*s when compared to wild-type flies under both normal and restrictive conditions, showing a role for the *mir-310*s in nutritional homeostasis and response to starvation.

Defects caused by mir-310s deficiency depend on nutrition

In correlation with the abnormal expression of the energy- and lipid metabolism-related genes, the analysis of *mir-310*s-deficient flies revealed several gross morphological and physiological phenotypes that are known to be related to nutrient availability. One of the most prominent phenotypes detected upon dissection of *mir-310*s mutants was the enlarged food storage organ or crop (Figure S1, A and A′), the size of which is highly diet dependent and is capable of expansion after starvation and refeeding (Lemaitre and Miguel-Aliaga 2013). It is also known that the enlarged crop is a persisting signature of poststarvation response, since females switched from nutrient-poor to nutrient-rich food consume more food (Edgecomb *et al.* 1994; Al-Anzi *et al.* 2010). We found that even under normal feeding conditions, average crop size of *mir-310*s females was 30% larger than crops of wild-type females of comparable size (Figure S1A′′). This suggests that due to their abnormal metabolism, *mir-310*s females exhibit a phenotype consistent with the physiology elicited during poststarvation.

Interestingly, studies on the physiology of starvation-selected flies demonstrate that their entire life history is disturbed; as adults, these animals contain more lipids, but at the cost of reduced fecundity (Masek *et al.* 2014). To determine whether *mir-310*s flies exhibit these phenotypes, first we evaluated the fat storage characteristics of mutant females using a colorimetric assay. Under well-fed conditions, the total body fat content of *mir-310*s females was ~2-fold lower than that of controls (Figure S1B). Consistent with previously reported data (Musselman *et al.* 2011), 10 days of protein starvation resulted in a 1.3-fold increase in the total body fat content in controls. However, upon the same restriction, *mir-310*s females accumulated dramatically higher amounts of lipids, 2.5- and 4-fold increases in comparison to the starved and well-fed controls, respectively (Figure S1, B and B′).

It is well known that the nutrient-sensitive and energy-demanding egg production process is stopped due to nutrient deficit (Drummond-Barbosa and Spradling 2001). In *mir-310*s females, the cessation of egg production is delayed compared to wild type in response to starvation (Figure S1C). However, even on a normal diet, *mir-310*s females laid ~2.5-fold fewer eggs (Figure S1, D–E). If egg-laying ability is a direct readout of metabolic status, these results imply that *mir-310*s-deficient females in general have deficient energy resources and in addition, they cannot properly respond to dietary restriction. Taken together, the proteomic and qRT-PCR expression assays (Figure 1) in combination with the physiological defects caused by *mir-310*s loss, which include increased crop size and reduced egg production under normal diet and dramatic fat accumulation under starvation (Figure S1, Table S3), confirm that the *mir-310*s are essential factors in regulation of energy metabolism in various physiological and cellular elements of the whole organism.

The mir-310s function in the ovarian soma

Next, we aimed to dissect the *mir-310*s function at the cellular level and identify their direct targets involved in starvation response. Therefore, we focused on oogenesis, which is one of the best-studied nutrition-dependent processes. *Drosophila* oogenesis takes place in the ovaries, which are paired organs consisting of individual ovarioles—the egg production units made of progressively developing egg chambers. While developing egg chambers move toward the posterior and develop into mature eggs, they stay attached to the neighboring egg chambers by small groups of cells forming stalks (Figure 2A). Each egg chamber is surrounded by a monolayer of epithelium composed of follicle cells, and specialized polar cells are specified at each end of the egg chamber.

To identify the possible involvement of the *mir-310*s in oogenesis, we analyzed their expression pattern, which was visualized by nuclear β-gal and membrane-bound GFP driven by *mir-310*s–*Gal4*. Expression of reporters was detected in subsets of different somatic cell types, and their expression levels were fluctuating (Figure 2A). For example, some of the stalk and follicular epithelium cells were expressing nuclear β-gal and/or membrane GFP, but some were not (Figure 2, B and C). Since β-gal and GFP proteins have different turnover rates (Timmons *et al.* 1997), we conclude that expression of the *mir-310*s in the ovarian soma is dynamic. Similarly, a dynamic *mir-310*s expression pattern was observed in the brain, where the precision of these miRNAs' expression is achieved via the perceptive–executive mechanism orchestrated by their target (Yatsenko *et al.* 2014).

Upon in-depth examination of *mir-310*s mutant ovaries in well-fed conditions, we identified several phenotypes in the ovarian soma, which could be categorized into three distinct groups. First, supernumerary stalk cells accumulated between egg chambers: in control ovarioles, up to eight stalk cells properly line up between adjacent egg chambers, while in *mir-310*s ovarioles, excessive numbers of disorganized cells at the stalk region formed a multilayered epithelium (Figure 2D). Second, the follicular epithelium cells surrounding egg chambers of different stages were distorted in shape and had irregular cellular polarity, assembling random multilayered

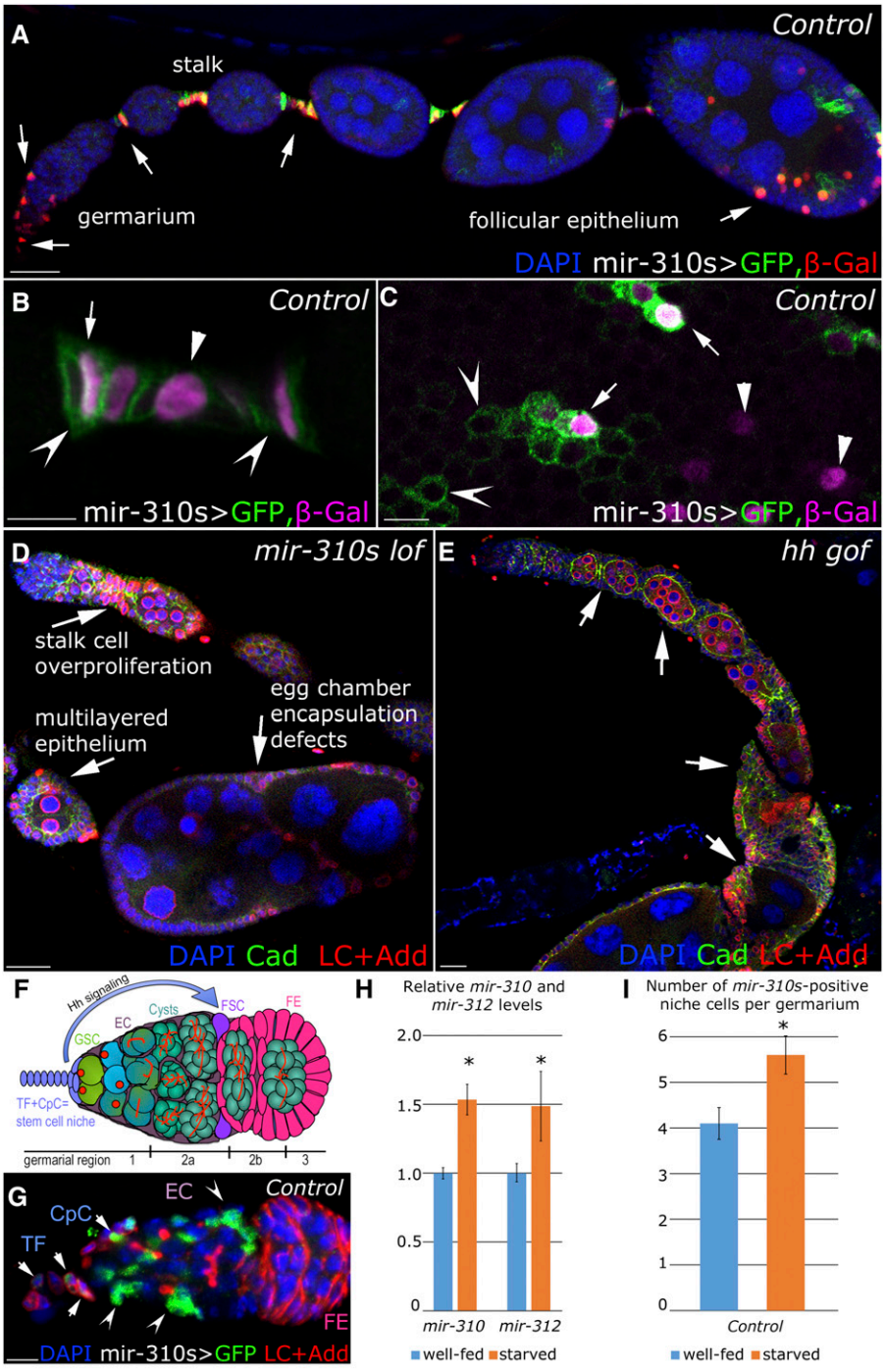

Figure 2 The *mir-310*s are expressed in the ovarian soma. (A–C) The *mir-310*s are expressed in the somatic cells in the germarium, stalk, and follicular epithelium, as visualized by nuclear β-gal and membrane-bound GFP reporters (*mir-310*s-*Gal4*/+; *UAS-mCD8*::*GFP*, *UAS-nLacZ*/+). Some of the stalk (B) and follicular epithelium cells (C) express exclusively β-gal (arrowheads) or GFP (concave arrowheads), whereas others coexpress both reporters (arrows). Different turnover rates of the reporter proteins indicate the dynamic *mir-310*s locus activity. (D) In *mir-310*s mutants (*KT40/Df6070*), ovarioles contain excessive numbers of cells at the stalk region, deformed and multilayered follicular epithelia, and abnormal numbers of nurse cells per egg chamber as a result of defects in egg chamber encapsulation. These phenotypes resemble phenotypes caused by Hh signaling deregulation (Forbes *et al.* 1996a). (E) Overexpression of *hh* in TF and CpCs by shifting 2-day-old *tub-Gal80*^{ts}/+; *bab1-Gal4/ UAS-hh* females to restrictive temperature (29°) for 7 days causes the stalk region and egg chambers to be filled by excessive numbers of epithelial cells in multilayers and egg chambers to bear abnormal numbers of nurse cells. These phenotypes look similar to those of the *mir-310*s mutant shown in D. (F) Schematic of the *Drosophila* germarium. *Drosophila* oogenesis depends on the presence of two to three adult germline stem cells (GSCs) per germarium that continuously divide. The GSCs reside in a specialized microenvironment, the GSC niche, which consists of specialized somatic cells, namely terminal filaments and cap cells (TFs and CpCs). The differentiating GSC progeny is enveloped by the escort cells (ECs) that assemble the differentiation niche. Another type of somatic cells, the follicle stem cells (FSCs) and their progeny, the follicular epithelium (FE) cells divide and surround the 16-cell germline cysts at region 2b. At region 3, the germline cyst encapsulated by the FE pinches off of the germarium as an individual egg chamber. The Hh ligand is expressed in the TF and CpCs and acts long range to FSCs, inducing their division and the differentiation of their progeny. (G) The *mir-310*s are expressed in the stem cell niche, TF and CpCs (arrowheads), and in the differentiation niche, ECs (concave arrowheads), as visualized by anti-GFP staining (*mir-310*s-*Gal4*/+; *UAS-mCD8*::*GFP*, *UAS-nlacZ*/+). (H) The *mir-310*s (*mir-310* and *mir-312*) are significantly upregulated upon starvation. Whole ovary extracts from 7-day-starved females show an ~1.5-fold increase in miRNA levels compared to well-fed controls (Table S5). The bar graph indicates AVE ± SEM. Significances were calculated with two-tailed Student's *t*-test. *$P < 0.05$, **$P < 0.005$, ***$P < 0.0005$. At least three biological replicates per genotype and condition were analyzed. (I) Upon 7 days of nutritional restriction, the number of *mir-310*s expressing CpCs significantly increases as visualized by anti-GFP staining (*mir-310*s-*Gal4*/+; *UAS-mCD8*::*GFP*, *UAS-nLacZ*/+) AVE ± SEM values are reported from the measurements done from 20 germaria (4.1 ± 0.34 well-fed, 5.6 ± 0.42 starved, statistical significance is calculated using Mann–Whitney *U*-test and *Z*-statistic, $P = 0.0078$). In A–G, anterior is to the left. B and C represent single optical sections. A, D, E, and G represent maximum intensity projections of confocal *Z*-stacks. Bars, 20 μm in A, D, and E and 5 μm in B, C, and G.

patches (Figure 2D). Third, abnormally encapsulated egg chambers, easily identifiable by the aberrant numbers of polyploid nurse cells, appeared (Figure 2D). These defects were very similar to the previously described ovarian phenotypes caused by defective Hh signaling (Figure 2E). Hh signaling is important for cell fate establishment of all ovarian somatic cell types (Forbes *et al.* 1996a,b; Tworoger *et al.* 1999; Besse *et al.* 2002; Chang *et al.* 2013) and its ligand is

produced by the terminal filament and cap cells (TFs and CpCs) forming the stem cell niche, and also escort cells (ECs) forming the germline differentiation niche (Rojas-Rios *et al.* 2012). The dynamic *mir-310*s expression was detected in all of these niche cell types (Figure 2, F and G). Importantly, this expression appeared to be diet-sensitive; upon starvation, *mir-310*s expression levels were upregulated (Figure 2H), and the number of *mir-310*s-expressing GSC niche cells (CpCs and TFs) was significantly increased (Figure 2I). These results suggest that the *mir-310*s have a cell-autonomous role in the stem cell niche during dietary changes.

The analysis of the *mir-310*s expression pattern revealed that the *mir-310*s are dynamically expressed in the Hh signal-sending cells (TFs, CpCs, and ECs in the germarium) as well as in the Hh signal-receiving cells (the stalk and follicular epithelium cells in the developing egg chambers) (Figure 2, A–C and G). These results, combined with the similarities of the observed *mir-310*s loss- and Hh gain-of-function mutant phenotypes (Figure 2, D and E), led us to hypothesize that the *mir-310*s regulate Hh signaling via targeting one or multiple components of this pathway.

mir-310s target three genes associated with the Hedgehog signaling pathway

To confirm this hypothesis and define the molecular mechanism responsible for *mir-310*s ovarian phenotypes, we acquired a list of *in silico*-predicted *mir-310*s targets using several miRNA target search databases (Enright *et al.* 2003; Kheradpour *et al.* 2007; Betel *et al.* 2008) and selected among the putative *mir-310*s targets all known or predicted Hh pathway elements and their interaction partners. The *mir-310*s are recently evolved miRNAs, which have highly evolutionarily conserved seed sequences (Figure 3A). As predicted by different algorithms, the *mir-310*s have 350– 450 putative targets, among which only three [*Rab23*, *tramtrack* (*ttk*), and *Hormone receptor-like in 96* (*DHR96*)] have been associated with Hh signaling.

To verify that the *mir-310*s indeed target these three genes, we performed a *Drosophila* S2 cell-based luciferase reporter assay, which depends on the readout from a reporter plasmid with a luciferase gene containing the 3′UTR of the gene of interest with the predicted miRNA target site. The luciferase assay showed that *in vitro*, the *mir-310*s could target the *Rab23*, *DHR96*, and *ttk* transcripts via their 3′UTRs (Figure 3B; Table S4).

Next, we tested *in vivo* the responsiveness of these three putative target genes to the *mir-310*s as well as to nutrient restriction. We found that the expression of all three genes is nutrition dependent, showing significant reduction under starvation conditions. In *mir-310*s mutants, *Rab23* and *DHR96* levels were significantly upregulated (>1.5-fold; Figure 3C), and their expression levels were not as efficiently reduced under starvation. In contrast, *ttk* mRNA expression levels were similar to controls in *mir-310*s-deficient flies under well-fed conditions. *ttk* expression was controlled by the *mir-310*s only under nutritional stress, where *mir-310*s mutants had 1.5-fold higher *ttk* mRNA levels when compared to controls (Figure 3C and Table S5). These data demonstrate that the *mir-310*s act to fine tune the expression of the nutrition-dependent genes *Rab23*, *DHR96*, and *ttk*; furthermore, the *mir-310*s regulate *ttk* only upon dietary restriction.

The above results confirm that the *mir-310*s are important regulators of at least three components associated with Hh signaling (Figure 3D). *DHR96* encodes a cholesterol receptor responsible for sensing the nutritional status of the cell environment (Horner *et al.* 2009; Bujold *et al.* 2010; Sieber and Thummel 2012) and promoting Hh ligand release upon dietary cholesterol intake (Hartman *et al.* 2013). *ttk* encodes a transcription factor that acts as a controller of the cell cycle switch during midoogenesis through regulation of Hh target gene expression (Sun and Deng 2007). *Rab23* encodes a membrane organization and trafficking Rab GTPase (Zerial and McBride 2001; Zhang *et al.* 2007; Chan *et al.* 2011). Mouse Rab23 was shown to act as a negative regulator of the Sonic Hh signaling pathway in signal-receiving cells during embryonic neural patterning (Eggenschwiler *et al.* 2001). However, *Drosophila* Rab23 is known not to function in Hh signaling through the same mechanism [at least in the process of wing development (Pataki *et al.* 2010)], and its role in Hh signaling has not been confirmed.

The mir-310s and Rab23 regulate Hh ligand release

As the involvement of Rab23 in the Hh pathway remains an open question in *Drosophila* (Zhang *et al.* 2007; Pataki *et al.* 2010), we decided to further focus on the *mir-310*s–*Rab23* interaction. First, we analyzed the spatial distribution of Rab23 protein using a *Rab23*::*YFP* line generated via homologous recombination (see *Materials and Methods*). Similarly to the *mir-310*s, the endogenous Rab23 protein was detected in the germline stem cell niche (TFs and CpCs) and in the differentiation niche (ECs), and this expression was dynamic: some of the niche cells were Rab23 negative and the others could be classified as high or low Rab23-expressing cells (Figure 2G, Figure 4, A–D). Upon close examination, we found significantly more Rab23-positive CpCs in *mir-310*s mutant germaria in comparison to controls (Figure 4E). Moreover, upon starvation, the number of cells with high Rab23 levels was significantly increased in *mir-310*s mutants (Figure 4E; Table S6).

In wild type, Hh is produced in the stem cell niche and travels into the posterior compartment to activate FSC division. We observed that the elevated levels of Rab23 in *mir-310*s mutants in different conditions coincided with higher levels and a broader expression pattern of the Hh ligand, as detected by an anti-Hh antibody (Figure 4, A–D). To confirm the roles of Rab23 and the *mir-310*s in the dispersion of the Hh ligand, we calculated the number of Hh protein speckles in the germarium (Figure 4, A–D, F, and G). Indeed, *mir-310*s loss and Rab23 overexpression in the stem cell niche both resulted in significantly higher numbers of Hh speckles distributed throughout the whole germarium (Figure 4, C and F, red line). Moreover, although starvation results in the restriction of

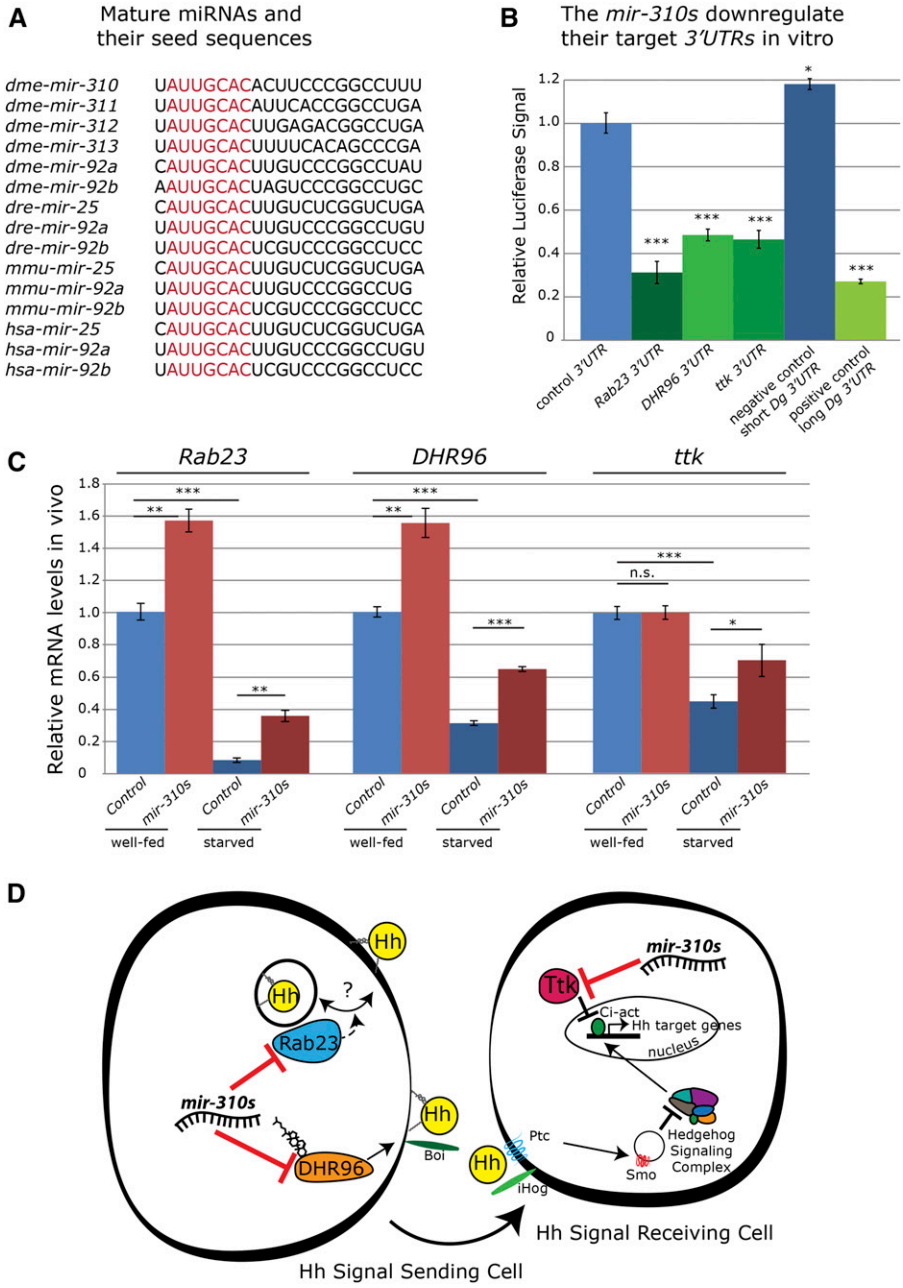

Figure 3 The *mir-310*s target three genes associated with the Hh pathway. (A) The *mir-310*s share a highly conserved seed sequence (red) with their ancestral miRNAs *mir-92a* and *mir-92b*, and their orthologous miRNAs from zebrafish, mouse, and human. (B) Overexpression of *mir-310*s downregulates *Rab23*, *DHR96*, and *ttk* 3′ UTR luciferase reporters in *Drosophila* S2 cells. The long 3′ UTR of a confirmed target gene (*Dg*) with *mir-310*s binding site serves as positive, the short *Dg* 3′ UTR without a *mir-310*s binding site serves as negative control (Table S4). (C) *mir-310*s mutant (*KT40*/*KT40*) females have significantly higher *Rab23* and *DHR96* mRNA levels (whole RNA extracts from adult females were used). This elevation is even more pronounced under starvation conditions (10 days). The change in *ttk* mRNA levels, however, illustrates *mir-310*s-dependent regulation exclusive to the starvation condition (Table S5). (D) Model shows major conserved components of Hh signaling, including the Hh receptor Patched (Ptc), the transmembrane protein Smoothened (Smo), and the transcriptional effector Cubitus interruptus (Ci), which act in the signal-receiving cells (Forbes *et al.* 1996a; Zhang and Kalderon 2001). Additional Hh receptors and close homologs, Ihog and Boi, promote intrinsic Hh signaling and extrinsic Hh ligand release (Hartman *et al.* 2010). Hh signaling governs adult stem cell division and differentiation depending on the cholesterol modification of the ligand, which is required for long-range signaling and is sensitive to changes in the nutritional status of the animal (Panakova *et al.* 2005). Particularly, ovarian FSCs rely on this signal to initiate the division and differentiation process, which can be slowed down, stopped, and reinitiated upon changing dietary conditions (Rojas-Rios *et al.* 2012; Hartman *et al.* 2013). Upon starvation, Hh is sequestered by Boi, while upon feeding, cholesterol binds to DHR96 and promotes Boi phosphorylation and Hh release, which positively affects FSC proliferation (Hartman *et al.* 2013). The *mir-310*s are present in the niche and follicle cells that also express *DHR96* and *ttk*, respectively (Sun and Deng 2007; Hartman *et al.* 2013), which suggests that the *mir-310*s could intrinsically regulate these targets in both the Hh signal-sending and Hh signal-receiving cells of the ovarian soma in response to nutrient availability. For B and C, bar graphs indicate AVE ± SEM. Significances were calculated with two-tailed Student's *t*-test. $*P < 0.05$, $**P < 0.005$, $***P < 0.0005$.

Hh ligand to the anterior part of the germarium (Hartman *et al.* 2013) (Figure 4B, red line), in the starved *mir-310*s loss-of-function and Rab23 overexpressing germaria, this spatial restriction was less pronounced (Figure 4, D–H, red lines; Table S7). These results confirm a role for Rab23 in the cell-autonomous positive regulation of Hh release and suggest that the effect of *mir-310*s deficiency on Hh ligand distribution occurs via Rab23.

Next, we tested if starvation-mediated regulation of *hh* expression occurs at the transcriptional level. However, expression of a *hh-lacZ* reporter transgene in the stem cell and differentiation niches did not change upon starvation (compare Figure 4I and 4J, arrows and arrowheads, respectively). These data indicate that upon dietary restriction, Hh is not regulated at the transcriptional level; on the contrary, the *mir-310*s and Rab23 play a role in Hh spatial distribution.

Next, we aimed to understand how Rab23 is involved in regulation of the Hh ligand. Analysis of Rab23 and Hh protein expression in CpCs revealed dynamic expression patterns such that some cells coexpressed both proteins and others were positive for either Hh or Rab23 (Figure 4, A–D). At the subcellular level, the proteins formed puncta, some of which

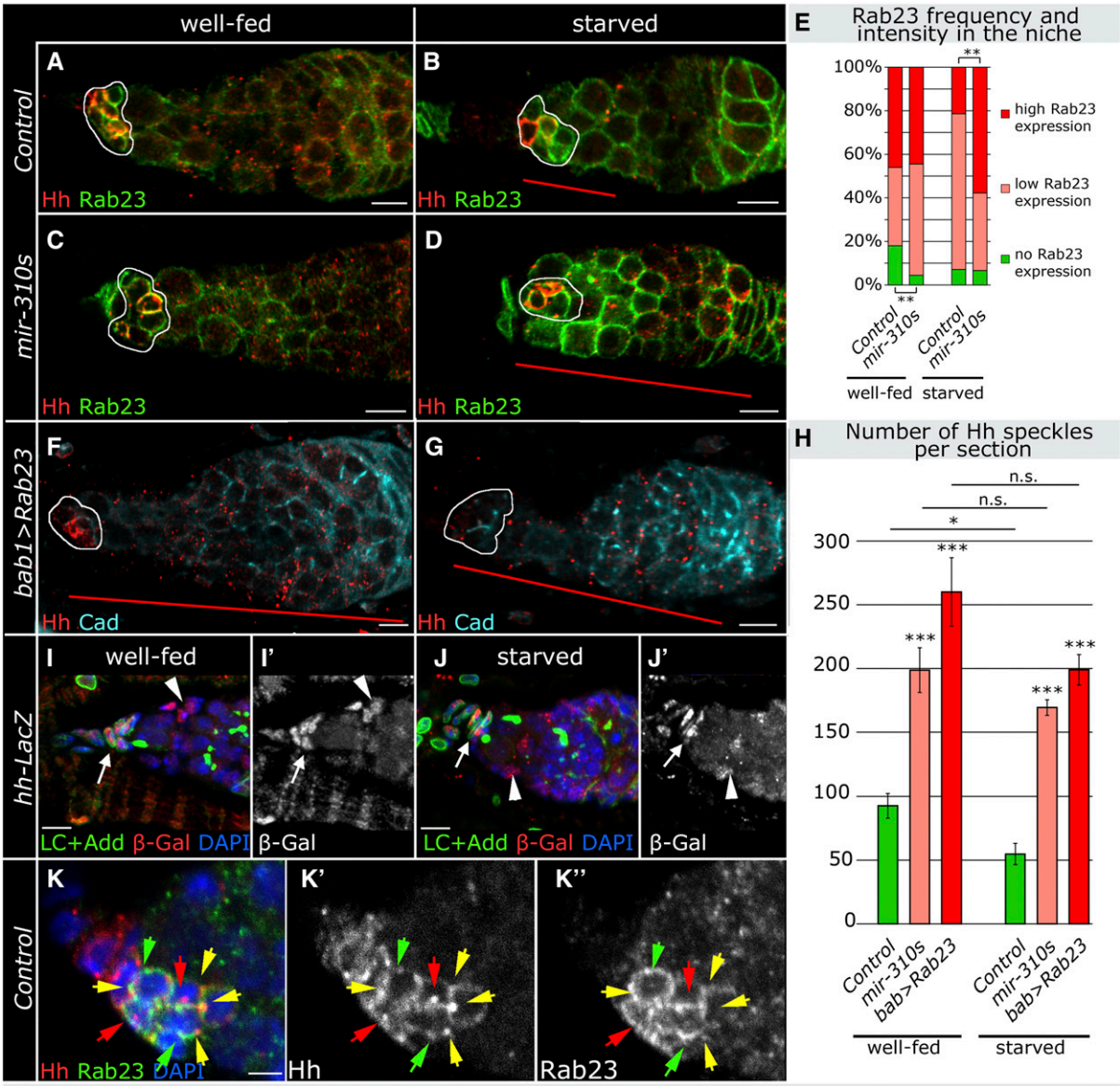

L Rab23 co-immunoprecipitates with vesicle-associated proteins

CG Number	Gene Name	GO Term
CG14813	deltaCOP	vesicle-mediated transport
CG3029	or	vesicle coating
CG11785	bai	Golgi vesicle transport
CG7359	Sec22	ER to Golgi vesicle-mediated transport
CG4780	Membrin	ER to Golgi vesicle-mediated transport
CG5864	AP-1sigma	vesicle-mediated transport
CG9128	Sac1	axon cargo transport
CG8385	Arf79F	post-Golgi vesicle-mediated transport
CG6582	Aac11	negative regulation of apoptotic process
CG3564	CHOp24	ER to Golgi vesicle-mediated transport
CG4422	Gdi	vesicle-mediated transport
CG33104	eca	ER to Golgi vesicle-mediated transport

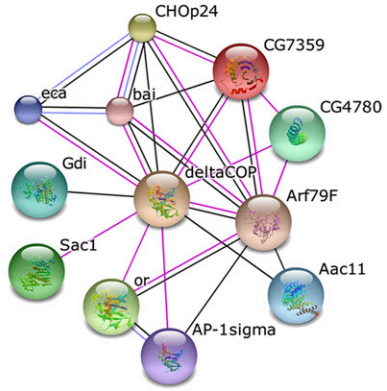

Figure 4 *Rab23* is targeted by the *mir-310*s, controlling Hh ligand availability. (A–D) The *mir-310*s negatively regulate Rab23 expression. Rab23 has a stronger and more widespread expression pattern in *mir-310*s mutant (C, *KT40/KT40*; *Rab23*::*YFP*::*4xmyc*) compared to control germaria (A, w^{1118}; *Rab23*::*YFP*::*4xmyc*). As a result of 7-day starvation, in controls, Rab23 has more widespread staining (B), which is more obvious in *mir-310*s mutants (D). The Hh ligand is produced by CpCs in the niche (outlined in white) and is visualized by anti-Hh antibody (red). Hh protein is detected along the length of the germarium under normal conditions (A). Upon starvation, Hh speckles are confined at the anterior half of the germarium (B, red line), while in the

contained Hh or Rab23 only (Figure 4K, red and green arrows, respectively) and some had both proteins colocalized (Figure 4K, yellow arrows). In general, Rab proteins are vesicle-tethering proteins, regulating intracellular trafficking (Zerial and McBride 2001). Therefore, we hypothesized that Rab23 is involved in transport and trafficking of Hh-loaded vesicles in the GSC niche cells. To test this idea, we performed a coimmunoprecipitation using *Rab23*::*YFP*::*4xmyc* flies to identify Rab23 interaction partners. Subsequently, mass spectrometry analysis followed by GO term analysis of identified proteins (UniProt Consortium 2014) and evaluation of functional association networks (Franceschini *et al.* 2013) revealed a group of 12 proteins as components of COPI-coated vesicle machinery among a larger number of other identified proteins (Figure 4L; Table S8). Importantly, this implicates Rab23 as a novel regulator of precisely controlled Hh ligand secretion in *Drosophila*. In summary, our results suggest a model in which *mir-310*s act in the stem cell niche to repress expression of Rab23, which is involved in intracellular vesicle trafficking and release of the Hh ligand in COPI vesicles.

mir-310s moderate ovarian Hh signaling via downregulation of the positive regulator Rab23

If our model is correct, then the diet-dependent *mir-310*s–Rab23–Hh trafficking cascade should have a direct effect on Hh signaling strength, and manipulation of the levels of these components may allow the rescue of phenotypes associated with abnormal Hh signaling. Therefore, we performed such an epistasis analysis, quantifying several ovarian phenotypes previously described as Hh signaling defects (Forbes *et al.* 1996a,b). First, we analyzed the posterior germarium architecture at the intersection of regions 2a and 2b (Figure 2F). In controls, ~75% of germaria had germline cysts fully encapsulated by the follicular epithelial cell precursors (Figure 5A, marked by FasIII, arrow), while ectopic Hh expression in the GSC niche results in the accumulation of germ cells in germarial region 2b (Figure 5, A, A′, and B). Next we analyzed *mir-310*s loss-of-function and *Rab23* niche-specific gain-of-function phenotypes and compared their frequencies to those caused by Hh overexpression. Only 20% of *mir-310*s mutant germaria had this region properly structured (Figure 5, A and B). This phenotype is *mir-310*s specific, since it was observed in different *mir-310*s mutant allelic combinations and could be fully rescued by the introduction of a *mir-310*s genomic fragment (Figure 5, A′′′ and B; Table S9). Similar frequencies of disorganization were observed due to Rab23 overexpression (Figure 5, A′′′′ and B). If this defect is caused by the increased levels of the Hh ligand, trafficking and release of which depend on Rab23, which is in turn negatively regulated by the *mir-310*s, then downregulation of Hh or Rab23 should alleviate *mir-310*s-deficient phenotypes in the germarium. Indeed, this germarial defect was significantly rescued by reducing Rab23 or Hh levels via RNAi in a *mir-310*s mutant background (Figure 5B; Table S9).

Second, we analyzed the germline pinching-off defects. Abnormal cyst encapsulation in the germarium coupled with defective epithelial cell fate determination results in the appearance of egg chambers containing atypical numbers of germline cells (Figure 2, D and E; Figure 5, C–E). This phenotype was detected in ~40% of *mir-310*s-deficient and Rab23-overexpressing ovarioles and was even more pronounced (~90%) in the ovarioles with Hh overexpression (Figure 5, C–F). Importantly, the introduction of a *mir-310*s genomic fragment or reduction of Hh or Rab23 in *mir-310*s mutants fully rescued this phenotype, demonstrating that Rab23 and Hh act downstream of the *mir-310*s in this process (Figure 5F; Table S9).

Third, we analyzed the state of stalk cell specification. Increased Hh levels cause abnormal differentiation of the stalk cells, resulting in the accumulation of excessive precursor stage-like cells (Tworoger *et al.* 1999). A total of 70% of all ovarioles contained multilayered stalks in *mir-310*s loss of function (Figure 5G) and Rab23 gain of function (Figure 5E), and again this phenotype was even stronger in the Hh gain of function (Figure 2E). This phenotype was fully rescued upon the introduction of a *mir-310*s genomic fragment (Figure 5H) or downregulation of Rab23 or Hh in *mir-310*s-deficient animals (Figure 5I; Table S9).

Normally, the stalk cells are terminally differentiated epithelial cells that never divide; thus, a multilayered stalk phenotype can result if stalk cell differentiation is delayed

mir-310s mutant this restriction does not happen under the same conditions (D, red line). (E) The *mir-310*s affect the frequency and intensity of Rab23 expression in CpCs. In well-fed conditions, *mir-310*s mutants have lower numbers of Rab23-negative CpCs compared to controls (green bars). Upon 7 days of starvation, *mir-310*s mutant germaria contain a higher number of CpCs expressing high levels of Rab23 compared to controls (red bars), visualized by the intensity of Rab23 fluorescence (Table S6). (F–H) Germaria overexpressing Rab23 in the stem cell niche (*bab1-Gal4/UAS-Rab23*) similarly to *mir-310*s mutants, have increased Hh staining (increased number of Hh speckles) compared to controls under well-fed and starved conditions (F and G red lines, Table S7). (I and J) The expression activity of the *hh* gene locus (as visualized using *hh-LacZ*) does not change significantly upon starvation and is comparable in the stem cell niche (arrows) and in the escort cells (arrowheads) in well-fed (I) and starved conditions (J). (K) Both Rab23 and Hh proteins are expressed in the CpCs and their expression patterns are dynamic; some of the stem cell niche cells express Rab23 (visualized by *Rab23*::*YFP*::*4xmyc*) and/or Hh (green and red arrows, respectively). In addition, these proteins colocalize in subcellular foci (yellow arrows). (L) Interaction network and related their GO term analysis of Rab23 coimmunoprecipitated multiple coatomer-associated proteins (COPI) that act in intracellular vesicular trafficking are shown. The edges connecting the protein nodes indicate database-derived (Franceschini *et al.* 2013) interactions based on coexpression (black edges), experiments (pink edges), and homology (purple edges). The complete list of Rab23 coimmunoprecipitated proteins is given in Table S8. Significances were calculated with two-tailed Student's *t*-test. $*P < 0.05$, $**P < 0.005$, $***P < 0.0005$. A–G and K represent single optical sections; CpCs are outlined; and I and J represent maximum intensity projections of confocal *Z*-stacks. Anterior is to the left. Bars, 5 μm in A–G, I ,and J and 2 μm in K.

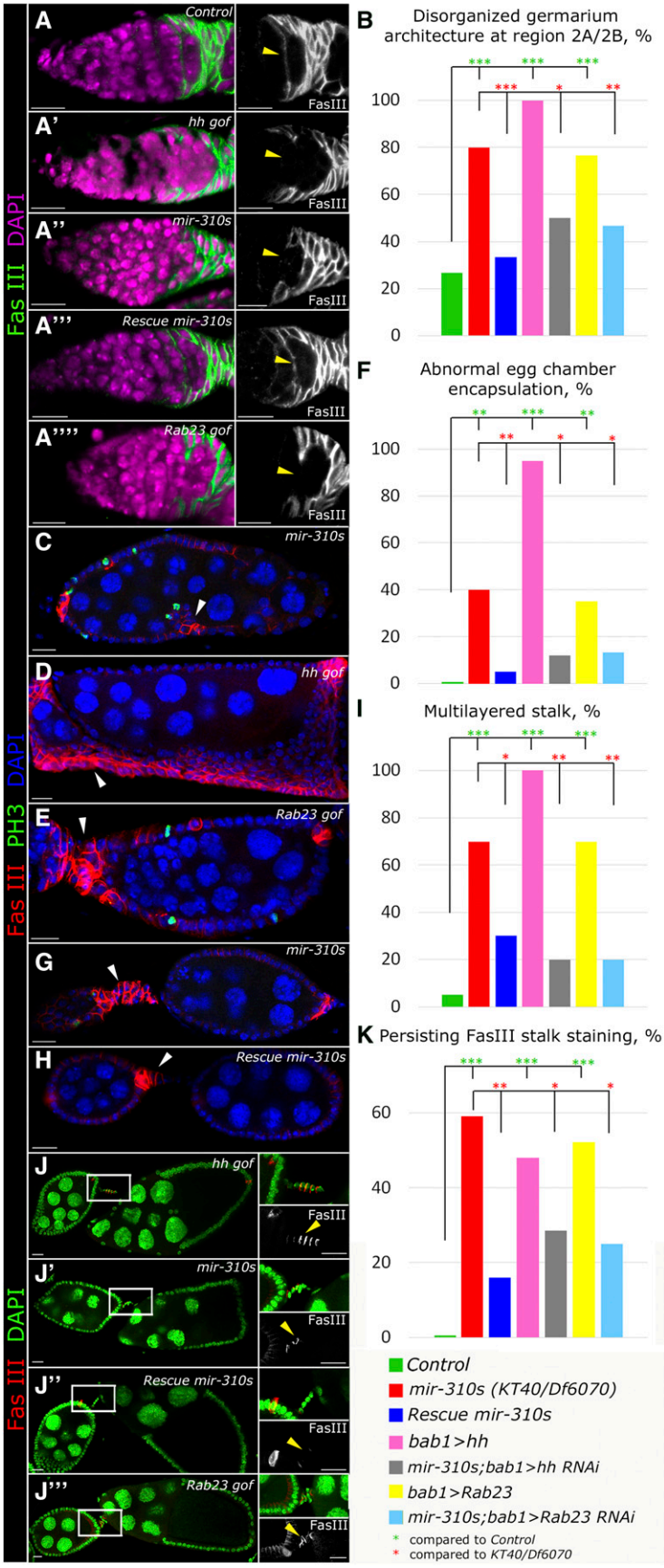

Figure 5 The *mir-310*s and Rab23 regulate Hh signaling in the ovary. (A and B) Prior to the pinching off of the egg chamber from the germarium, the germline cysts are encapsulated by follicle cell precursors marked with FasIII, which move toward the interior of the germarium and envelop the cyst (A, arrowhead) as shown in a control (*w*^{1118}*/Oregon-R-C*) germarium. Hh overexpressing (A′, *tub-Gal80*^{ts}; *bab1-Gal4/ UAS-hh* at 29°), *mir-310*s mutant (A′′, *KT40/Df6070*), and Rab23 overexpressing (A′′′′, *bab1-Gal4/UAS-Rab23*) germaria have disorganized architecture at the posterior end, with a significantly lower frequency of properly encapsulated cysts than in controls. This phenotype can be rescued by introducing a *mir-310*s genomic rescue construct in the *mir-310*s mutant background (A′′′, *KT40/KT40*; *attB2 mir-310*s *rescue long2/+*) (Table S9). (C–F) *mir-310*s deficiency causes the appearance of egg chambers with abnormal sizes and an abnormal number of nurse cells (C). In addition, the follicular epithelium becomes multilayered in irregular patches (arrowhead in C). Similarly, Hh or Rab23 overexpression results in the occurrence of egg chambers with similar defects (D and E). The frequency of this phenotype is comparable for *mir-310*s mutation and Rab23 overexpression. This phenotype can be rescued by downregulating the Rab23 or Hh levels in a *mir-310*s mutant background (*KT40/KT40*; *bab1-Gal4/UAS-Rab23-RNAi* and *KT40/KT40*; *bab1-Gal4/UAS-hh-RNAi*) (Table S9). (G–I) Loss of the *mir-310*s results in an excess number of cells accumulating between the egg chambers (arrowhead), forming an overcrowded, multilayered stalk. This phenotype can be rescued by introducing the *mir-310*s genomic rescue construct in a *mir-310*s mutant background (H, *KT40/KT40*; *attB2 mir-310*s *rescue long2/+*) (Table S9). (J and K) *mir-310*s mutant stalks connecting stages 6–10 egg chambers have disorganized shapes and continue to express the precursor marker FasIII (J′, arrowhead), reproducing the cell specification phenotype caused by very mild *hh* overexpression (*tub-Gal80*^{ts}; *bab1-Gal4/UAS-hh* at 18°) (J, arrowhead). Higher levels of Hh overexpression result in a severe phenotype (depicted in Figure 2E). *Rab23* overexpression causes the same stalk defects (J′′′). This phenotype can be rescued by introducing the *mir-310*s genomic rescue construct in the *mir-310*s mutant background (J′′, *KT40/KT40*; *attB2 mir-310*s *rescue long2/+*) (Table S9). In A, C–E, G, H, and J, anterior is to the left. A, C–E, G, and H represent single optical sections. J′–J′′′ represent maximum intensity projections of confocal *Z*-stacks. Bars, 10 μm. Significances were calculated using Pearson's chi-square test. $*P < 0.05$, $**P < 0.005$, $***P < 0.0005$ (Table S9).

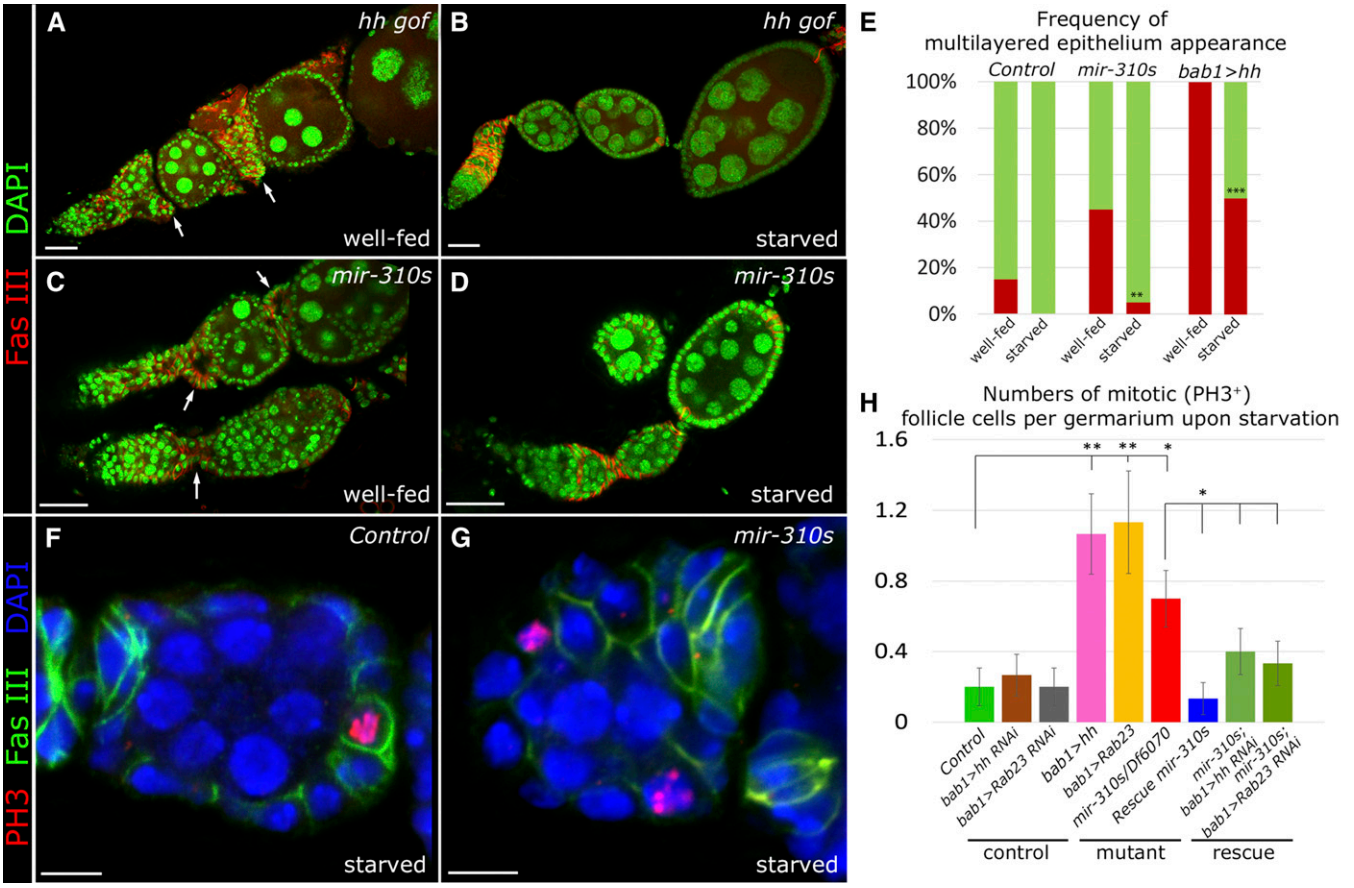

Figure 6 The phenotypes caused by *mir-310*s loss or *hh* overexpression can be alleviated by dietary restriction. (A–E) *hh* gain of function causes epithelial defects resulting from somatic cell overproliferation (A, arrows). Upon nutritional restriction for 3 days, the dramatic *hh* gain-of-function (*tub-Gal80^{ts}*/+; *bab1-Gal4/UAS-hh* at 29°) phenotypes become significantly less penetrant (B and E). Similarly, the appearance of the atypical multilayered epithelium in *mir-310*s mutant (C, arrows, *KT40/Df6070*) ovaries is dramatically reduced upon nutritional restriction (C–E) (Table S9). (F–H) Under nutritional stress, on average less than one mitotically active follicle cell (marked by PH3) per stage 2 egg chamber is found in controls (F and H). In the *mir-310*s mutant, this number is increased (G and H). After nutritional restriction for 7 days, egg production is slowed down, which results in a reduction of follicular epithelial cell proliferation. However, the number of PH3-positive cells is fourfold higher due to *mir-310*s loss (H). Similarly, upon starvation, overexpression of Rab23 (*tub-Gal80^{ts}*; *bab1-Gal4/UAS-Rab23*) and Hh (*tub-Gal80^{ts}*; *bab1-Gal4/UAS-hh*) (4 days at 29°) results in an approximately fivefold higher PH3-positive cell number compared to control (H). The high mitotic activity in *mir-310*s mutant egg chambers is rescued by an independent genomic *mir-310*s rescue construct (*KT40/KT40*; *attB2 mir-310*s *rescue long2/+*), or by downregulating the Rab23 (*KT40/KT40*; *bab1-Gal4/UAS-Rab23-RNAi*) or Hh levels (*KT40/KT40*; *bab1-Gal4/UAS-hh-RNAi*) (Table S10). A–D, F, and G represent single optical sections and anterior is to the left. Bars, 20 μm in A–D and 5 μm in F and G. In H, the bar graph indicates AVE ± SEM. Significances were calculated for E using Pearson's chi-square test (Table S9) and for H, using Mann–Whitney *U*-test and *Z*-statistic. *$P < 0.05$, **$P < 0.005$, ***$P < 0.0005$ (Table S10).

and proliferation continues. In this case, these cells would express undifferentiated epithelial precursor cell markers and undergo additional divisions. Therefore we analyzed the expression of a precursor cell marker, FasIII, in stalks between late-stage egg chambers (later than stage 6) that normally no longer express FasIII (Figure 5, J–J′′′). Overexpression of the Hh ligand in the GSC niche results in a very dramatic phenotype, in which all the stalk cells were abnormally differentiated (Figure 2E and Figure 5D). Therefore, to obtain stalks with a less severe phenotype more amenable to quantification, we overexpressed Hh in a short pulse during adulthood using the Gal4/Gal80^{ts} system. Hh overexpression in the stem cell niche led to the appearance of stalk cells with persistent FasIII expression between late-stage egg chambers (Figure 5J). Similarly, we found FasIII-positive stalk cells in >50% of the analyzed stalks in *mir-310*s loss-of-function and Rab23 overexpressing ovarioles (Figure 5, J and J′′; Table S9). Importantly, downregulation of Hh signaling, either by *mir-310*s genomic rescue or by downregulation of Rab23 or Hh ligand expression in the GSC niche, rescued the stalk cell specification phenotype (Figure 5K; Table S9).

Together, these phenotypic analyses indeed show that higher levels of Rab23 in *mir-310*s mutants phenocopy overactive Hh signaling and confirm that the effect the *mir-310*s have on Hh signaling is accomplished via their regulation of Rab23. Thus, Hh signaling can be intensified via Rab23-mediated enhancement of Hh ligand trafficking/release and the *mir-310*s moderate this signaling cascade via the upstream targeting of *Rab23*.

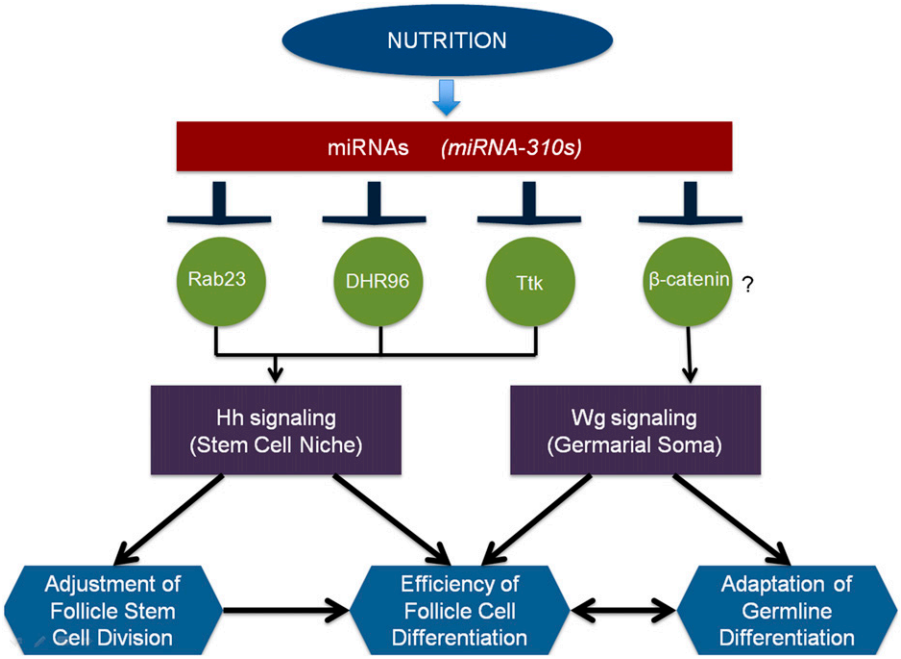

Figure 7 Model of a miRNA-based nutritional stress response signaling relay. In the ovary, upon dietary fluctuations, the *mir-310*s target multiple components associated with Hh signaling, which ensures fast dietary response and adapts oogenesis. miRNAs can also act on other targets that belong to other critical pathways (for example, Wg), further coordinating the efficiency of the process. See also *Discussion* for details.

Hh signaling is regulated by the mir-310s in response to diet

Since our data show that *mir-310*s mutants show defective metabolic status (Figure S1), and that the *mir-310*s act upstream of Hh signaling via repression of *Rab23* (Figure 3C; Figure 4, C–E), we decided to test whether these miRNAs would aid in adjusting Hh signaling efficiency in response to nutritional stress. Remarkably, we observed that the dramatic ovarian phenotypes associated with excessive Hh signaling were radically improved upon dietary restriction (compare Figure 6A and 6B). Similarly, the appearance of mutant phenotypes in *mir-310*s ovaries was significantly rescued upon starvation (compare Figure 6C and 6D). To quantify the effect of starvation, we focused on the overproliferated stalk phenotype, since it is a hallmark of hyperactive Hh signaling. A total of 100% of Hh-overexpressing ovarioles contained patches of multilayered stalk cells, while upon starvation the frequency of this phenotype was reduced by half; in *mir-310*s, this phenotype was fully rescued by dietary restriction (Figure 6E; Table S9).

It is known (Forbes *et al.* 1996a,b) that ectopic *hh* expression results in excessive somatic cell proliferation and that stimulated Hh release can induce ligand accumulation on the follicle cells, hence promoting their division even under nutrient-restricted conditions (Hartman *et al.* 2013). Therefore, we analyzed the number of mitotically active cells among follicular epithelium cells wrapping stage 2 egg chambers using phosphohistone 3 (PH3) as a mitotic marker. Under normal conditions, *mir-310*s mutant, Hh and Rab23 overexpressing egg chambers also have a mild increase (1.2- to 2-fold) in the number of follicle cells in mitosis (Table S10). This tendency became even more pronounced under starvation, as *mir-310*s mutants had almost 4-fold higher numbers of follicle cells in mitosis when compared to controls (Figure 6, F–H). To determine whether this proliferation phenotype is caused by excessive Rab23 levels and, thus, overactive Hh signaling, we overexpressed Rab23 or Hh ligand in Hh-sending cells. As expected, even upon starvation, both of the overexpression experiments resulted in ~5-fold higher numbers of dividing follicle cells in the follicular epithelium, suggesting that Rab23 cell-autonomous involvement in the Hh signaling pathway is diet dependent. Notably, the excessive *mir-310*s follicle cell division phenotype under starvation was significantly rescued by the introduction of the *mir-310*s genomic locus or downregulation of *Rab23* or *hh* in a *mir-310*s mutant background (Figure 6H; Table S10). These results show that the abnormal follicle cell proliferation upon dietary restriction is caused by the higher levels of *Rab23*, and, consequently, overactive Hh signaling as a result of *mir-310*s loss of function. Furthermore, this confirms our hypothesis that the *mir-310*s–Rab23–Hh ligand signaling cascade regulates Hh signaling activity, and this regulation becomes even more prominent in response to dietary fluctuations.

Together, our data show that the miRNAs pathway plays an important role in adjusting the metabolic status of an organism to nutritional signals. In particular, we found that the *mir-310*s are diet-sensitive and that *mir-310*s-deficient flies exhibit severe abnormalities in metabolic homeostasis, including altered gene and protein expression profiles. In addition, multiple diet-sensitive physiological processes, such as crop size, lipid storage, and fecundity are perturbed. Furthermore, we found that the *mir-310*s are capable of targeting at least three genes associated with the Hh signaling pathway, ensuring a robust, fast, and precise response to diet alterations via modulation of this vital signaling pathway. Particularly, in the Hh signal-sending cells, the *mir-310*s

represses expression of factors regulating Hh ligand production: DHR96, which senses systemic cholesterol levels and promotes Hh release; and Rab23 which, as we propose here, functions in vesicles required for Hh trafficking. In the Hh signal-receiving cells, *ttk* mRNA encoding the negative Hh signaling transducer and transcription factor, is targeted by the *mir-310*s. Possibly, targeting of several components of the same signaling pathway is a critical principle of miRNA regulation of stress signaling pathways that should be specifically considered in our understanding of the roles of miRNAs in physiologic and pathophysiologic stress.

Discussion

Here we propose a model for a prompt dietary stress response in which nutritional signals are transduced via miRNAs that act upstream of vital cellular signaling pathways to fine tune their activity and efficiently adapt organismal metabolism to ensure healthy homeostasis (Figure 7). Here we found that the *mir-310*s, via targeting of multiple Hh pathway components, ensure rapid and robust adjustment of Hh signaling in response to dietary signals. Normally, the capacity of organisms to adapt quickly to changeable food conditions is crucial for their survival since dietary components and food availability can vary rapidly. It is known that adult miRNA mutants rarely show extreme phenotypes in well-controlled laboratory conditions; however, upon stress, a miRNA deficiency frequently has a profound effect on organism survival and adaptability (Bhattacharyya *et al.* 2006; Leung and Sharp 2010; Mendell and Olson 2012; Edeleva and Shcherbata 2013). Therefore, our interpretations that miRNAs act only upon stress may not be entirely reasonable; their functions may be broader and more basic to control organismal homeostasis. Unique challenges and opportunities for miRNA studies, and in particular for miRNA research focused on the stress response, are to identify the biologically relevant downstream targets regulated by miRNAs, which will allow not only to better understand the mechanisms of stress responses, but also to provide the understanding of how organisms constantly fine tune gene expression to maintain healthy homeostasis in the ever-changing external and internal environments. Here we propose a new workflow that facilitates the identification of miRNA targets and conditions under which studied miRNAs might function.

During embryonic development, miRNAs often act only as fine tuners of gene expression, differentiation guardians, and canalization factors, as embryonic development is extremely well programmed and protected from environmental stimuli and, therefore, it should just be stabilized to succeed (Siegal and Bergman 2002; Hornstein and Shomron 2006; Yatsenko and Shcherbata 2014). However, during adulthood, miRNAs often greatly influence the responses of adult tissues to stressful conditions or hormonal fluctuations (Leung and Sharp 2010; Fagegaltier *et al.* 2014). To have a profound effect on gene expression, several mechanisms assuring the effectiveness of miRNA-based gene expression regulation have been developed, such as high expression of the miRNA, positive feedback loops, or targeting of multiple components of the critical pathway. For the newly emerged *mir-310*s family, misexpression would be damaging since the *mir-310*s have hundreds of putative and several already confirmed critical targets, such as *Khc-73*, *armadillo* (*arm*), and *Dystroglycan*, deregulation of which could be fatal (Tsurudome *et al.* 2010; Pancratov *et al.* 2013; Yatsenko *et al.* 2014). Positive feedback signaling is also somewhat unlikely because then miRNAs would be expressed in all Hh signal-receiving cells, which, as we have shown, is not the case for the *mir-310*s. Instead, the *mir-310*s are expressed dynamically only in some of the Hh signal-sending and signal-receiving cells. Previously it was shown that the *mir-310*s gene expression is sensitive to nitric oxide levels (Yatsenko *et al.* 2014), which via nitrosylation of histone deacetylases regulates the cellular epigenetic profile. Epigenetic modifications that play a key role in the regulation of gene expression can also be influenced by both the quality and quantity of the diet (Daniel and Tollefsbol 2015). Based on the previous data, it is logical to hypothesize that the dynamic *mir-310*s expression in ovaries could also be dependent on specific histone modifications. Currently, it is unknown which signaling induces *mir-310*s expression in response to deficit of nutrients; however, *mir-310*s ability to target both the factors required for Hh ligand release in the signal-sending cells (Rab23 and DHR96) and the Hh signal transducer (the transcription factor Ttk) in the signal-receiving cells, ensures that the diet-dependent Hh pathway is securely downregulated upon restrictive diet. While previous data propose that modulation of Hh signaling is a primary dietary stress-response mechanism controlling stem cell proliferation (Horner *et al.* 2009; Hartman *et al.* 2013), we show that the *mir-310*s act upstream of this signaling, demonstrating that miRNAs fine tune a major cell signaling pathway to adjust its strength in the stem cell niche to changing dietary conditions. Even though the miRNAs are generally not well conserved between *Drosophila* and humans, the processes they regulate are. Therefore, it would be interesting to study whether Hh signaling is also regulated via miRNAs in vertebrates upon diet.

Hh is one of the canonical developmental pathways crucial for the development of a variety of tissues in all bilaterians; thus, finding new components of this pathway is of great importance. We identified the *mir-310*s as a novel upstream regulatory element of this pathway in *Drosophila*. Namely, the post-transcriptional control of the expression levels of at least three genes from the Hh pathway (*Rab23*, *DHR96*, and *ttk)* depends on these miRNAs to sustain tissue homeostasis, which has to assume new equilibrium under changing environmental/nutritional conditions. Interestingly, the highly evolutionarily conserved Hh signaling pathway has been shown to play a role in obesity-like fat accumulation in *Drosophila* and mouse adult stem cells (Pospisilik *et al.* 2010).

Importantly, we identified a new regulator of Hh signaling in *Drosophila*, Rab23. Rab proteins are a family of small

GTPases that play key roles in vesicle cargo transport, docking, and fusion and are important for fine tuning of various canonical pathways, safeguarding proper development, tissue morphogenesis, and homeostasis (Zhang *et al.* 2007). It is known that Rab proteins can have redundant functions (Chan *et al.* 2011); therefore, deficiency or downregulation of only one of them might not have a dramatic effect on animal viability. Indeed, *Rab23* loss of function did not result in any of the analyzed ovarian phonotypes, demonstrating that Rab23 is dispensable for Hh signaling function in the ovary, while its upregulation had an important effect on Hh signaling strength. Based on the proposed Rab23 vertebrate homolog function, *Drosophila* Rab23 was expected to regulate the trafficking of vesicle-associated components in the Hh signal receiving cells (Evans *et al.* 2003; Pataki *et al.* 2010). However, our data demonstrate Rab23-based regulation in the Hh signal sending cells. We propose a new mechanism in which Rab23 has a cell-autonomous role in Hh signal-sending cells in the ovary and that diet-sensitive *mir-310*s are potent regulators of *Rab23* and its downstream trafficking events. Interestingly, *Drosophila* and human Rab23 are highly evolutionarily conserved (with 59% protein sequence homology) and human *Rab23* is a putative target for the human *mir-310*s orthologs *mir-25*, *mir-32*, *mir-92a/b/c*, *mir-363*, and *mir-367* (Enright *et al.* 2003; Kheradpour *et al.* 2007; Betel *et al.* 2008). miRNA-based control of conserved pathways is also generally conserved between species, implying that their regulatory role could have ancient origins. Therefore it will be important to test whether human *Rab23* is regulated via miRNAs as well.

In addition, Rab23 (Wang *et al.* 2012) and the COPI complex (Beller *et al.* 2008) have been shown to play a role in lipid homeostasis by affecting lipid droplet size, and the COPI complex also takes part in cholesterol-modified Hh ligand release (Lum *et al.* 2003; Nybakken *et al.* 2005; Aikin *et al.* 2012). Together, our data show that miRNAs can fine tune cell signaling to tailor adult oogenesis to changing dietary conditions. Since miRNAs usually are capable of targeting multiple genes, components of the Hh signaling are not the only *mir-310*s targets. At least in the male germline stem cell niche, a *Drosophila* homolog of vertebrate *beta-catenin*, *arm* is a *bona fide mir-310*s target, and *mir-310*s deficiency has an effect on male fertility (Pancratov *et al.* 2013). Arm is not only a major cell adhesion protein that is involved in homophilic cell adhesion via its binding to cadherins, but also it is the major transcription factor involved in Wingless (Wg) signaling (Wodarz *et al.* 2006; Somorjai and Martinez-Arias 2008). Recently we found that Wg signaling acts in the germline to regulate the efficiency of germline stem cell progeny differentiation (Konig and Shcherbata 2015). At the same time, the strength of the homophilic cell adhesion between the germline and the soma regulates Wg signaling. Thus, somatic cells communicate to the germline via cell adhesion (Cadherin–Arm complexes), adjusting the speed of germline differentiation (Konig and Shcherbata 2015). Therefore, amounts of Arm available either for cell adhesion or Wg signaling have a profound effect on oogenesis progression. Since the *mir-310*s expression in the GSC niche and differentiation niche cells is very dynamic and depends on dietary fluctuations, it would be interesting to study whether the diet-dependent *mir-310*s could also be involved in regulation of GSC progeny differentiation via targeting of *arm* levels (Figure 7). This *mir-310*s-mediated soma–germline communication mechanism (the *mir-310*s-regulating *arm*) could additionally be used to coordinate the speed of oogenesis with the nutritional status of the whole organism. Theoretically, the simultaneous management of different signaling pathways via the same miRNAs may aid in coordinating the stress response. In particular, modification of vital cell signaling via miRNAs in response to dietary changes might be commonly implicated in the process of adapting egg production to dietary conditions to ensure sufficient progeny survival.

Acknowledgments

We thank Eric Lai, Frank Hirth, Christian Bökel, Wu-Min Deng, Todd Nystul, Acaimo González-Reyes, Josef Mihaly, and Matthias Selbach for flies and reagents, Philip Hehlert and Ronald Kühnlein for help in CCA, Travis Carney for critical reading and comments on the manuscript, and the Jäckle and Shcherbata labs for discussions. This work was supported by the Max Planck Society.

Author contributions: I.Ö.Ç. and H.R.S. contributed research design, data acquisition, analysis and interpretation, manuscript draft, and figure design; M.B. and S.E., generation of *Rab23*::*YFP*::*4xmyc* line; and S.K. and H.U., proteomic analysis by mass spectrometry. The authors declare no competing financial interests.

Literature Cited

Aikin, R., A. Cervantes, G. D'Angelo, L. Ruel, S. Lacas-Gervais *et al.*, 2012 A genome-wide RNAi screen identifies regulators of cholesterol-modified hedgehog secretion in Drosophila. PLoS One 7: e33665.

Al-Anzi, B., E. Armand, P. Nagamei, M. Olszewski, V. Sapin *et al.*, 2010 The leucokinin pathway and its neurons regulate meal size in Drosophila. Curr. Biol. 20: 969–978.

Barrio, L., A. Dekanty, and M. Milan, 2014 MicroRNA-mediated regulation of Dp53 in the Drosophila fat body contributes to metabolic adaptation to nutrient deprivation. Cell Reports 8: 528–541.

Beller, M., C. Sztalryd, N. Southall, M. Bell, H. Jackle *et al.*, 2008 COPI complex is a regulator of lipid homeostasis. PLoS Biol. 6: e292.

Besse, F., D. Busson, and A.-M. Pret, 2002 Fused-dependent Hedgehog signal transduction is required for somatic cell differentiation during Drosophila egg chamber formation. Development 129: 4111–4124.

Betel, D., M. Wilson, A. Gabow, D. S. Marks, and C. Sander, 2008 The microRNA.org resource: targets and expression. Nucleic Acids Res. 36: D149–D153.

Bhattacharyya, S. N., R. Habermacher, U. Martine, E. I. Closs, and W. Filipowicz, 2006 Relief of microRNA-mediated translational repression in human cells subjected to stress. Cell 125: 1111–1124.

Bujold, M., A. Gopalakrishnan, E. Nally, and K. King-Jones, 2010 Nuclear receptor DHR96 acts as a sentinel for low cholesterol concentrations in Drosophila melanogaster. Mol. Cell. Biol. 30: 793–805.

Chan, C. C., S. Scoggin, D. Wang, S. Cherry, T. Dembo *et al.*, 2011 Systematic discovery of Rab GTPases with synaptic functions in Drosophila. Curr. Biol. 21: 1704–1715.

Chang, Y. C., A. C. Jang, C. H. Lin, and D. J. Montell, 2013 Castor is required for Hedgehog-dependent cell-fate specification and follicle stem cell maintenance in Drosophila oogenesis. Proc. Natl. Acad. Sci. USA 110: E1734–E1742.

Daniel, M., and T. O. Tollefsbol, 2015 Epigenetic linkage of aging, cancer and nutrition. J. Exp. Biol. 218: 59–70.

Drummond-Barbosa, D., and A. C. Spradling, 2001 Stem cells and their progeny respond to nutritional changes during Drosophila oogenesis. Dev. Biol. 231: 265–278.

Edeleva, E. V., and H. R. Shcherbata, 2013 Stress-induced ECM alteration modulates cellular microRNAs that feedback to readjust the extracellular environment and cell behavior. Front. Genet. 4: 305.

Edgecomb, R. S., C. E. Harth, and A. M. Schneiderman, 1994 Regulation of feeding behavior in adult Drosophila melanogaster varies with feeding regime and nutritional state. J. Exp. Biol. 197: 215–235.

Efeyan, A., W. C. Comb, and D. M. Sabatini, 2015 Nutrient-sensing mechanisms and pathways. Nature 517: 302–310.

Eggenschwiler, J. T., E. Espinoza, and K. V. Anderson, 2001 Rab23 is an essential negative regulator of the mouse Sonic hedgehog signalling pathway. Nature 412: 194–198.

Enright, A. J., B. John, U. Gaul, T. Tuschl, C. Sander *et al.*, 2003 MicroRNA targets in Drosophila. Genome Biol. 5: R1.

Evans, T. M., C. Ferguson, B. J. Wainwright, R. G. Parton, and C. Wicking, 2003 Rab23, a negative regulator of hedgehog signaling, localizes to the plasma membrane and the endocytic pathway. Traffic 4: 869–884.

Fagegaltier, D., A. Konig, A. Gordon, E. C. Lai, T. R. Gingeras *et al.*, 2014 A genome-wide survey of sexually dimorphic expression of *Drosophila* miRNAs identifies the steroid hormone-induced miRNA let-7 as a regulator of sexual identity. Genetics 198: 647–668.

Farhadian, S. F., M. Suarez-Farinas, C. E. Cho, M. Pellegrino, and L. B. Vosshall, 2012 Post-fasting olfactory, transcriptional, and feeding responses in Drosophila. Physiol. Behav. 105: 544–553.

Forbes, A. J., H. Lin, P. W. Ingham, and A. C. Spradling, 1996a hedgehog is required for the proliferation and specification of ovarian somatic cells prior to egg chamber formation in Drosophila. Development 122: 1125–1135.

Forbes, A. J., A. C. Spradling, P. W. Ingham, and H. Lin, 1996b The role of segment polarity genes during early oogenesis in Drosophila. Development 122: 3283–3294.

Franceschini, A., D. Szklarczyk, S. Frankild, M. Kuhn, M. Simonovic *et al.*, 2013 STRING v9.1: protein-protein interaction networks, with increased coverage and integration. Nucleic Acids Res. 41: D808–D815.

Gilboa, L., and R. Lehmann, 2006 Soma-germline interactions coordinate homeostasis and growth in the Drosophila gonad. Nature 443: 97–100.

Hartman, T. R., D. Zinshteyn, H. K. Schofield, E. Nicolas, A. Okada *et al.*, 2010 Drosophila Boi limits Hedgehog levels to suppress follicle stem cell proliferation. J. Cell Biol. 191: 943–952.

Hartman, T. R., T. I. Strochlic, Y. Ji, D. Zinshteyn, and A. M. O'Reilly, 2013 Diet controls Drosophila follicle stem cell proliferation via Hedgehog sequestration and release. J. Cell Biol. 201: 741–757.

Horner, M. A., K. Pardee, S. Liu, K. King-Jones, G. Lajoie *et al.*, 2009 The Drosophila DHR96 nuclear receptor binds cholesterol and regulates cholesterol homeostasis. Genes Dev. 23: 2711–2716.

Hornstein, E., and N. Shomron, 2006 Canalization of development by microRNAs. Nat. Genet. 38(Suppl): S20–S24.

Kheradpour, P., A. Stark, S. Roy, and M. Kellis, 2007 Reliable prediction of regulator targets using 12 Drosophila genomes. Genome Res. 17: 1919–1931.

Konig, A., and H. R. Shcherbata, 2015 Soma influences GSC progeny differentiation via the cell adhesion-mediated steroid-let-7-Wingless signaling cascade that regulates chromatin dynamics. Biol. Open 4: 285–300.

Konig, A., A. S. Yatsenko, M. Weiss, and H. R. Shcherbata, 2011 Ecdysteroids affect Drosophila ovarian stem cell niche formation and early germline differentiation. EMBO J. 30: 1549–1562.

Kuhnlein, R. P., 2011 The contribution of the Drosophila model to lipid droplet research. Prog. Lipid Res. 50: 348–356.

Lai, E. C., 2015 Two decades of miRNA biology: lessons and challenges. RNA 21: 675–677.

Lemaitre, B., and I. Miguel-Aliaga, 2013 The digestive tract of Drosophila melanogaster. Annu. Rev. Genet. 47: 377–404.

Leung, A. K., and P. A. Sharp, 2010 MicroRNA functions in stress responses. Mol. Cell 40: 205–215.

Lum, L., S. Yao, B. Mozer, A. Rovescalli, D. Von Kessler *et al.*, 2003 Identification of Hedgehog pathway components by RNAi in Drosophila cultured cells. Science 299: 2039–2045.

Marrone, A. K., E. V. Edeleva, M. M. Kucherenko, N. H. Hsiao, and H. R. Shcherbata, 2012 Dg-Dys-Syn1 signaling in Drosophila regulates the microRNA profile. BMC Cell Biol. 13: 26.

Masek, P., L. A. Reynolds, W. L. Bollinger, C. Moody, A. Mehta *et al.*, 2014 Altered regulation of sleep and feeding contributes to starvation resistance in Drosophila melanogaster. J. Exp. Biol. 217: 3122–3132.

Mendell, J. T., and E. N. Olson, 2012 MicroRNAs in stress signaling and human disease. Cell 148: 1172–1187.

Morrison, S. J., and A. C. Spradling, 2008 Stem cells and niches: mechanisms that promote stem cell maintenance throughout life. Cell 132: 598–611.

Musselman, L. P., J. L. Fink, K. Narzinski, P. V. Ramachandran, S. S. Hathiramani *et al.*, 2011 A high-sugar diet produces obesity and insulin resistance in wild-type Drosophila. Dis. Model. Mech. 4: 842–849.

Nybakken, K., S. A. Vokes, T. Y. Lin, A. P. McMahon, and N. Perrimon, 2005 A genome-wide RNA interference screen in Drosophila melanogaster cells for new components of the Hh signaling pathway. Nat. Genet. 37: 1323–1332.

Nystul, T., and A. Spradling, 2007 An epithelial niche in the Drosophila ovary undergoes long-range stem cell replacement. Cell Stem Cell 1: 277–285.

O'Reilly, A. M., H. H. Lee, and M. A. Simon, 2008 Integrins control the positioning and proliferation of follicle stem cells in the Drosophila ovary. J. Cell Biol. 182: 801–815.

Panakova, D., H. Sprong, E. Marois, C. Thiele, and S. Eaton, 2005 Lipoprotein particles are required for Hedgehog and Wingless signalling. Nature 435: 58–65.

Pancratov, R., F. Peng, P. Smibert, S. Yang, Jr., E. R. Olson *et al.*, 2013 The miR-310/13 cluster antagonizes beta-catenin function in the regulation of germ and somatic cell differentiation in the Drosophila testis. Development 140: 2904–2916.

Pataki, C., T. Matusek, E. Kurucz, I. Ando, A. Jenny *et al.*, 2010 *Drosophila* Rab23 is involved in the regulation of the number and planar polarization of the adult cuticular hairs. Genetics 184: 1051–1065.

Piper, M. D., E. Blanc, R. Leitao-Goncalves, M. Yang, X. He *et al.*, 2014 A holidic medium for Drosophila melanogaster. Nat. Methods 11: 100–105.

Pospisilik, J. A., D. Schramek, H. Schnidar, S. J. Cronin, N. T. Nehme *et al.*, 2010 Drosophila genome-wide obesity screen reveals hedgehog as a determinant of brown *vs.* white adipose cell fate. Cell 140: 148–160.

Rojas-Rios, P., I. Guerrero, and A. Gonzalez-Reyes, 2012 Cytoneme-mediated delivery of hedgehog regulates the expression of bone morphogenetic proteins to maintain germline stem cells in Drosophila. PLoS Biol. 10: e1001298.

Ross, S. A., and C. D. Davis, 2011 MicroRNA, nutrition, and cancer prevention. Adv. Nutr. 2: 472–485.

Sahai-Hernandez, P., and T. G. Nystul, 2013 A dynamic population of stromal cells contributes to the follicle stem cell niche in the Drosophila ovary. Development 140: 4490–4498.

Sieber, M. H., and C. S. Thummel, 2012 Coordination of triacylglycerol and cholesterol homeostasis by DHR96 and the Drosophila LipA homolog magro. Cell Metab. 15: 122–127.

Siegal, M. L., and A. Bergman, 2002 Waddington's canalization revisited: developmental stability and evolution. Proc. Natl. Acad. Sci. USA 99: 10528–10532.

Somorjai, I. M., and A. Martinez-Arias, 2008 Wingless signalling alters the levels, subcellular distribution and dynamics of Armadillo and E-cadherin in third instar larval wing imaginal discs. PLoS One 3: e2893.

Song, X., and T. Xie, 2002 DE-cadherin-mediated cell adhesion is essential for maintaining somatic stem cells in the Drosophila ovary. Proc. Natl. Acad. Sci. USA 99: 14813–14818.

Sun, J., and W. M. Deng, 2007 Hindsight mediates the role of notch in suppressing hedgehog signaling and cell proliferation. Dev. Cell 12: 431–442.

Sury, M. D., J. X. Chen, and M. Selbach, 2010 The SILAC fly allows for accurate protein quantification in vivo. Mol. Cell. Proteomics 9: 2173–2183.

Teleman, A. A., S. Maitra, and S. M. Cohen, 2006 Drosophila lacking microRNA miR-278 are defective in energy homeostasis. Genes Dev. 20: 417–422.

Timmons, L., J. Becker, P. Barthmaier, C. Fyrberg, A. Shearn *et al.*, 1997 Green fluorescent protein/beta-galactosidase double reporters for visualizing Drosophila gene expression patterns. Dev. Genet. 20: 338–347.

Tsurudome, K., K. Tsang, E. H. Liao, R. Ball, J. Penney *et al.*, 2010 The Drosophila miR-310 cluster negatively regulates synaptic strength at the neuromuscular junction. Neuron 68: 879–893.

Tworoger, M., M. K. Larkin, Z. Bryant, and H. Ruohola-Baker, 1999 Mosaic analysis in the drosophila ovary reveals a common hedgehog-inducible precursor stage for stalk and polar cells. Genetics 151: 739–748.

UniProt Consortium, 2014 Activities at the Universal Protein Resource (UniProt). Nucleic Acids Res. 42: D191–D198.

Wang, C., Z. Liu, and X. Huang, 2012 Rab32 is important for autophagy and lipid storage in Drosophila. PLoS One 7: e32086.

Wei, Y., and M. A. Lilly, 2014 The TORC1 inhibitors Nprl2 and Nprl3 mediate an adaptive response to amino-acid starvation in Drosophila. Cell Death Differ. 21: 1460–1468.

Wodarz, A., D. B. Stewart, W. J. Nelson, and R. Nusse, 2006 Wingless signaling modulates cadherin-mediated cell adhesion in Drosophila imaginal disc cells. J. Cell Sci. 119: 2425–2434.

Xu, P., S. Y. Vernooy, M. Guo, and B. A. Hay, 2003 The Drosophila microRNA Mir-14 suppresses cell death and is required for normal fat metabolism. Curr. Biol. 13: 790–795.

Yatsenko, A. S., and H. R. Shcherbata, 2014 Drosophila miR-9a targets the ECM receptor Dystroglycan to canalize myotendinous junction formation. Dev. Cell 28: 335–348.

Yatsenko, A. S., A. K. Marrone, and H. R. Shcherbata, 2014 miRNA-based buffering of the cobblestone-lissencephaly-associated extracellular matrix receptor dystroglycan via its alternative 3′-UTR. Nat. Commun. 5: 4906.

Zerial, M., and H. McBride, 2001 Rab proteins as membrane organizers. Nat. Rev. Mol. Cell Biol. 2: 107–117.

Zhang, J., K. L. Schulze, P. R. Hiesinger, K. Suyama, S. Wang *et al.*, 2007 Thirty-one flavors of *Drosophila* rab proteins. Genetics 176: 1307–1322.

Zhang, Y., and D. Kalderon, 2001 Hedgehog acts as a somatic stem cell factor in the Drosophila ovary. Nature 410: 599–604.

Communicating editor: H. J. Bellen

GENETICS

Supporting Information
www.genetics.org/lookup/suppl/doi:10.1534/genetics.115.185371/-/DC1

Hedgehog Signaling Strength Is Orchestrated by the *mir-310* Cluster of MicroRNAs in Response to Diet

Ibrahim Ömer Çiçek, Samir Karaca, Marko Brankatschk, Suzanne Eaton, Henning Urlaub, and Halyna R. Shcherbata

DOI: 10.1534/genetics.115.185371

Supplemental Information

Hedgehog signaling strength is orchestrated by the *mir-310* cluster of microRNAs in response to diet

Ibrahim Ömer Çiçek[1], Samir Karaca[2], Marko Brankatschk[3], Suzanne Eaton[3], Henning Urlaub[2], and Halyna R. Shcherbata[1]*

[1] Max Planck Research Group of Gene Expression and Signaling, Max Planck Institute for Biophysical Chemistry, Am Fassberg 11, 37077, Göttingen, Germany

[2] Bioanalytical Mass Spectrometry Research Group**,** Max Planck Institute for Biophysical Chemistry, Am Fassberg 11, 37077, Göttingen, Germany

[3] Max Planck Institute of Molecular Cell Biology and Genetics, Pfotenhauerstrasse 108, 01307, Dresden, Germany

*corresponding author: halyna.shcherbata@mpibpc.mpg.de

Running title: upon diet, miRNAs modulate Hh signaling

Keywords: *Drosophila*; oogenesis; follicle stem cell; Hedgehog signaling; miRNA; the *mir-310s*; *Rab23*; dietary restriction; metabolic stress; Hh ligand

Supplemental Figures

Figure S1

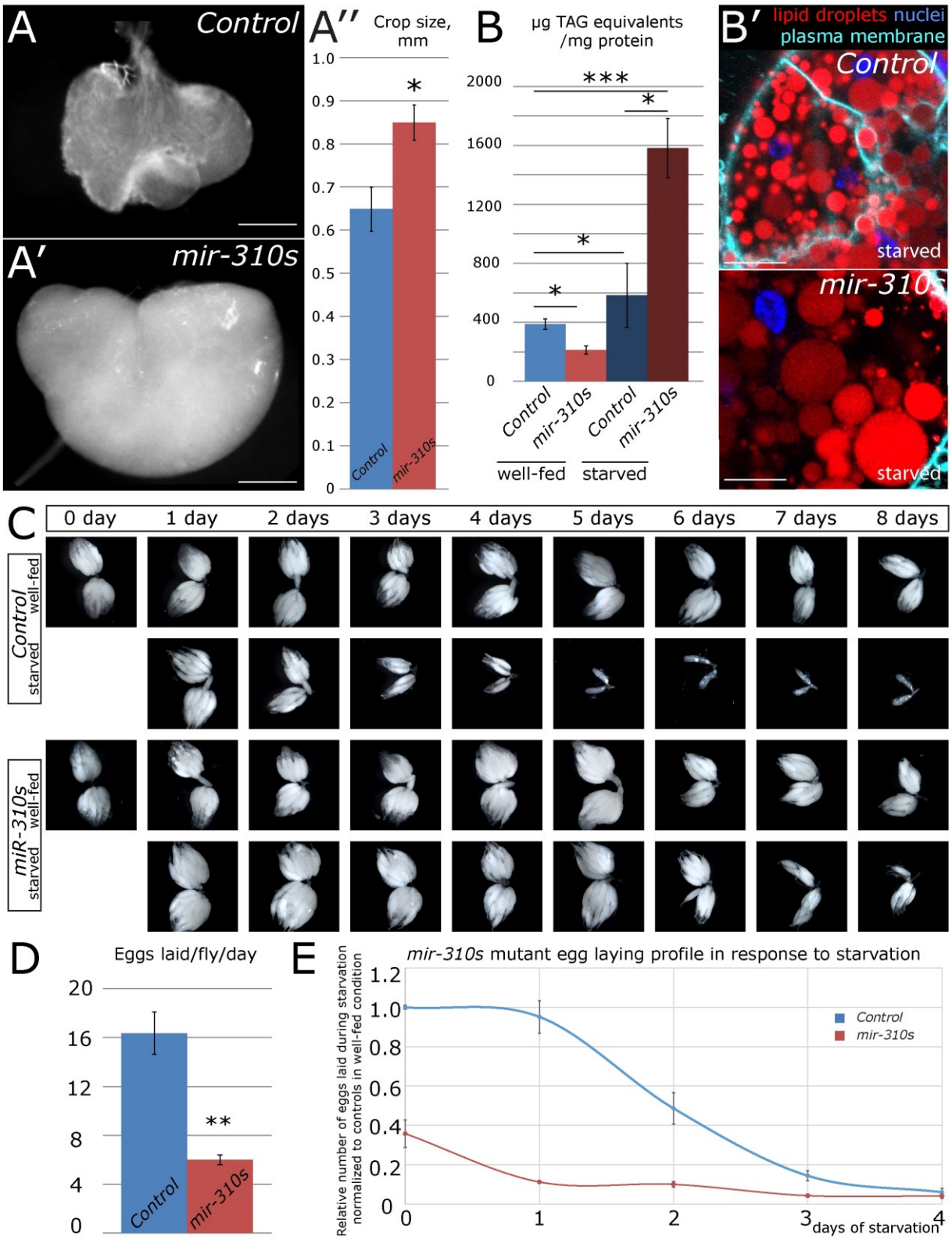

Figure S1. The *mir-310s* mutant female ovaries respond to protein starvation abnormally

(A, A`) Bright field images of control (w^{1118}) and *mir-310s* mutant (*KT40/KT40*) crops dissected from comparably sized females kept under normal conditions. Note the enlarged crop size of *mir-310s* mutant females (A``) (Table S3).

(B) *mir-310s* mutant females have abnormal energy metabolism as measured by the total body fat. However, upon nutritional restriction for 10 days, *mir-310s* mutants accumulate ~2.5-fold more lipids and larger lipid droplets than controls (B`) (Table S3).

(C) In response to nutritional restriction, control females cease egg production after day 4. *mir-310s* mutant ovaries contain substantial amounts of late egg chambers even after 7-8 days of nutritional restriction (Table S3). *mir-310s* loss-of-function mutants, similarly to *hh* (*tub-Gal80^{ts}/+; bab1-Gal4/UAS-hh* at 29°C) and *Rab23* (*bab1-Gal4/UAS-Rab23*) overexpression (data not shown), demonstrate a delayed cessation of egg chamber production after stage 6 in response to starvation.

(D) Note that even under well-fed condition, *mir-310s* mutant females lay significantly fewer eggs than controls (Table S3).

(E) Egg laying profiles for control and *mir-310s* mutant females (Table S3).

In (A``), (B), (D), and (E) the data points indicate AVE±SEM (Table S3). Significances were calculated using two-tailed Student's t-test. *p<0.05, **p<0.005, ***p<0.0005. Scale bar represents 250μm in (A, A`) and 20μm in B`.

Supplemental Tables

Table S1, related to Figure 1. Proteins significantly deregulated in *mir-310s* mutants

CG number	Gene name
Energy metabolism	
CG10924	CG10924
CG11594	CG11594
CG17530	GstE6
CG2827	Tal
CG30360	**Mal-A6**
CG31692	fbp
CG33138	CG33138
CG3763	Fbp2
CG4178	Lsp1beta
CG5177	CG5177
CG6806	Lsp2
CG8036	CG8036
CG8094	Hex-C
CG8696	**LvpH**
CG9092	Gal
CG9232	Galt
Lipid metabolism	
CG10622	Sucb
CG10932	CG10932
CG11064	Rfabg
CG11129	Yp3
CG11198	ACC
CG15828	Apoltp
CG1648	CG1648
CG1742	Mgstl
CG18212	**alt**
CG2979	Yp2
CG2985	Yp1
CG3050	**Cyp6d5**
CG31150	crossveinless d
CG3481	Adh
CG3523	CG3523
CG3524	v(2)k05816
CG3699	EG:BACR7A4.14
CG3752	Aldh
CG4581	Thiolase
CG4729	CG4729
CG5170	**Dp1**
CG5590	CG5590
CG5885	CG5885
CG5958	CG5958
CG7400	**Fatp**
CG8256	Gpo-1
CG8628	CG8628
CG8778	CG8778
CG9035	Tapdelta
CG9412	**rin**
CG9577	**CG9577**
CG9914	CG9914
Protein homeostasis	
CG10236	LanA
CG10302	bsf
CG10686	tral
CG11512	GstD4
CG11899	CG11899
CG12163	CG12163
CG13393	lethal (2) k12914
CG14715	CG14715
CG15261	UK114
CG15369	CG15369
CG2852	CG2852
CG3011	CG3011
CG31198	CG31198
CG31343	CG5839
CG33103	Ppn
CG3926	Spat
CG3949	hoip
CG3999	CG3999
CG4067	pug
CG4181	GstD2
CG4463	Hsp23
CG4659	Srp54k
CG4916	me31B
CG4954	eIF3-S8
CG5064	Srp68
CG5330	Nap1
CG5394	Aats-glupro
CG5474	SsRbeta
CG5839	CG31233
CG6287	CG6287
CG6370	CG6370
CG6512	CG6512
CG6781	se
CG6950	CG6950
CG7014	RpS5b
CG7637	CG7637
CG8396	Ssb-c31a
CG8431	Aats-cys
CG8858	CG8858
CG8938	GstS1
CG9012	Chc
CG9423	**Kap-alpha3**
CG9539	**Sec61alpha**
CG9805	eIF3-S10
CG9842	**Pp2B-14D**
CG9897	CG9897
Mitochondria	
CG3902	CG3902
CG10340	CG10340
CG12203	CG12203
CG12079	CG12079
CG12151	Pdp
CG14757	CG14757
CG16944	sesB
CG2286	ND75
CG32531	mRpS14
CG3283	SdhB
CG34073	mt:ATPase6
CG3566	CG3566
CG4169	CG4169
CG4769	CG4769
CG5670	**Atpalpha**
CG5889	Men-b
CG6022	Cchl
CG6455	CG6455
CG6612	Adk3
CG6647	**porin**

CG6666	SdhC
CG6782	**sea**
CG6878	**CG6878**
CG7580	CG7580
CG7610	ATPsyn-gamma
CG8479	opa1-like
CG8790	Dic1
CG8844	Pdsw
CG9090	CG9090
Nucleotide synthesis	
CG11089	CG11089
CG16758	CG16758
CG18572	r
CG2194	su(r)
CG31628	ade3
CG3989	ade5
CG4584	dUTPase
CG7917	Nlp
CG8132	CG8132
CG9127	ade2
CG9193	mus209
CG9242	bur
CG9674	CG9674
Muscle	
CG10067	Act57B
CG1106	Gel
CG11949	cora
CG12408	TpnC4
CG15792	zip
CG17927	Mhc
CG17927	MHC isoforms
CG18290	Act87E
CG2184	Mlc2
CG2981	**TpnC41C**
CG4183	Hsp26
CG4466	Hsp27
CG4843	Tm2
CG4898	**Tm1**
CG5125	ninaC
CG5178	Act88F
CG5596	Mlc1
CG7107	up
CG7178	wupA
CG7445	**fln**
CG7478	Act79B
CG7930	TpnC73F
CG9138	**uif**
CG9432	l(2)01289
CG9480	Glycogenin
Neural	
CG11797	Obp56a
CG12202	Nat1
CG12908	Ndg
CG15457	Obp19c
CG1618	comt
CG1634	Nrg
CG17029	CG17029
CG1744	chp
CG17870	**14-3-3zeta**
CG18102	shi
CG18111	Obp99a
CG1873	Ef1alpha100E
CG1977	alpha-Spec
CG2028	CkIalpha
CG2297	Obp44a
CG30021	metro
CG32234	axo
CG33950	trol
CG3620	norpA
CG3725	Ca-P60A, CG3725
CG3747	Eaat1
CG43079	nrm
CG4609	fax
CG5119	pAbp
CG5711	Arr1
CG5779	proPO-A1
CG5779	proPo
CG5870	beta-Spec
CG7088	bnb
CG7576	Rab3
CG7592	Obp99b
CG8462	**Obp56e**
CG8663	nrv3
CG9206	Gl
CG9261	Nrv2
Cuticle	
CG10112	Cpr51A
CG10287	Gasp
CG12045	Cpr100A
CG17052	obst-A
CG1919	Cpr62Bc
CG3244	Clect27
CG4475	CG4475
CG4784	Cpr72Ec
CG7532	l(2)34Fc
CG8505	Cpr49Ae
CG8511	Cpr49Ag
CG9079	Cpr47Ea
Histone	
CG10638	CG10638
CG11765	Prx2540-2
CG12171	CG12171
CG12405	Prx2540-1
CG12896	CG12896
CG18547	CG18547
CG1982	Sodh-1
CG3609	CG3609
CG3835	EG:87B1.3
CG6084	CG6084
CG6776	GStO3
CG6776	CG6776
CG7322	CG7322
CG8503	CG8503
CG9119	CG9119
CG9331	CG9331
His2B	His2B
His4	His4
No association	
CG12008	kst
CG10031	CG10031
CG10527	CG10527
CG10691	l(2)37Cc
CG10978	jagn
CG11785	bai
CG11920	CG11920
CG11999	CG11999
CG12403	Vha68-1
CG14168	Zasp67
CG1444	CG1444
CG1462	Aph-4
CG14661	CG14661
CG15081	l(2)03709
CG15881	**CG15881**
CG16884	BG:DS00180.3
CG16985	CG16985
CG18591	SmE

CG1885	CG1885
CG2082	CG2082
CG2216	Fer1HCH
CG2233	**CG2233**
CG2310	CG2310
CG2943	CG2943
CG30222	**CG30222**
CG3082	l(2)k09913
CG31195	CG31195

CG34026	CG34026
CG34215	CG34215
CG42314	PMCA
CG4239	CG4239
CG5945	CG5945
CG6214	MRP
CG6544	fau
CG6702	Cbp53E
CG6815	bor

CG6851	Mtch
CG6917	Est-6
CG6950	CG6950
CG7646	CG7646
CG8108	CG8108
CG8790	CG8790
CG9297	CG9297

Putative *mir-310s* target

Table S2, related to Figure 1. Relative mRNA expression levels of the starvation-sensitive genes upon *mir-310s* deficit and/or nutritional stress

Genotype/ Condition	Target Gene	C_T AVE±SEM[b]	ΔC_T AVE±SEM[b]	$\Delta\Delta C_T$ AVE±SEM[b]	Relative mRNA level[a,c] AVE± SEM[b]	log_{10} Relative mRNA level AVE± SEM[b]
Plate 1						
Control (w^{1118}) well-fed	*Act88F*	2.76E+01 ±5.57E-02	9.47 ±6.27E-02	3.18E-07 ±5.57E-02	1.00 ±3.80E-02	-9.57E-08 ±1.68E-02
Control (w^{1118}) starved		2.16E+01 ±1.79E-02	3.58 ±2.69E-02	-5.88 ±1.79E-02	5.90E+01 ±7.30E-01 $p^{Control\ well\text{-}fed}$=1.52E-07	1.77 ±5.38E-03
mir-310s (KT40/KT40) well-fed		2.50E+01 ±3.11E-02	6.45 ±4.29E-02	-3.02 ±3.11E-02	8.09 ±1.73E-01 $p^{Control\ well\text{-}fed}$=2.30E-06	9.08E-01 ±9.37E-03
mir-310s (KT40/KT40) starved		2.40E+01 ±9.20E-03	5.79 ±1.19E-02	-3.68 ±9.20E-03	1.28E+01 ±8.18E-02 $p^{Control\ well\text{-}fed}$=2.05E-08	1.11 ±2.77E-03
Control (w^{1118}) well-fed	*ade2*	2.29E+01 ±3.16E-02	4.70 ±4.28E-02	1.59E-07 ±3.16E-02	1.00 ±2.18E-02	-4.78E-08 ±9.52E-03
Control (w^{1118}) starved		2.32E+01 ±4.70E-02	5.17 ±5.12E-02	4.65E-01 ±4.70E-02	7.25E-01 ±2.35E-02 $p^{Control\ well\text{-}fed}$=1.01E-03	-1.40E-01 ±1.42E-02
mir-310s (KT40/KT40) well-fed		2.19E+01 ±2.31E-02	3.32 ±3.75E-02	-1.38 ±2.31E-02	2.61 ±4.15E-02 $p^{Control\ well\text{-}fed}$=4.30E-06	4.16E-01 ±6.95E-03
mir-310s (KT40/KT40) starved		2.25E+01 ±1.49E-02	4.36 ±1.67E-02	-3.45E-01 ±1.49E-02	1.27 ±1.32E-02 $p^{Control\ well\text{-}fed}$=4.48E-04	1.04E-01 ±4.49E-03
Control (w^{1118}) well-fed	*ade3*	2.34E+01 ±1.77E-02	5.21 ±3.38E-02	-1.59E-07 ±1.77E-02	1.00 ±1.22E-02	4.78E-08 ±5.33E-03
Control (w^{1118}) starved		2.49E+01 ±2.39E-02	6.91 ±3.13E-02	1.70 ±2.39E-02	3.09E-01 ±5.09E-03 $p^{Control\ well\text{-}fed}$=8.01E-07	-5.11E-01 ±7.19E-03
mir-310s (KT40/KT40) well-fed		2.27E+01 ±1.78E-02	4.15 ±3.45E-02	-1.06 ±1.78E-02	2.08 ±2.56E-02 $p^{Control\ well\text{-}fed}$=2.82E-06	3.18E-01 ±5.36E-03
mir-310s (KT40/KT40) starved		2.39E+01 ±2.81E-02	5.73 ±2.91E-02	5.16E-01 ±2.81E-02	6.99E-01 ±1.37E-02 $p^{Control\ well\text{-}fed}$=8.16E-05	-1.55E-01 ±8.46E-03
Control (w^{1118}) well-fed	*Arr1*	2.30E+01 ±9.35E-03	4.80 ±3.03E-02	0.00 ±9.35E-03	1.00 ±6.49E-03	0.00 ±2.82E-03
Control (w^{1118}) starved		2.03E+01 ±4.21E-02	2.27 ±4.67E-02	-1.83 ±7.03E-01	3.56 ±1.49 $p^{Control\ well\text{-}fed}$=4.02E-05	5.52E-01 ±1.27E-02
mir-310s (KT40/KT40) well-fed		2.28E+01 ±1.09E-01	4.27 ±1.13E-01	-9.41E-01 ±5.17E-01	1.92 ±8.63E-01 $p^{Control\ well\text{-}fed}$=2.35E-01	2.83E-01 ±1.56E-01
mir-310s (KT40/KT40) starved		2.14E+01 ±3.34E-02	3.19 ±3.43E-02	-8.18E-01 ±8.12E-01	1.76 ±8.43E-01 $p^{Control\ well\text{-}fed}$=2.11E-01	2.46E-01 ±2.44E-01
Control (w^{1118}) well-fed	*CG3699*	2.39E+01 ±5.05E-02	5.72 ±5.81E-02	-1.59E-07 ±5.05E-02	1.00 ±3.55E-02	4.78E-08 ±1.52E-02
Control (w^{1118}) starved		2.53E+01 ±2.82E-02	7.28 ±3.47E-02	1.56 ±2.82E-02	3.38E-01 ±6.55E-03 $p^{Control\ well\text{-}fed}$=5.16E-05	-4.71E-01 ±8.49E-03

mir-310s (KT40/KT40) well-fed		2.50E+01 ±7.56E-03	6.43 ±3.05E-02	7.14E-01 ±7.56E-03	6.09E-01 ±3.19E-03 $p^{Control\ well\text{-}fed}$=3.88E-04	-2.15E-01 ±2.28E-03
mir-310s (KT40/KT40) starved		2.52E+01 ±7.45E-03	7.03 ±1.06E-02	1.31 ±7.45E-03	4.03E-01 ±2.08E-03 $p^{Control\ well\text{-}fed}$=7.28E-05	-3.95E-01 ±2.24E-03
Control (w^{1118}) well-fed	*CG3902*	2.29E+01 ±1.99E-03	4.78 ±2.89E-02	1.59E-07 ±1.99E-03	1.00 ±1.38E-03	-4.78E-08 ±5.99E-04
Control (w^{1118}) starved		2.43E+01 ±2.56E-02	6.32 ±3.26E-02	1.54 ±2.56E-02	3.44E-01 ±6.17E-03 $p^{Control\ well\text{-}fed}$=5.18E-08	-4.63E-01 ±7.72E-03
mir-310s (KT40/KT40) well-fed		2.26E+01 ±1.72E-02	4.04 ±3.41E-02	-7.34E-01 ±1.72E-02	1.66 ±1.98E-02 $p^{Control\ well\text{-}fed}$=4.79E-06	2.21E-01 ±5.16E-03
mir-310s (KT40/KT40) starved		2.33E+01 ±1.23E-02	5.18 ±1.45E-02	3.97E-01 ±1.23E-02	7.60E-01 ±6.46E-03 $p^{Control\ well\text{-}fed}$=3.42E-06	-1.19E-01 ±3.71E-03
Control (w^{1118}) well-fed	*Rpl32*	1.82E+01 ±2.88E-02	0.00 ±2.88E-02			
Control (w^{1118}) starved		1.80E+01 ±2.02E-02	6.36E-07 ±2.02E-02			
mir-310s (KT40/KT40) well-fed		1.86E+01 ±2.95E-02	1.91E-06 ±2.95E-02			
mir-310s (KT40/KT40) starved		1.82E+01 ±7.58E-03	6.36E-07 ±7.58E-03			
No Reverse Transcriptase						
Control (w^{1118}) well-fed	*Rpl32*	3.34E+01 ±2.44E-01	1.53E+01 ±2.44E-01	1.53E+01 ±2.44E-01	2.53E-05 ±4.68E-06	-4.60 ±7.35E-02
Control (w^{1118}) starved		3.30E+01 ±2.87E-01	1.50E+01 ±2.87E-01	1.50E+01 ±2.87E-01	3.06E-05 ±5.89E-06	-4.51 ±8.65E-02
mir-310s (KT40/KT40) well-fed		3.28E+01 ±1.09E-01	1.43E+01 ±1.09E-01	1.43E+01 ±1.09E-01	5.06E-05 ±3.98E-06	-4.30 ±3.29E-02
mir-310s (KT40/KT40) starved		3.37E+01 ±1.36E-01	1.56E+01 ±1.36E-01	1.56E+01 ±1.36E-01	2.08E-05 ±1.95E-06	-4.68 4.10E-02
Plate 2						
Control (w^{1118}) well-fed	*CG3999*	2.69E+01 ±1.07E-02	9.08 ±2.33E-02	-6.36E-07 ±1.07E-02	1.00 ±7.44E-03	1.91E-07 ±3.22E-03
Control (w^{1118}) starved		2.85E+01 ±2.78E-02	1.08E+01 ±2.98E-02	1.72 ±2.78E-02	3.04E-01 ±5.90E-03 $p^{Control\ well\text{-}fed}$=2.08E-07	-5.17E-01 ±8.36E-03
mir-310s (KT40/KT40) well-fed		2.68E+01 ±3.90E-02	8.55 ±4.82E-02	-5.30E-01 ±3.90E-02	1.44 ±3.95E-02 $p^{Control\ well\text{-}fed}$=3.79E-04	1.60E-01 ±1.17E-02
mir-310s (KT40/KT40) starved		2.76E+01 ±4.55E-02	9.69 ±4.81E-02	6.09E-01 ±4.55E-02	6.56E-01 ±2.10E-02 $p^{Control\ well\text{-}fed}$=1.03E-04	-1.83E-01 ±1.37E-02
Control (w^{1118}) well-fed	*CG9914*	3.08E+01 ±4.14E-02	1.30E+01 ±4.63E-02	-9.54E-07 ±4.14E-02	1.00 ±2.83E-02	2.87E-07 ±1.25E-02
Control (w^{1118}) starved		3.19E+01 ±2.46E-02	1.42E+01 ±2.69E-02	1.20 ±2.46E-02	4.34E-01 ±7.41E-03 $p^{Control\ well\text{-}fed}$=4.19E-05	-3.62E-01 ±7.42E-03

mir-310s (KT40/KT40) well-fed		3.08E+01 ±2.57E-02	1.25E+01 ±3.83E-02	-4.46E-01 ±2.57E-02	1.36 ±2.44E-02 $p^{Control\ well\text{-}fed}$=6.35E-04	1.34E-01 ±7.74E-03
mir-310s (KT40/KT40) starved		3.06E+01 ±5.07E-02	1.27E+01 ±5.30E-02	-2.91E-01 ±5.07E-02	1.22 ±4.31E-02 $p^{Control\ well\text{-}fed}$=1.22E-02	8.76E-02 ±1.53E-02
Control (w^{1118}) well-fed	*CG11089*	2.22E+01 ±2.57E-02	4.41 ±3.30E-02	-7.95E-07 ±2.57E-02	1.00 ±1.80E-02	2.39E-07 ±7.73E-03
Control (w^{1118}) starved		2.30E+01 ±1.08E-02	5.33 ±1.54E-02	9.29E-01 ±1.08E-02	5.25E-01 ±3.96E-03 $p^{Control\ well\text{-}fed}$=1.33E-05	-2.80E-01 ±3.27E-03
mir-310s (KT40/KT40) well-fed		2.15E+01 ±9.71E-03	3.30 ±3.00E-02	-1.10 ±9.71E-03	2.15 ±1.44E-02 $p^{Control\ well\text{-}fed}$=9.64E-07	3.32E-01 ±2.92E-03
mir-310s (KT40/KT40) starved		2.30E+01 ±1.41E-02	5.10 ±2.10E-02	6.99E-01 ±1.41E-02	6.16E-01 ±6.07E-03 $p^{Control\ well\text{-}fed}$=3.49E-05	-2.10E-01 ±4.26E-03
Control (w^{1118}) well-fed	*CG15369*	3.29E+01 ±8.65E-03	1.51E+01 ±2.24E-02	-3.18E-07 ±8.65E-03	1.00 ±5.97E-03	9.57E-08 ±2.60E-03
Control (w^{1118}) starved		3.17E+01 ±1.71E-01	1.40E+01 ±1.72E-01	-1.12 ±1.71E-01	2.18 ±2.56E-01 $p^{Control\ well\text{-}fed}$=9.14E-03	3.38E-01 ±5.15E-02
mir-310s (KT40/KT40) well-fed		3.29E+01 ±8.31E-02	1.47E+01 ±8.78E-02	-4.16E-01 ±8.31E-02	1.33 ±7.67E-02 $p^{Control\ well\text{-}fed}$=1.17E-02	1.25E-01 ±2.50E-02
mir-310s (KT40/KT40) starved		3.11E+01 ±8.40E-02	1.32E+01 ±8.54E-02	-1.86 ±8.40E-02	3.64 ±2.06E-01 $p^{Control\ well\text{-}fed}$=2.12E-04	5.61E-01 ±2.53E-02
Control (w^{1118}) well-fed	*CG16884*	3.60E+01 ±1.55E-01	1.82E+01 ±1.57E-01	0.00 ±1.55E-01	1.00 ±1.03E-01	0.00 ±4.68E-02
Control (w^{1118}) starved		3.48E+01 ±6.19E-02	1.70E+01 ±6.29E-02	-1.13 ±6.19E-02	2.20 ±9.23E-02 $p^{Control\ well\text{-}fed}$=1.02E-03	3.41E-01 ±1.86E-02
mir-310s (KT40/KT40) well-fed		3.63E+01 ±5.23E-02	1.81E+01 ±5.95E-02	-8.92E-02 ±5.23E-02	1.06 ±3.80E-02 $p^{Control\ well\text{-}fed}$=6.50E-01	2.69E-02 ±1.57E-02
mir-310s (KT40/KT40) starved		3.49E+01 ±1.49E-01	1.71E+01 ±1.50E-01	-1.13 ±1.49E-01	2.18 ±2.27E-01 $p^{Control\ well\text{-}fed}$=8.67E-03	3.39E-01 ±4.48E-02
Control (w^{1118}) well-fed	*CG30360*	2.19E+01 ±1.06E-02	4.11 ±2.32E-02	-7.95E-07 ±1.06E-02	1.00 ±7.30E-03	2.39E-07 ±3.18E-03
Control (w^{1118}) starved		2.30E+01 ±1.63E-02	5.32 ±1.96E-02	1.22 ±1.63E-02	4.30E-01 ±4.86E-03 $p^{Control\ well\text{-}fed}$=3.35E-07	-3.67E-01 ±4.91E-03
mir-310s (KT40/KT40) well-fed		2.27E+01 ±1.47E-02	4.50 ±3.19E-02	3.92E-01 ±1.47E-02	7.62E-01 ±7.78E-03 $p^{Control\ well\text{-}fed}$=2.40E-05	-1.18E-01 ±4.41E-03
mir-310s (KT40/KT40) starved		2.34E+01 ±2.02E-02	5.52 ±2.55E-02	1.41 ±2.02E-02	3.76E-01 ±5.23E-03 $p^{Control\ well\text{-}fed}$=2.58E-07	-4.24E-01 ±6.08E-03
Control (w^{1118}) well-fed	*Rpl32*	1.78E+01 ±2.07E-02	-6.36E-07 ±2.07E-02			
Control (w^{1118}) starved		1.77E+01 ±1.09E-02	0.00 ±1.09E-02			
mir-310s (KT40/KT40) well-fed		1.82E+01 ±2.84E-02	-1.27E-06 ±2.84E-02			

mir-310s (KT40/KT40) starved		1.79E+01 ±1.55E-02	6.36E-07 ±1.55E-02			
No Reverse Transcriptase						
Control (w^{1118}) well-fed	*Rpl32*	3.28E+01 ±1.19E-01	1.50E+01 ±1.19E-01	1.50E+01 ±1.19E-01	3.07E-05 ±2.64E-06	-4.51 ±3.59E-02
Control (w^{1118}) starved		3.28E+01 ±1.03E-01	1.51E+01 ±1.03E-01	1.51E+01 ±1.03E-01	2.92E-05 ±2.16E-06	-4.53 ±3.10E-02
mir-310s (KT40/KT40) well-fed		3.22E+01 ±9.10E-02	1.40E+01 ±9.10E-02	1.40E+01 ±9.10E-02	6.13E-05 ±3.82E-06	-4.21 ±2.74E-02
mir-310s (KT40/KT40) starved		3.27E+01 ±2.33E-01	1.49E+01 ±2.33E-01	1.49E+01 ±2.33E-01	3.37E-05 ±5.94E-06	-4.47 ±7.00E-02
Plate 3						
Control (w^{1118}) well-fed	*CG31233*	2.54E+01 ±1.38E-02	7.51 ±2.92E-02	0.00 ±1.38E-02	1.00 ±9.53E-03	0.00 ±4.14E-03
Control (w^{1118}) starved		2.36E+01 ±1.64E-03	5.80 ±9.31E-03	-1.72 ±1.64E-03	3.29 ±3.73E-03 $p^{Control\ well\text{-}fed}$=2.41E-09	5.17E-01 ±4.93E-04
mir-310s (KT40/KT40) well-fed		2.59E+01 ±3.60E-02	7.76 ±1.04E-01	2.41E-01 ±3.60E-02	8.46E-01 ±2.13E-02 $p^{Control\ well\text{-}fed}$=2.79E-03	-7.25E-02 ±1.09E-02
mir-310s (KT40/KT40) starved		2.43E+01 ±1.91E-02	6.43 ±2.24E-02	-1.08 ±1.91E-02	2.12 ±2.82E-02 $p^{Control\ well\text{-}fed}$=2.96E-06	3.26E-01 ±5.74E-03
Control (w^{1118}) well-fed	*Cpr62Bc*	3.45E+01 ±7.64E-02	1.66E+01 ±8.06E-02	6.36E-07 ±7.64E-02	1.00 ±5.16E-02	-1.91E-07 ±2.30E-02
Control (w^{1118}) starved		3.15E+01 ±3.45E-02	1.37E+01 ±3.57E-02	-2.93 ±3.45E-02	7.64 ±1.84E-01 $p^{Control\ well\text{-}fed}$=4.10E-06	8.83E-01 ±1.04E-02
mir-310s (KT40/KT40) well-fed		3.20E+01 ±5.19E-02	1.38E+01 ±1.11E-01	-2.79 ±5.19E-02	6.90 ±2.46E-01 $p^{Control\ well\text{-}fed}$=1.94E-05	8.39E-01 ±1.56E-02
mir-310s (KT40/KT40) starved		3.01E+01 ±1.61E-02	1.23E+01 ±2.00E-02	-4.31 ±1.61E-02	1.98E+01 ±2.22E-01 $p^{Control\ well\text{-}fed}$=1.29E-07	1.30 ±4.84E-03
Control (w^{1118}) well-fed	*Cpr72Ec*	3.25E+01 ±8.92E-02	1.46E+01 ±9.28E-02	-3.18E-07 ±8.92E-02	1.00 ±6.37E-02	9.57E-08 ±2.68E-02
Control (w^{1118}) starved		3.29E+01 ±1.73E-02	1.51E+01 ±1.96E-02	5.13E-01 ±1.73E-02	7.01E-01 ±8.41E-03 $p^{Control\ well\text{-}fed}$=9.22E-03	-1.54E-01 ±5.22E-03
mir-310s (KT40/KT40) well-fed		2.80E+01 ±9.14E-03	9.84 ±9.80E-02	-4.76 ±9.14E-03	2.70E+01 ±1.71E-01 $p^{Control\ well\text{-}fed}$=1.46E-08	1.43 ±2.75E-03
mir-310s (KT40/KT40) starved		2.62E+01 ±3.01E-02	8.39 ±3.24E-02	-6.21 ±3.01E-02	7.40E+01 ±1.54 $p^{Control\ well\text{-}fed}$=1.19E-06	1.87 ±9.07E-03
Control (w^{1118}) well-fed	*Cpr100A*	3.18E+01 ±1.13E-01	1.39E+01 ±1.16E-01	0.00 ±1.13E-01	1.00 ±8.06E-02	0.00 ±3.41E-02
Control (w^{1118}) starved		2.79E+01 ±1.96E-02	1.01E+01 ±2.17E-02	-3.78 ±1.96E-02	1.38E+01 ±1.89E-01 $p^{Control\ well\text{-}fed}$=4.00E-07	1.14 ±5.91E-03
mir-310s (KT40/KT40) well-fed		2.78E+01 ±4.13E-02	9.63 ±1.06E-01	-4.27 ±4.13E-02	1.93E+01 ±5.45E-01 $p^{Control\ well\text{-}fed}$=4.90E-06	1.29 ±1.24E-02

mir-310s (KT40/KT40) starved		2.84E+01 ±3.03E-02	1.06E+01 ±3.25E-02	-3.31 ±3.03E-02	9.93 ±2.10E-01 $p^{Control\ well\text{-}fed}$=2.43E-06	9.97E-01 ±9.11E-03
Control (w^{1118}) well-fed	*Gal*	2.76E+01 ±6.26E-02	9.77 ±6.77E-02	-3.18E-07 ±6.26E-02	1.00 ±4.26E-02	9.57E-08 ±1.89E-02
Control (w^{1118}) starved		2.79E+01 ±4.60E-02	1.01E+01 ±4.69E-02	3.15E-01 ±4.60E-02	8.04E-01 ±2.55E-02 $p^{Control\ well\text{-}fed}$=1.65E-02	-9.50E-02 ±1.38E-02
mir-310s (KT40/KT40) well-fed		2.86E+01 ±1.76E-02	1.04E+01 ±9.91E-02	6.79E-01 ±1.76E-02	6.25E-01 ±7.62E-03 $p^{Control\ well\text{-}fed}$=9.55E-04	-2.04E-01 ±5.31E-03
mir-310s (KT40/KT40) starved		2.80E+01 ±1.89E-02	1.01E+01 ±2.23E-02	3.70E-01 ±1.89E-02	7.74E-01 ±1.02E-02 $p^{Control\ well\text{-}fed}$=6.50E-03	-1.11E-01 ±5.68E-03
Control (w^{1118}) well-fed	*Gasp*	2.99E+01 ±4.09E-02	1.20E+01 ±4.83E-02	3.18E-07 ±4.09E-02	1.00 ±2.79E-02	-9.57E-08 ±1.23E-02
Control (w^{1118}) starved		2.61E+01 ±1.95E-02	8.34 ±2.16E-02	-3.67 ±1.95E-02	1.27E+01 ±1.73E-01 $p^{Control\ well\text{-}fed}$=2.97E-07	1.10 ±5.88E-03
mir-310s (KT40/KT40) well-fed		2.90E+01 ±2.72E-02	1.08E+01 ±1.01E-01	-1.16 ±2.72E-02	2.23 ±4.20E-02 $p^{Control\ well\text{-}fed}$=1.66E-05	3.49E-01 ±8.20E-03
mir-310s (KT40/KT40) starved		2.76E+01 ±1.90E-02	9.77 ±2.24E-02	-2.24 ±1.90E-02	4.72 ±6.19E-02 $p^{Control\ well\text{-}fed}$=6.65E-07	6.74E-01 ±5.72E-03
Control (w^{1118}) well-fed	*Rpl32*	1.79E+01 ±2.57E-02	0.00 ±2.57E-02			
Control (w^{1118}) starved		1.78E+01 ±9.16E-03	6.36E-07 ±9.16E-03			
mir-310s (KT40/KT40) well-fed		1.81E+01 ±9.76E-02	0.00 ±9.76E-02			
mir-310s (KT40/KT40) starved		1.78E+01 ±1.18E-02	0.00 ±1.18E-02			
No Reverse Transcriptase						
Control (w^{1118}) well-fed	*Rpl32*	3.30E+01 ±6.88E-02	1.51E+01 ±6.88E-02	1.51E+01 ±6.88E-02	2.81E-05 ±1.34E-06	-4.55 2.07E-02
Control (w^{1118}) starved		3.29E+01 ±1.01E-01	1.51E+01 ±1.01E-01	1.51E+01 ±1.01E-01	2.90E-05 ±2.03E-06	-4.54 3.04E-02
mir-310s (KT40/KT40) well-fed		3.23E+01 ±2.68E-01	1.42E+01 ±2.68E-01	1.42E+01 ±2.68E-01	5.32E-05 ±9.93E-06	-4.27 8.06E-02
mir-310s (KT40/KT40) starved		3.30E+01 ±9.89E-03	1.52E+01 ±9.89E-03	1.52E+01 ±9.89E-03	2.67E-05 ±1.83E-07	-4.57 2.98E-03
Plate 4						
Control (w^{1118}) well-fed	*GstD4*	2.55E+01 ±3.46E-02	8.26 ±3.85E-02	-3.18E-07 ±3.46E-02	1.00 ±2.42E-02	9.57E-08 ±1.04E-02
Control (w^{1118}) starved		2.56E+01 ±2.51E-02	8.55 ±2.63E-02	2.91E-01 ±2.51E-02	8.17E-01 ±1.43E-02 $p^{Control\ well\text{-}fed}$=2.85E-03	-8.77E-02 ±7.57E-03
mir-310s (KT40/KT40) well-fed		2.54E+01 ±1.23E-02	7.72 ±3.97E-02	-5.38E-01 ±1.23E-02	1.45 ±1.24E-02 $p^{Control\ well\text{-}fed}$=7.65E-05	1.62E-01 ±3.71E-03

mir-310s (KT40/KT40) starved		2.59E+01 ±1.08E-02	8.72 ±1.58E-02	4.55E-01 ±1.08E-02	7.30E-01 ±5.46E-03 $p^{Control\ well\text{-}fed}$=3.97E-04	-1.37E-01 ±3.26E-03
Control (w^{1118}) well-fed	*Lsp1beta*	2.69E+01 ±3.96E-02	9.65 ±4.31E-02	-6.36E-07 ±3.96E-02	1.00 ±2.73E-02	1.91E-07 ±1.19E-02
Control (w^{1118}) starved		3.17E+01 ±9.43E-03	1.47E+01 ±1.23E-02	5.08 ±9.43E-03	2.95E-02 ±1.93E-04 $p^{Control\ well\text{-}fed}$=3.72E-06	-1.53 ±2.84E-03
mir-310s (KT40/KT40) well-fed		2.39E+01 ±2.93E-02	6.26 ±4.78E-02	-3.39 ±2.93E-02	1.05E+01 ±2.12E-01 $p^{Control\ well\text{-}fed}$=1.54E-06	1.02 ±8.82E-03
mir-310s (KT40/KT40) starved		2.40E+01 ±2.88E-02	6.85 ±3.11E-02	-2.80 ±2.88E-02	6.98 ±1.38E-01 $p^{Control\ well\text{-}fed}$=1.83E-06	8.44E-01 ±8.67E-03
Control (w^{1118}) well-fed	*Lsp2*	1.98E+01 ±1.86E-02	2.57 ±2.52E-02	-6.36E-07 ±1.86E-02	1.00 ±1.28E-02	1.91E-07 ±5.61E-03
Control (w^{1118}) starved		2.87E+01 ±4.05E-02	1.17E+01 ±4.12E-02	9.17 ±4.05E-02	1.74E-03 ±4.95E-05 $p^{Control\ well\text{-}fed}$=1.64E-07	-2.76 ±1.22E-02
mir-310s (KT40/KT40) well-fed		2.19E+01 ±2.81E-03	4.30 ±3.78E-02	1.72 ±2.81E-03	3.03E-01 ±5.89E-04 $p^{Control\ well\text{-}fed}$=6.91E-07	-5.19E-01 ±8.45E-04
mir-310s (KT40/KT40) starved		2.34E+01 ±2.49E-02	6.17 ±2.74E-02	3.59 ±2.49E-02	8.28E-02 ±1.44E-03 $p^{Control\ well\text{-}fed}$=2.36E-07	-1.08 ±7.49E-03
Control (w^{1118}) well-fed	*LvpH*	2.17E+01 ±4.82E-02	4.53 ±5.10E-02	-4.77E-07 ±4.82E-02	1.00 ±3.29E-02	1.44E-07 ±1.45E-02
Control (w^{1118}) starved		2.18E+01 ±2.57E-02	4.76 ±2.69E-02	2.35E-01 ±2.57E-02	8.50E-01 ±1.52E-02 $p^{Control\ well\text{-}fed}$=1.41E-02	-7.06E-02 ±7.74E-03
mir-310s (KT40/KT40) well-fed		2.23E+01 ±2.06E-02	4.63 ±4.30E-02	1.01E-01 ±2.06E-02	9.32E-01 ±1.34E-02 $p^{Control\ well\text{-}fed}$=1.26E-01	-3.04E-02 ±6.21E-03
mir-310s (KT40/KT40) starved		2.29E+01 ±2.60E-03	5.74 ±1.19E-02	1.21 ±2.60E-03	4.32E-01 ±7.80E-04 $p^{Control\ well\text{-}fed}$=6.58E-05	-3.64E-01 ±7.84E-04
Control (w^{1118}) well-fed	*Mgstl*	2.29E+01 ±1.60E-02	5.71 ±2.33E-02	-4.77E-07 ±1.60E-02	1.00 ±1.11E-02	1.44E-07 ±4.82E-03
Control (w^{1118}) starved		2.34E+01 ±1.61E-02	6.38 ±1.79E-02	6.76E-01 ±1.61E-02	6.26E-01 ±6.96E-03 $p^{Control\ well\text{-}fed}$=8.94E-06	-2.04E-01 ±4.83E-03
mir-310s (KT40/KT40) well-fed		2.24E+01 ±5.28E-03	4.78 ±3.81E-02	-9.32E-01 ±5.28E-03	1.91 ±6.99E-03 $p^{Control\ well\text{-}fed}$=2.62E-07	2.80E-01 ±1.59E-03
mir-310s (KT40/KT40) starved		2.24E+01 ±1.72E-01	5.22 ±1.72E-01	-4.89E-01 ±1.72E-01	1.40 ±1.76E-01 $p^{Control\ well\text{-}fed}$=7.43E-02	1.47E-01 ±5.17E-02
Control (w^{1118}) well-fed	*mus209*	2.19E+01 ±1.36E-02	4.70 ±2.17E-02	-6.36E-07 ±1.36E-02	1.00 ±9.37E-03	1.91E-07 ±4.08E-03
Control (w^{1118}) starved		2.44E+01 ±9.25E-03	7.39 ±1.21E-02	2.69 ±9.25E-03	1.55E-01 ±9.93E-04 $p^{Control\ well\text{-}fed}$=9.25E-08	-8.10E-01 ±2.78E-03
mir-310s (KT40/KT40) well-fed		2.19E+01 ±5.19E-03	4.24 ±3.81E-02	-4.61E-01 ±5.19E-03	1.38 ±4.96E-03 $p^{Control\ well\text{-}fed}$=3.74E-06	1.39E-01 ±1.56E-03
mir-310s (KT40/KT40) starved		2.34E+01 ±3.90E-03	6.20 ±1.22E-02	1.51 ±3.90E-03	3.52E-01 ±9.51E-04 $p^{Control\ well\text{-}fed}$=2.67E-07	-4.54E-01 ±1.18E-03

Control (w^{1118}) well-fed	*Rpl32*	1.72E+01 ±1.69E-02	-6.36E-07 ±1.69E-02			
Control (w^{1118}) starved		1.70E+01 ±7.88E-03	6.36E-07 ±7.88E-03			
mir-310s (KT40/KT40) well-fed		1.76E+01 ±3.77E-02	0.00 ±3.77E-02			
mir-310s (KT40/KT40) starved		1.72E+01 ±1.16E-02	1.27E-06 ±1.16E-02			
No Reverse Transcriptase						
Control (w^{1118}) well-fed	*Rpl32*	3.19+E01	1.47E+01	1.47E+01	3.70E-05	-4.43
Control (w^{1118}) starved		3.30E+01	1.33E+01	1.33E+01	9.94E-05	-4.00
mir-310s (KT40/KT40) well-fed		3.03E+01	1.27E+01	1.27E+01	1.50E-04	-3.82
mir-310s (KT40/KT40) starved		3.05E+01	1.33E+01	1.33E+01	9.94E-05	-4.00
Plate 5						
Control (w^{1118}) well-fed	*Obp44a*	2.69E+01 ±3.37E-02	8.55 ±3.55E-02	-3.18E-07 ±3.37E-02	1.00 ±2.36E-02	9.57E-08 ±1.01E-02
Control (w^{1118}) starved		2.67E+01 ±1.68E-02	8.41 ±5.16E-02	-1.33E-01 ±1.68E-02	1.10 ±1.29E-02 $p^{Control\ well\text{-}fed}$=2.30E-02	4.01E-02 ±5.07E-03
mir-310s (KT40/KT40) well-fed		2.68E+01 ±3.72E-02	7.95 ±5.92E-02	-6.01E-01 ±3.72E-02	1.52 ±3.89E-02 $p^{Control\ well\text{-}fed}$=3.42E-04	1.81E-01 ±1.12E-02
mir-310s (KT40/KT40) starved		2.66E+01 ±1.28E-02	8.12 ±3.78E-02	-4.28E-01 ±1.28E-02	1.35 ±1.19E-02 $p^{Control\ well\text{-}fed}$=1.98E-04	1.29E-01 ±3.84E-03
Control (w^{1118}) well-fed	*Obp56a*	2.57E+01 ±2.06E-02	7.32 ±2.34E-02	-1.59E-07 ±2.06E-02	1.00 ±1.43E-02	4.78E-08 ±6.20E-03
Control (w^{1118}) starved		2.49E+01 ±7.92E-03	6.70 ±4.94E-02	-6.17E-01 ±7.92E-03	1.53 ±8.39E-03 $p^{Control\ well\text{-}fed}$=5.50E-06	1.86E-01 ±2.38E-03
mir-310s (KT40/KT40) well-fed		2.79E+01 ±2.00E-02	9.05 ±5.02E-02	1.73 ±2.00E-02	3.02E-01 ±4.16E-03 $p^{Control\ well\text{-}fed}$=1.22E-06	-5.21E-01 ±6.01E-03
mir-310s (KT40/KT40) starved		2.75E+01 ±5.34E-02	9.00 ±6.41E-02	1.68 ±5.34E-02	3.11E-01 ±1.17E-02 $p^{Control\ well\text{-}fed}$=3.07E-06	-5.07E-01 ±1.61E-02
Control (w^{1118}) well-fed	*Obp56e*	2.46E+01 ±3.45E-02	6.25 ±3.63E-02	0.00 ±3.45E-02	1.00 ±2.41E-02	0.00 ±1.04E-02
Control (w^{1118}) starved		2.56E+01 ±1.69E-02	7.36 ±5.16E-02	1.11 ±1.69E-02	4.64E-01 ±5.41E-03 $p^{Control\ well\text{-}fed}$=2.63E-05	-3.34E-01 ±5.10E-03
mir-310s (KT40/KT40) well-fed		2.76E+01 ±1.19E-02	8.76 ±4.76E-02	2.51 ±1.19E-02	1.76E-01 ±1.45E-03 $p^{Control\ well\text{-}fed}$=4.35E-06	-7.55E-01 ±3.59E-03
mir-310s (KT40/KT40) starved		2.69E+01 ±2.14E-02	8.36 ±4.15E-02	2.11 ±2.14E-02	2.32E-01 ±3.47E-03 $p^{Control\ well\text{-}fed}$=5.96E-06	-6.35E-01 ±6.45E-03

Control (w^{1118}) well-fed	*Obp99b*	2.56E+01 ±2.63E-02	7.30 ±2.85E-02	1.59E-07 ±2.63E-02	1.00 ±1.83E-02	-4.78E-08 ±7.90E-03
Control (w^{1118}) starved		2.93E+01 ±5.85E-02	1.10E+01 ±7.62E-02	3.75 ±5.85E-02	7.44E-02 ±3.05E-03 $p^{Control\ well\text{-}fed}$=9.65E-07	-1.13 ±1.76E-02
mir-310s (KT40/KT40) well-fed		2.17E+01 ±5.31E-03	2.88 ±4.64E-02	-4.42 ±5.31E-03	2.14E+01 ±7.86E-02 $p^{Control\ well\text{-}fed}$=1.48E-09	1.33 ±1.60E-03
mir-310s (KT40/KT40) starved		2.39E+01 ±6.43E-03	5.36 ±3.61E-02	-1.94 ±6.43E-03	3.83 ±1.71E-02 $p^{Control\ well\text{-}fed}$=3.68E-08	5.83E-01 ±1.94E-03
Control (w^{1118}) well-fed	*Obst-A*	2.99E+01 ±3.09E-02	1.15E+01 ±3.29E-02	-3.18E-07 ±3.09E-02	1.00 ±2.16E-02	9.57E-08 ±9.31E-03
Control (w^{1118}) starved		2.86E+01 ±5.96E-02	1.04E+01 ±7.70E-02	-1.15 ±5.96E-02	2.21 ±8.97E-02 $p^{Control\ well\text{-}fed}$=1.92E-04	3.45E-01 ±1.79E-02
mir-310s (KT40/KT40) well-fed		2.88E+01 ±4.78E-02	9.92 ±6.64E-02	-1.62 ±4.78E-02	3.07 ±1.04E-01 $p^{Control\ well\text{-}fed}$=3.97E-05	4.88E-01 ±1.44E-02
mir-310s (KT40/KT40) starved		2.80E+01 ±2.56E-02	9.46 ±4.38E-02	-2.07 ±2.56E-02	4.20 ±7.39E-02 $p^{Control\ well\text{-}fed}$=2.00E-06	6.24E-01 ±7.71E-03
Control (w^{1118}) well-fed	*pro-PO-A1*	2.67E+01 ±3.29E-02	8.33 ±3.47E-02	3.18E-07 ±3.29E-02	1.00 ±2.26E-02	-9.57E-08 ±9.89E-03
Control (w^{1118}) starved		2.67E+01 ±4.36E-02	8.46 ±6.54E-02	1.27E-01 ±4.36E-02	9.16E-01 ±2.75E-02 $p^{Control\ well\text{-}fed}$=7.73E-02	-3.83E-02 ±1.31E-02
mir-310s (KT40/KT40) well-fed		3.62E+01 ±2.55E-01	1.73E+01 ±2.59E-01	8.99 ±2.55E-01	1.96E-03 ±3.78E-04 $p^{Control\ well\text{-}fed}$=1.56E-06	-2.71 ±7.68E-02
mir-310s (KT40/KT40) starved		3.62E+01 ±5.30E-01	1.77E+01 ±5.31E-01	9.39 ±5.30E-01	1.50E-03 ±6.56E-04 $p^{Control\ well\text{-}fed}$=1.56E-06	-2.83 ±1.59E-01
Control (w^{1118}) well-fed	*Rpl32*	1.83E+01 ±1.11E-02	0.00 ±1.11E-02			
Control (w^{1118}) starved		1.82E+01 ±4.88E-02	0.00 ±4.88E-02			
mir-310s (KT40/KT40) well-fed		1.89E+01 ±4.61E-02	-6.36E-07 ±4.61E-02			
mir-310s (KT40/KT40) starved		1.85E+01 ±3.56E-02	0.00 ±3.56E-02			
No Reverse Transcriptase						
Control (w^{1118}) well-fed -RT	*Rpl32*	3.06E+01 ±1.02E-01	1.22E+01 ±1.02E-01	1.22E+01 ±1.02E-01	9.15E-05	-4.04
Control (w^{1118}) starved -RT		3.08E+01 ±1.01E-01	1.27E+01 ±1.01E-01	1.27E+01 ±1.01E-01	1.05E-04	-3.98
mir-310s (KT40/KT40) well-fed -RT		3.06E+01 ±1.08E-01	1.20E+01 ±1.08E-01	1.20E+01 ±1.08E-01	1.39E-04	-3.86
mir-310s (KT40/KT40) starved -RT		2.99E+01 ±7.07E-01	1.17E+01 ±7.07E-01	1.17E+01 ±7.07E-01	9.03E-05	-4.04
Plate 6						

Control (w^{1118}) well-fed	*Sucb*	2.38E+01 ±3.20E-02	5.40 ±4.19E-02	1.11E-06 ±3.20E-02	1.00 ±2.20E-02	-3.35E-07 ±9.62E-03
Control (w^{1118}) starved		2.43E+01 ±2.38E-02	6.23 ±5.19E-02	8.30E-01 ±2.38E-02	5.62E-01 ±9.29E-03 $p^{Control\ well\text{-}fed}$=5.23E-05	-2.50E-01 ±7.16E-03
mir-310s (KT40/KT40) well-fed		2.39E+01 ±3.60E-02	5.24 ±6.33E-02	-1.59E-01 ±3.60E-02	1.12 ±2.80E-02 $p^{Control\ well\text{-}fed}$=3.08E-02	4.78E-02 ±1.08E-02
mir-310s (KT40/KT40) starved		2.43E+01 ±1.63E-02	5.99 ±4.23E-02	5.95E-01 ±1.63E-02	6.62E-01 ±7.46E-03 $p^{Control\ well\text{-}fed}$=1.30E-04	-1.79E-01 ±4.90E-03
Control (w^{1118}) well-fed	*Rpl32*	1.84E+01 ±2.71E-02	1.27E-06 ±2.71E-02			
Control (w^{1118}) starved		1.81E+01 ±4.62E-02	-6.36E-07 ±4.62E-02			
mir-310s (KT40/KT40) well-fed		1.86E+01 ±5.21E-02	6.36E-07 ±5.21E-02			
mir-310s (KT40/KT40) starved		1.83E+01 ±3.91E-02	-6.36E-07 ±3.91E-02			
No Reverse Transcriptase						
Control (w^{1118}) well-fed	*Rpl32*	3.06E+01 ±1.02E-01	1.22E+01 ±1.02E-01	1.22E+01 ±1.02E-01	2.11E-05 ±1.45E-05	-3.68 3.08E-02
Control (w^{1118}) starved		3.08E+01 ±1.01E-01	1.27E+01 ±1.01E-01	1.27E+01 ±1.01E-01	1.51E-05 ±1.03E-05	-3.82 3.05E-02
mir-310s (KT40/KT40) well-fed		3.06E+01 ±1.08E-01	1.20E+01 ±1.08E-01	1.20E+01 ±1.08E-01	2.45E-05 ±1.81E-05	-3.61 3.24E-02
mir-310s (KT40/KT40) starved		2.99E+01 ±7.07E-01	1.17E+01 ±7.07E-01	1.17E+01 ±7.07E-01	3.05E-04 ±1.43E-04	-3.52 2.13E-01

[a] The relative mRNA levels were calculated by $2^{-\Delta\Delta CT}$.

[b] Average (AVE) and standard error of the mean (SEM) values were calculated based on three replicates for each genotype/condition/gene value.

[c] Significance was calculated using two-tailed non-paired Student's t-test.

Flies were fed with nutritionally rich or poor medium for 10 days before analysis.

Table S3, related to Figure S1. *mir-310s* mutants exhibit global defects associated with nutritional stress

Genotype/Condition / Phenotype	*Control* (w^{1118}) well-fed[a]	*mir-310s* (*KT40/KT40*) well-fed[a]	*Control* (w^{1118}) starved[a]	*mir-310s* (*KT40/KT40*) starved[a]
Crop diameter[b]: (in mm) (AVE±SEM) n=number of crops analyzed	0.65±0.05 n=12	0.85±0.04 n=10 $p^{Control\ well\text{-}fed}$=0.007	0.44±0.05 n=10	0.44±0.04 n=10 $p^{Control\ starved}$=1,00
Lipid Accumulation: µg TAG equivalents per mg protein (AVE±SEM) n=number of females analyzed	(3 days) 386.77±35.68 n=30	(3 days) 210.67±28.57 n=20 $p^{Control\ well\text{-}fed}$=0.008	(10 days) 582.07±217.43 n = 30 $p^{Control\ well\text{-}fed}$=0.04	(10 days) 1581.0±202.03 n=30 $p^{Control\ well\text{-}fed}$=0.0002 $p^{Control\ starved}$=0.006
Fecundity: Eggs laid per fly per day (AVE±SEM) n=number of females analyzed	16.48±1.76 n=49	6.03±0.4 n=50 $p^{Control}$=0.004		

Relative egg laying efficiency under starvation	well-fed	1 day starved	2 day starved	3 day starved	4 day starved
Control (w^{1118}) n=50	1±0.01	0.95±0.08	0.49±0.08	0.14±0.03	0.06±0.02
mir-310s (*KT40/KT40*) n=50	1±0.19 $p^{Control\ well\text{-}fed}$= 7.82E-04	0.31±0.01 $p^{Control\ 1\ day}$ = 5.48E-04	0.28±0.04 $p^{Control\ 2\ day}$ = 8.9E-03	0.12±0.03 $p^{Control\ 3\ day}$ = 2.22E-02	0.11±0.04 $p^{Control\ 4\ day}$ = 4.5E-01

[a] Flies were fed with nutritionally rich and starvation medium for 10 days prior to analysis.

[b] Maximum crop diameters were measured from bright field images using Adobe Photoshop software.

Three biological replicates were analyzed for each genotype/condition.

Significance was tested using two-tailed non-paired Student's t-test.

Table S4, related to Figure 3. The *mir-310s* target *Rab23, DHR96,* and *ttk in vitro*

3'UTR Reporter	Control *3'UTR* without *mir-310s* binding site	*Rab23 3`UTR*	*DHR96 3`UTR*	*ttk 3`UTR*	negative control short *Dg 3'UTR* without *mir-310s* binding site[a]	positive control long *Dg 3'UTR* with *mir*-310s binding site[b]
Luciferase Signal (*Renilla/Firefly*) AVE±SEM	7.76E-02 ±3.62E-03	2.41E-02 ±3.96E-03	3.75E-02 ±2.10E-03	3.60E-02 ±3.18E-03	9.16E-02 ±1.96E-03	2.09E-02 ±8.29E-04
Relative Luciferase Signal AVE±SEM	1.00 ±4.67E-02	3.11E-01 ±5.10E-02 p=2.09E-04	4.83E-01 ±2.71E-02 p=1.54E-04	4.63E-01 ±4.10E-02 p=3.48E-04	1.18 ±2.52E-02 p=1.14E-02	2.69E-01 ±1.07E-02 p=1.03E-05

Luciferase reporter assays were performed in three biological replicates for each gene.

Significance was tested using two-tailed non-paired Student's t-test.

The short ([a]) and long ([b]) *3`UTR*s of a confirmed *mir-310s* target gene, *Dystroglycan* (*Dg*) (YATSENKO *et al.* 2014), were used as negative and positive controls, respectively.

Table S5, related to Figure 2 and 3. Relative mRNA and miRNA expression levels

qRT-PCR					
Genotype/ Condition	C_T *Rab23* AVE±SEM[b]	C_T *Rpl32* AVE±SEM[b]	Δ C_T AVE±SEM[b]	ΔΔ C_T AVE±SEM[b]	Relative ***Rab23*** mRNA level[a,c] AVE± SEM[b]
Control (w^{1118}) well-fed	2.42E+01 ±2.7E-01	1.85E+01 ±1.97E-01	5.71 ±8.18E-02	0.00 ±8.18E-02	1.00 ±5.18E-02
mir-310s (*KT40/KT40*) well-fed	2.41E+01 ±1.04E-01	1.9E+01 ±5.34E-02	5.06 ±6.22E-02	-6.48E-01 ±7.23E-02	1.57 ±7.08E-02 $p^{Control\ well\text{-}fed}$ =2.9E-03
Control (w^{1118}) starved	2.8E+01 ±3.1E-01	1.86E+01 ±1.21E-01	9.32 ±1.79E-01	3.61 ±2.67E-01	8.17E-02 ±1.4E-02 $p^{Control\ well\text{-}fed}$ =1.04E-05
mir-310s (*KT40/KT40*) starved	2.59E+01 ±1.98E-01	1.87E+01 ±9.29E-02	7.2 ±1.15E-01	1.49 ±1.52E-01	3.56E-01 ±3.47E-02 $p^{Control\ starved}$ =5.64E-04
	C_T *DHR96* AVE±SEM	C_T *Rpl32* AVE±SEM	Δ C_T AVE±SEM	ΔΔ C_T AVE±SEM	Relative ***DHR96*** mRNA level AVE± SEM
Control (w^{1118}) well-fed	2.66E+01 ±1.87E-01	1.83E+01 ±1.34E-01	8.24 ±1.21E-01	0.00 ±6.43E-02	1.00 ±3.23E-02
mir-310s (*KT40/KT40*) well-fed	2.66E+01 ±1.52E-01	1.90E+01 ±5.72E-02	7.61 ±8.62E-02	-6.35E-01 ±1.11E-01	1.55 ±9.1E-02 $p^{Control\ well\text{-}fed}$ =5.52E-03
Control (w^{1118}) starved	2.85E+01 ±1.14E+01	1.86E+01 ±1.14E-01	9.93 ±9.17E-02	1.69 ±9.36E-02	3.12E-01 ±1.43E-02 $p^{Control\ well\text{-}fed}$ =7.99E-06
mir-310s (*KT40/KT40*) starved	2.75E+01 ±1.1E-01	1.86E+01 ±5.7E-02	8.87 ±5.79E-02	6.28E-01 ±6.06E-02	6.47E-01 ±1.53E-02 $p^{Control\ starved}$ =1.3E-04
	C_T *ttk* AVE±SEM	C_T *Rpl32* AVE±SEM	Δ C_T AVE±SEM	ΔΔ C_T AVE±SEM	Relative ***ttk*** mRNA level AVE± SEM
Control (w^{1118}) well-fed	2.56E+01 ±2.48E-01	1.89E+01 ±2.06E-01	6.67 ±1.72E-01	0.00 ±5.53E-02	1.00 ±4.04E-02
mir-310s (*KT40/KT40*) well-fed	2.64E+01 ±9.0E-02	1.97E+01 ±2.12E-01	6.66 ±1.61E-01	-4.0E-03 ±1.22E-01	1.002 ±8.94E-02 $p^{Control\ well\text{-}fed}$=9.54E-01
Control (w^{1118}) starved	2.69E+01 ±1.18E-01	1.91E+01 ±1.08E-01	7.82 ±1.03E-01	1.16 ±3.42E-01	0.45 ±4.2E-02 $p^{Control\ well\text{-}fed}$ =5.63E-05
mir-310s (*KT40/KT40*) starved	2.64E+01 ±1.13E-01	1.93E+01 ±1.53E-01	7.17 ±1.61E-01	5.06E-01 ±1.39E-01	0.70 ±9.93E-02 $p^{Control\ starved}$=2.14E-02
TaqMan MicroRNA Assay					
	C_T *mir-310* AVE±SEM	C_T *2S rRNA* AVE±SEM	Δ C_T AVE±SEM	ΔΔ C_T AVE±SEM	Relative ***mir-310*** level AVE± SEM
Control (w^{1118}/*Oregon-R-C*) well-fed	2.54E+01 ±2.26E+00	1.05E+01 ±2.26E+00	1.49E+01 ±4.45E-02	0.00 ±5.86E-02	1.00 ±4.07E-02
Control (w^{1118}/*Oregon-R-C*) starved	2.42E+01 ±2.01E+00	9.83E+00 ±2.01E+00	1.43E+01 ±6.58+E-02	-6.14E-01 ±1.03E-01	1.54 ±1.12E-01 $p^{Control\ well\text{-}fed}$ =1.07E-02
	C_T *mir-312* AVE±SEM	C_T *2S rRNA* AVE±SEM	Δ C_T AVE±SEM	ΔΔ C_T AVE±SEM	Relative ***mir-312*** level AVE± SEM
Control (w^{1118}/*Oregon-R-C*) well-fed	2.55E+01 ±2.26E+00	9.48E+00 ±1.60E+00	1.60E+01 ±6.67E-01	0.00 ±1.03E-01	1.00 ±6.62E-02
Control (w^{1118}/*Oregon-R-C*) starved	2.86E+01 ±2.23E+00	1.13E+01 ±1.31E+00	1.54E+01 ±1.00E+00	-5.27E-01 ±2.54E-01	1.49 ±2.53E-01 $p^{Control\ well\text{-}fed}$ = 2.94E-02

[a] The relative mRNA levels were calculated by $2^{-\Delta\Delta CT}$.

[b] Average (AVE) and standard error of the mean (SEM) values were calculated using at least three biological replicates for each genotype and condition.

[c] Significance was tested using two-tailed non-paired Student's t-test.

Flies were fed with nutritionally rich and poor medium for 10 days prior analysis.

Table S6, related to Figure 4. Rab23 is upregulated at the germarial niche upon *mir-310s* loss

Genotype/ Condition	Rab23-expressing CpC percentage AVE±SEM[a]		
	negative	positive	
		low	high
w^{1118}; Rab23::YFP::4xmyc well-fed n=6	17.75±2.41%	36.33±5.34%	45.92±6.19%
mir-310s; Rab23::YFP::4xmyc well-fed n=6	4.46±3.1% $p^{w1118;\ Rab23::YFP::4xmyc}_{well\text{-}fed}$=0.0035	51.19±9.4%	44.35±10.95%
w^{1118}; Rab23::YFP::4xmyc starved n=6	6.94±3.47%	72.22±4.36%	20.83±4.08%
mir-310s; Rab23::YFP::4xmyc starved n=6	7.54±3.71%	35.19±3.09%	57.28±4.7% $p^{w1118;\ Rab23::YFP::4xmyc}_{starved}$=0.00082

[a] Averages and the standard errors of the means were calculated using five replicates.

Significances between the percentages of the cap cells (CpCs) that differentially express Rab23 protein: Rab23 negative CpCs under well-fed condition and the CpCs that have high Rab23 expression under starvation condition were calculated using a two tailed Student's t-test.

In order to analyze the significance between the frequencies of CpCs that differentially express Rab23 protein [negative or positive (high or low)] in control and *mir-310s* mutant germaria under well-fed and starved conditions, two-way tables and chi-squared test with 6 degrees of freedom were used. Chi-square value is 11.311 and p value is 0.079227.

Table S7, related to Figure 4. Upon *mir-310s* loss or Rab23 overexpression, the number of Hh-positive speckles in the germarium increases

Genotype	number Hh speckles AVE±SEM	
	well-fed	starved
Control (w^{1118}/*Oregon-R-C*)	92.67±3.66 n=9	55.11±8.62 n=9 $p^{Control\ well\text{-}fed}$ =1.04E-02
mir-310s (*KT40/KT40*)	198.67±17.53 n=9 $p^{Control\ well\text{-}fed}$ =7.25E-05	169.33±6.09 n=9 $p^{Control\ starved}$ =9.04E-09 $p^{mir\text{-}310s\ well\text{-}fed}$ =1.33E-01
bab1>Rab23 (*bab1-Gal4/UAS-Rab23*)	260.0±26.86 n=9 $p^{Control\ well\text{-}fed}$ =2.41E-05	198.89±11.96 n=9 $p^{Control\ starved}$ =3.89E-08 $p^{bab1>Rab23\ well\text{-}fed}$ =5.41E-02

Confocal images were analyzed using the particle analyzer tool from ImageJ software to quantify Hedgehog (Hh) speckle numbers.

p-values were calculated using two-tailed non-paired Student's t-test.

Table S8, related to Figure 4. Rab23 co-immunoprecipitated proteins

CG number	Gene name
CG2108	Rab23
CG7920	CG7920
CG2152	Pcmt
CG4916	me31B
CG7445	fln
CG30395	CG30395
CG6821	Lsp1gamma
CG6803	Mf
CG8867	Jon25Bi
CG9769	eIF3-S5-1
CG5887	desat1
CG5654	yps
CG7113	scu
CG4153	eIF-2beta
CG4466	Hsp27
CG1742	Mgstl
CG16765	ps
CG7178	wupA
CG11844	vig2;fdy
CG5330	Nap1
CG2229	Jon99Fii
CG4769	CG4769
CG10306	CG10306
CG3800	CG3800
CG4533	l(2)efl
CG4183	Hsp26
CG18811	Capr
CG8308	alphaTub67C
CG1633	Jafrac1
CG9641	CG9641
CG45077	fau
CG34069	mt:CoII
CG5422	Rox8
CG8871	Jon25Biii
CG5885	BEST:CK01296
CG13425	bl
CG5258	NHP2
CG10922	La
CG10578	DnaJ-1
CG10849	Sc2
CG6543	CG6543
CG4302	BEST:GH09393

CG5641	CG5641
CG8053	eIF-1A
CG6341	Ef1beta
CG4008	und
CG4170	vig
CG4666	CG4666
CG10279	Rm62
CG1469	Fer2LCH
CG13849	Nop56
CG6987	SF2
CG8189	ATPsyn-b
CG4193	dhd
CG4912	eEF1delta
CG6258	RfC38
CG8427	SmD3
CG10851	B52
CG3972	Cyp4g1
CG14999	RfC4
CG6617	CG6617
CG4003	pont
CG17136	Rbp1
CG31362	Jon99Cii
CG14813	deltaCOP
CG10206	nop5
CG5313	RfC3
CG5352	SmB
CG32701	l(1)G0320
CG8231	Tcp-1zeta
CG4376	Actn
CG8142	CG8142
CG4978	Mcm7
CG4611	CG4611
CG13240	l(2)35Di
CG11835	CG11835
CG45076	fau
CG7172	CG7172
CG7436	Nmt
CG6693	CG6693
CG9306	CG9306
CG7917	Nlp
CG15092	Jabba
CG8977	Cctgamma
CG13887	CG13887
CG7637	CG7637

CG18067	CG18067
CG8844	Pdsw
CG17686	DIP1
CG5289	Pros26.4
CG5047	mTerf3
CG4799	Pen
CG11107	CG11107
CG5374	T-cp1
CG4422	Gdi
CG18591	SmE
CG8715	lig
CG4082	Mcm5
CG2216	Fer1HCH
CG12203	CG12203
CG10628	CG10628
CG3029	or
CG5167	CG5167
CG12306	polo
CG4729	CG4729
CG6519	Cp15
CG30185	Gr59f
CG7182	CG7182
CG17566	gammaTub37C
CG11999	CG11999
CG16725	Smn
CG17280	levy
CG3446	CG3446
CG12400	CG12400
CG4553	CG4553
CG8322	ATPCL
CG3039	ogre
CG6094	CG6094
CG10097	CG10097
CG1489	Pros45
CG14207	HspB8
CG17611	eIF6
CG3333	Nop60B
CG7409	CG7409
CG3944	ND23
CG30008	CG12138
CG5371	RnrL
CG3267	l(2)04524
CG4824	BicC
CG5903	CG5903

CG15481	Ski6
CG14476	BcDNA.GH04962
CG3436	CG3436
CG31249	CG7477
CG6746	CG6746
CG7581	Bub3
CG7378	CG7378
CG8905	Sod2
CG6013	CG6013
CG1616	dpa
CG1938	Dlic
CG4634	Nurf-38
CG7911	CG7911
CG3747	Eaat1
CG4164	CG4164
CG6202	Surf4
CG4619	CG4619
CG13126	CG13126
CG5703	CG5703
CG31523	CG9798
CG9155	Myo61F
CG8258	CG8258
CG30176	wibg
CG8947	26-29-p
CG3710	TfIIS
CG3606	caz
CG1249	SmD2
CG13163	CG13163
CG3683	CG3683
CG12984	CG12984
CG8547	CG8547
CG8542	Hsc70-5
CG7033	CG7033
CG4206	Mcm3
CG12163	CG12163
CG3564	CHOp24
CG10833	Cyp28d1
CG5826	Prx3
CG8190	eIF2B-gamma
CG5183	KdelR
CG7006	CG7006
CG12357	Cbp20
CG4274	fzy
CG7830	Ostgamma

CG16912	CG16912
CG5508	BcDNA
CG3416	Mov34
CG7483	eIF4AIII
CG17437	wds
CG4020	CG4020
CG9548	CG9548
CG18444	alphaTry
CG1101	Ref1
CG10297	Acp65Aa
CG5000	msps
CG3420	CG3420
CG14309	CG14309
CG9987	CG9987
CG7123	LanB1
CG1751	Spase25
CG8680	CG8680
CG6137	aub
CG3422	Pros28.1
CG10469	CG10469
CG7619	Pros54
CG1828	dre4
CG34026	CG34026
CG3359	mfas
CG7361	RFeSP
CG9054	Ddx1
CG8351	Tcp-1eta
CG16904	CG16904
CG11804	ced-6
CG9302	CG9302
CG7697	CstF-64
CG9172	CG9172
CG9383	asf1
CG10045	GstD1
CG7488	CG7488
CG4760	bol
CG1453	Klp10A
CG6782	sea
CG7008	Tudor-SN
CG11876	CG11876
CG4463	Hsp23
CG4279	LSm1
CG11989	vnc
CG5864	AP-1sigma
CG44255	CG13644
CG10212	SMC2
CG10470	CG10470

CG2910	nito
CG15735	CG15735
CG1877	lin19
CG8749	snRNP-U1-70K
CG5548	CG5548
CG8711	Cul-4
CG16983	skpA
CG18559	Cyp309a2
CG7946	CG7946
CG3845	NAT1
CG13298	CG13298
CG33104	eca;p24-2
CG2014	CG2014
CG5555	CG5555
CG9741	Dhod
CG3424	path
CG10687	Aats-asn
CG2621	sgg
CG13091	CG13091
CG42807	CG6183
CG3917	Grip84
CG3909	CG3909
CG3664	Rab5
CG3059	NTPase
CG15877	CG15877
CG32441	CG32441
CG6416	Zasp66
CG1548	cathD
CG8409	Su(var)205
CG13277	LSm7
CG10203	x16
CG4115	CG4115
CG13570	spag
CG12908	Ndg
CG11785	bai
CG15531	CG15531
CG6249	Csl4
CG8827	Ance
CG3200	Reg-2
CG1703	CG1703
CG4447	CG4447
CG11837	CG11837
CG7359	Sec22
CG5670	Atpalpha
CG10360	ref(2)P
CG2604	CG2604
CG5252	Ranbp9

CG30149	rig
CG6235	tws
CG3678	CG17556
CG10210	tst
CG8548	Kap-alpha1
CG3068	aur
CG2175	CG2175
CG6375	pit
CG3295	CG3295
CG9018	CG9018
CG3959	pelo
CG9799	CG9799
CG14224	Ubqn
CG11092	Nup93-1
CG6866	loqs
CG1119	Gnf1
CG8625	Iswi
CG9128	Sac1
CG3815	CG3815
CG4051	egl
CG34074	mt:CoIII
CG1091	CG1091
CG13935	Cpr62Bb
CG3299	Vinc
CG8397	CG8397
CG2867	Prat
CG11015	CoVb
CG9889	yellow-d
CG2071	Ser6
CG3582	U2af38
CG3561	Dbp21E2
CG8648	Fen1
CG7833	Orc5
CG33141	sns
CG7288	CG7288
CG2031	Hpr1
CG1307	CG1307
CG9749	Abi
CG5272	gnu
CG10159	BEAF-32
CG31368	CG31368
CG11137	CG11137
CG3071	EG:25E8.3
CG14788	ns3
CG4088	lat
CG7109	mts
CG3056	ssx

CG9159	Kr-h2
CG31717	CG31717
CG18347	CG18347
CG4038	CG4038
CG10498	cdc2c
CG13472	CG13472
CG6841	CG6841
CG9350	CG9350
CG10472	CG10472
CG6948	Clc
CG12000	Prosbeta7
CG1179	LysB;LysD;LysA;LysE
CG11777	CG11777
CG1685	pen
CG33129	CG6089
CG33503	Cyp12d1-d
CG4039	Mcm6
CG9547	CG9547
CG10333	CG10333
CG9441	Pu
CG3157	gammaTub23C
CG5001	CG5001
CG5193	TfIIB
CG18124	mTTF
CG7929	ocn
CG12128	CG12128
CG3320	Rab1
CG1401	Cul-5
CG3412	slmb
CG15433	Elp3
CG4152	l(2)35Df
CG3501	CG3501
CG11397	glu
CG9253	CG9253
CG4365	CG4365
CG17454	CG17454
CG7970	CG7970
CG1406	U2A
CG5099	msi
CG3625	CG3625
CG5358	Art4
CG8571	smid
CG11583	CG11583
CG10326	CG10326
CG17018	CG17018
CG8553	SelD

CG9267	CG9267
CG3262	CG3262
CG5205	CG5205
CG12325	CG12325
CG9191	Klp61F
CG4609	fax
CG7375	CG7375
CG5726	CG5726
CG4097	Pros26
CG11984	CG11984
CG10327	TBPH
CG9829	poly
CG11007	CG11007
CG6601	Rab6;Rab39
CG17608	fu12
CG12170	CG12170
CG6450	lva
CG17285	Fbp1
CG3509	CG3509
CG5655	Rsf1
CG2034	anon-i1
CG9246	CG9246
CG12333	CG12333
CG3605	CG3605
CG4086	Su(P)
CG1963	Pcd
CG12352	san
CG10673	CG10673
CG31137	twin
CG14100	CG14100
CG3224	CG3224
CG11077	CG11077
CG12343	Syf2
CG9802	Cap
CG2875	CG2875
CG9621	Adgf-D
CG8323	CG8323
CG33214	Glg1
CG5913	CG5913
CG4241	att-ORFA
CG5495	Txl
CG6907	CG6907
CG6796	CG6796
CG5553	DNApol-alpha60
CG2076	CG2076
CG11416	uri
CG11875	Nup37

CG11241	CG11241
CG4857	tyf
CG7910	CG7910
CG5442	SC35
CG2917	Orc4
CG5266	Pros25
CG5923	DNApol-alpha73
CG8385	Arf79F
CG4303	Bap60
CG1081	Rheb
CG8453	Cyp6g1
CG7382	CG7382
CG5677	Spase22-23
CG5581	Ote
CG1512	Cul-2
CG10850	ida
CG3265	Eb1
CG14542	vps2
CG7626	Spt5
CG10535	Elp1
CG7175	mTerf5
CG11943	Nup205
CG8454	Vps16A
CG14802	MED18
CG6311	Edc3
CG6339	rad50
CG7704	Taf5
CG5949	DNApol-delta
CG1768	dia
CG8360	CG8360
CG18125	Send2
CG10254	CG10254
CG18543	mtrm
CG9143	CG9143
CG33523	CG33523
CG12702	CG12702
CG8306	CG8306
CG3431	Uch-L5
CG9446	CG9446
CG9890	CG9890
CG1956	R
CG34325	CG34325
CG14995	CG14995
CG4798	l(2)k01209
CG32638	CG32638
CG10988	l(1)dd4
CG3808	CG3808

CG1634	Nrg
CG2161	Rga
CG6851	Mtch
CG14213	Rcd-1
CG2925	noi
CG2789	CG2789
CG12323	Prosbeta5
CG2051	CG2051
CG5942	brm
CG4901	CG4901
CG17255	nocte
CG9300	CG9300
CG9399	CG9399
CG2358	twr
CG12473	stnB
CG14472	poe
CG12320	CG12320
CG18259	CG18259
CG6113	Lip4
CG18190	CG18190
CG6768	DNApol-epsilon
CG6998	ctp;Cdlc2
CG4461	CG4461
CG3312	Rnp4F
CG6582	Aac11
CG8705	pnut
CG44248	Snp
CG45076	CG45076
CG10415	TfIIEalpha
CG1057	MED31
CG12363	Dlc90F
CG4254	tsr
CG5198	CG5198
CG6717	Spn28B
CG3697	mei-9
CG5222	IntS9
CG9742	SmG
CG7595	ck
CG4665	Dhpr
CG6958	Nup133
CG4118	nxf2
CG5989	CG5989
CG4215	spel1
CG31671	tho2
CG11887	Elp2
CG5208	Patr-1
CG3291	pcm

CG7238	sip1
CG3151	Rbp9
CG6197	CG6197
CG10622	Sucb
CG17492	mib2
CG12878	btz
CG9050	psd
CG12050	CG12050
CG31322	Aats-met
CG10189	CG10189
CG17337	CG17337
CG8156	Arf51F
CG32549	CG32549
CG4091	CG4091
CG18076	shot
CG9250	Mpp6
CG34387	futsch
CG2684	lds
CG12752	Nxt1
CG12031	MED14
CG12298	sub
CG6967	CG6967
CG1490	Usp7
CG4268	Pitslre
CG14257	CG14257
CG12217	PpV
CG32732	CG12542
CG6354	Rb97D
CG10153	CG10153
CG33113	Rtnl1
CG1750	CG1750
CG18273	CG18273
CG1216	mri
CG11981	Prosbeta3
CG6995	Saf-B
CG7351	PCID2
CG8545	CG8545
CG6805	CG6805
CG9323	CG9323
CG17259	CG17259
CG32075	CG6316
CG32211	Taf6
CG18069	CaMKII
CG9774	rok
CG9791	CG9791
CG17947	alpha-Cat
CG8778	CG8778

CG12272	CG12272
CG8602	CG8602
CG7433	CG7433
CG6349	DNApol-alpha180
CG5714	ecd
CG30021	metro
CG34033	CG34033
CG5819	CG5819
CG4780	membrin
CG12113	IntS4
CG1318	Hexo1
CG6233	Ufd1-like
CG1372	yl
CG7899	Acph-1
CG10418	CG10418
CG33217	CG33217
CG6363	MRG15
CG34407	Not1
CG6418	CG6418
CG11414	CG11414
CG18176	defl
CG32721	NELF-B
CG8725	CSN4
CG10215	Ercc1
CG7670	WRNexo
CG10990	Pdcd4
CG3460	Nmd3
CG11909	tobi
CG1669	kappaB-Ras
CG10545	Gbeta13F
CG4165	CG4165
CG8590	Klp3A
CG33505	U3-55K
CG4845	psidin
CG10630	blanks
CG3642	Clp
CG18600	CG18600
CG1276	TfIIEbeta
CG12391	CG12391
CG10572	Cdk8
CG42468	Sfp24F
CG10938	Prosalpha5
CG3093	dor
CG4572	CG4572
CG2699	Pi3K21B
CG5884	par-6
CG1597	CG1597

CG7831	ncd
CG7108	DNApol-alpha50
CG31852	Tap42
CG8448	mrj
CG3173	IntS1
CG5465	MED16
CG16892	CG16892
CG7718	CG7718
CG14444	APC7
CG8729	rnh1
CG40300	AGO3
CG4379	Pka-C1
CG3423	SA
CG31390	MED7
CG34034	CG34034
CG1440	CG1440
CG9104	CG9104
CG4764	CG4764
CG6769	CG6769
CG12372	spt4
CG7338	CG7338
CG18332	CSN3
CG8211	IntS2
CG32438	Smc5
CG11132	DMAP1
CG5168	CG5168
CG10261	aPKC
CG2146	didum
CG12018	CG12018
CG2941	CG2941
CG7003	Msh6
CG3699	EG:BACR7A4.14
CG34424	CG34424
CG18729	zwilch
CG5643	wdb
CG9630	CG9630
CG9623	if
CG31716	Cnot4
CG6603	Hsc70Cb
CG8392	Prosbeta1
CG1009	Psa
CG30488	CG30488
CG7843	Ars2
CG11334	CG11334
CG2072	Mad1
CG32498	dnc

CG1911	CAP-D2
CG7839	CG7839
CG31048	spg
CG14286	CG14286
CG15701	CG15701
CG6176	Grip75
CG8440	Lis-1
CG9916	Cyp1
CG1709	Vha100-1
CG4749	CG4749
CG18780	MED20
CG4261	Hel89B
CG2158	Nup50
CG6875	asp
CG9841	EfSec
CG33122	cutlet
CG9591	omd
CG5008	GNBP3
CG7741	CG7741
CG4364	CG4364
CG1666	Hlc
CG7764	mrn
CG4291	CG4291
CG9248	CG9248
CG12785	Mat89Ba
CG1945	faf
CG17665	IntS3
CG9755	pum
CG2206	l(1)G0193
CG5800	CG5800
CG11990	hyx
CG13957	CG13957
CG7999	MED24
CG8019	hay
CG9925	CG9925
CG11710	CG11710
CG2124	CG2124
CG16865	CG16865
CG17912	CG17912
CG12819	sle;CG12592
CG9953	CG9953
CG9067	CG9067
CG9297	CG9297
CG16812	CG16812
CG9997	CG9997
CG4633	Aats-ala-m
CG17242	CG17242

CG2244	MTA1-like
CG2078	Myd88
CG13492	CG13492
CG1725	dlg1
CG14215	CG14215
CG11722	CG11722
CG9601	CG9601
CG12267	CG12267
CG31418	CG31418
CG33106	mask
CG7261	CG7261
CG10347	CG10347
CG11821	Cyp12a5
CG10923	Klp67A
CG6364	CG6364
CG5116	CG5116
CG6673	GstO2
CG10092	CG10092
CG12896	Prx2540-2
CG15645	cerv
CG33180	Ranbp16
CG11061	GM130
CG14299	CG14299
CG8426	l(2)NC136
CG31278	CG31278
CG2669	hd
CG10582	Sin
CG8610	Cdc27
CG7180	CG7180
CG8815	Sin3A
CG33056	CG10517
CG7825	Rad17
CG4700	Sema-2a
CG42600	clos
CG8367	cg
CG11330	cort
CG4561	Aats-tyr
CG6814	Asun
CG30463	pgant9
CG1258	pav
CG42574	ctrip
CG3975	Pol32
CG8771	CG8771
CG11143	Inos
CG11799	fd68A
CG6760	Pex1
CG1664	sbr

CG34408	CG34408
CG9198	shtd
CG7989	wcd
CG33139	Ranbp11
CG32473	CG32473
CG9088	lid
CG10726	barr
CG8915	CG8915
CG8318	Nf1
CG10542	Bre1
CG11486	CG11486
CG33484	zormin
CG6677	ash2
CG15811	Rop
CG4589	Letm1
CG6170	HDAC6
CG2701	crm
CG31045	Mhcl
CG13142	CG13142
CG18140	Cht3
CG3999	CG3999
CG3329	Prosbeta2

CG4790	fs(1)M3
CG1569	rod
CG17704	Nipped-B
CG6379	CG6379
CG2049	Pkn
CG6415	CG6415
CG9911	CG9911
CG1345	Gfat2
CG4069	CG4069
CG3228	kz
CG9594	Chd3
CG2864	Parg
CG11120	CG11120
CG7235	Hsp60C
CG7162	MED1
CG4792	Dcr-1
CG12052	lola
CG6511	CG6511
CG6606	Rip11
CG17209	CG17209
CG1643	Atg5
CG3510	CycB

CG15737	wisp
CG31793	CG17338
CG10042	MBD-R2
CG7660	Pxt
CG1031	alpha-Est1
CG6623	SIDL
CG10837	eIF-4B
CG1782	Uba1
CG32562	xmas-2
CG12010	CG12010
CG11411	fs(1)N
CG1433	Atu
CG4453	Nup153
CG42250	lqfR
CG3041	Orc2
CG43078	CG43078
CG4554	CG4554
CG7487	RecQ4
CG12153	Hira
CG32604	l(1)G0007
CG12090	CG12090
CG12499	CG12499

CG2707	fs(1)Ya
CG8153	mus210
CG1915	sls
CG5859	IntS8
CG12196	egg
CG13397	ESTS:172F5T
CG6206	LM408
CG3520	CG3520
CG12005	Mms19
CG33554	Nipped-A
CG6535	tefu
CG31445	CG11955
CG5874	Nelf-A
CG6539	Gem3
CG7337	CG7337
CG44162	Strn-Mlck
CG2520	lap
CG14796	Mur2B
CG2747	CG2747

Co-immunoprecipitated protein hits were filtered for 5-fold enrichment in the tagged Rab23 sample (*w^{1118}; Rab23::YFP::4xmyc*) compared to control (w^{1118}), resulting in 821 unique proteins.

COPI-associated proteins are highlighted.

Table S9, related to Figures 5 and 6. The frequencies of the analyzed ovarian phenotypes

Genotype \ Phenotype	Disorganized germarium architecture at region 2A/B	Abnormal egg chamber encapsulation	Multilayered stalk	Persisting FasIII expression	Multilayered follicular epithelium	
Control (*w^{1118}/Oregon-R-C*)	26.7% n=30	0% n=20	5% n=20	0% n=35	well-fed[a] 15% n=20	starved[a] 0% n=20 $p^{well\text{-}fed}$=0.072
mir-310s (*KT40/KT40*)	86.7% n=30 $p^{Control}$<0.0001	35% n=20 $p^{Control}$=0.004	75% n=20 $p^{Control}$<0.0001	44.4% n=35 $p^{Control}$<0.0001	well-fed[a] 45% n=20	starved[a] 5% n=20 $p^{well\text{-}fed}$=0.003
mir-310s (*w[*]; Df(2R)mir-310-311-312-313 FRT42D*)	66.7% n=30 $p^{Control}$=0.002	5% n=20 $p^{Control}$=0.311	65% n=20 $p^{Control}$<0.0001	54.2% n=35 $p^{Control}$<0.0001	50% n=20 $p^{Control}$=0.018	
mir-310s/ Df6070 (*w[1118]; KT40/Df(2R)Exel6070, P{w[+mC]=XP-U}Exel6070*)	80% n=30 $p^{Control}$<0.0001	40% n=20 $p^{Control}$=0.002	70% n=20 $p^{Control}$<0.0001	59.1% n=35 $p^{Control}$<0.0001	70% n=20 $p^{Control}$<0.0001	
bab1>hh (*tub-Gal80^{ts}/+; bab1-Gal4/UAS-hh*)	100% n=30 $p^{Control}$<0.0001	95% n=20 $p^{Control}$<0.0001	100% n=20 $p^{Control}$<0.0001	48% n=35 $p^{Control}$<0.0001	well-fed[b] 100% n=20	starved[b] 50% n=20 $p^{well\text{-}fed}$<0.0001
bab1>Rab23 (*bab1-Gal4/UAS-Rab23*)	76.7% n=30 $p^{Control}$<0.0001	35% n=20 $p^{Control}$=0.004	70% n=20 $p^{Control}$<0.0001	52.2% n=35 $p^{Control}$<0.0001	35% n=20 $p^{Control}$=0.144	
Rescue *mir-310s* (*KT40/KT40; attB2 mir-310s res long 2 /+*)	33.3% n=30 $p^{KT40/Df6070}$<0.0001	5% n=20 $p^{KT40/Df6070}$=0.008	30% n=20 $p^{KT40/Df6070}$=0.011	16% n=35 $p^{KT40/Df6070}$=0.002	35% n=20 $p^{KT40/Df6070}$=0.027	
mir-310s; bab1>hh RNAi (*KT40/KT40; bab1-Gal4/ UAS-hh-RNAi*)	50% n=30 $p^{KT40/Df6070}$=0.015	12% n=20 $p^{KT40/Df6070}$=0.077	20% n=20 $p^{KT40/Df6070}$=0.001	28.6% n=35 $p^{KT40/Df6070}$=0.03	15% n=20 $p^{KT40/Df6070}$<0.0001	
mir-310s; bab1>Rab23 RNAi (*KT40/KT40; bab1-Gal4/ UAS-Rab23-RNAi*)	46.7% n=30 $p^{KT40/Df6070}$=0.007	20% n=20 $p^{KT40/Df6070}$=0.168	20% n=20 $p^{KT40/Df6070}$=0.001	25% n=35 $p^{KT40/Df6070}$=0.015	40% n=20 $p^{KT40/Df6070}$=0.057	

[a] Flies were kept on nutritionally rich or poor medium for 7 days prior to analysis.

[b] *tub-Gal80^{ts}/+; bab1-Gal4/UAS-hh* flies were kept for 3 days at restrictive temperature (29°C).

Occurrences of the listed phenotypes per ovariole are indicated as percentages.

Significance was tested using Pearson's chi-Square test and IBM SPSS Statistics software.

Table S10, related to Figure 6. The high mitotic activity in *mir-310s* mutant egg chambers is rescued by downregulating Rab23 or Hh levels

Genotype	Number of $PH3^+$ follicle cells (AVE±SEM) n=number of stage 2 egg chambers analyzed	
	well-fed (7 days)	Starved (7 days)
Control (*w^{1118}/Oregon-R-C*)	4.17±0.25 n=30	0.20±0.09 n=30
bab1>hh RNAi[a] (*tub-Gal80^{ts}/+; bab1-Gal4/ UAS-hh-RNAi*)	2.00±0.34 n=30 $p^{Control}$=1.6E-05	0.27±0.12 n=15 $p^{Control}$=0.378
bab1>Rab23 RNAi[a] (*tub-Gal80^{ts}/+; bab1-Gal4/ UAS-Rab23-RNAi*)	2.4±0.33 n=30 $p^{Control}$=1.04E-04	0.20±0.11 n=15 $p^{Control}$=0.50
bab1>hh (*tub-Gal80^{ts}/+; bab1-Gal4/UAS-hh*)	8.4±0.68[b] n=30 $p^{Control}$<0.00001	1.07±0.23[a] n=15 $p^{Control}$=0.006
bab1>Rab23 (*tub-Gal80^{ts}/+; bab1-Gal4/UAS-Rab23*)	6.37±0.68 n=30 $p^{Control}$=0.0036	1.13±0.29 n=15 $p^{Control}$=0.007
mir-310s/ Df6070 (*w[1118]; KT40/Df(2R)Exel6070, P{w[+mC]=XP-U}Exel6070*)	5.3±0.38 n=30 $p^{Control}$=0.0233	0.70±0.16 n=30 $p^{Control}$=0.011
mir-310s (*KT40/KT40*)	5.63±0.51 n=30 $p^{Control}$=0.0222	0.8±0.19 n=30 $p^{Control}$=0.015
Rescue *mir-310s* (*KT40/KT40; attB2 mir-310s res long 2 /+*)	4.23±0.27 n=30 $p^{KT40/Df6070}$=0.0367	0.13±0.29 n=15 $p^{KT40/Df6070}$=0.0197
mir-310s; bab1>hh RNAi (*KT40/KT40; bab1-Gal4/ UAS-hh-RNAi*)	4.03±0.26 n=30 $p^{KT40/Df6070}$=0.011	0.4±0.13 n=15 $p^{KT40/Df6070}$=0.1075
mir-310s; bab1>Rab23 RNAi (*KT40/KT40; bab1-Gal4/ UAS-Rab23-RNAi*)	4.2±0.27 n=30 $p^{KT40/Df6070}$=0.0367	0.33±0.13 n=15 $p^{KT40/Df6070}$=0.0735

Significance was tested using Mann-Whitney U test and z statistic.

[a] Flies were kept at restrictive temperature (29°C) for 7 days.

[b] Flies were kept at restrictive temperature (29°C) for 3 days.

Table S11, related to Figures 1 and 3. Primers used in this study

3`UTR Luciferase reporter cloning[a]	*Rab23*	*NotI*	Forward	GCAAGCGGCCGCTTTTTGCATAGAATGCGAGCAGC
		XhoI	Reverse	GCAACTCGAGCCAAGCCCAGATCACAGGTCC
	ttk	*XhoI*	Forward	GCAACTCGAGAAGCGCAATCAAATAATAAACAAG
		NotI	Reverse	GCAAGCGGCCGCGCGAGAAAATTGCTGAAGGTT
	DHR96	*XhoI*	Forward	GCAACTCGAGTGTCTGTTTTATCTTGTCGCTTGT
		NotI	Reverse	GCAAGCGGCCGCTCCTTTTTGCACAGAACCCAC
qRT-PCR	*Rab23*		Forward	AGCTGGCCATTAAAGTGGTCATT
			Reverse	GATCTCGATCTGTCGCTCTAGGA
	DHR96		Forward	CCTCAGCGCCCTGATGATGG
			Reverse	CAGCTGCAATAGCTTTGGGTTGTG
	ttk		Forward	CGAAACGATCAAAGAACTCCAAGG
			Reverse	CGCCTGCTCGTTGAGGTGACTAC
	Rpl32		Forward	AAGATGACCATCCGCCCAGC
			Reverse	GTCGATACCCTTGGGCTTGC
	Act88F		Forward	GCGCCACCCGAGAGGAAGTA
			Reverse	TGGAAGGTGGACAGCGAGGC
	ade2		Forward	TTCCGTCGGTTTGCCTACATCA
			Reverse	TCCGCGACGAGAAGCTCATTAG
	ade3		Forward	GCCCAAACCCAAAGCCAAGG
			Reverse	CATCCAGCTGGTGGAGAAGTGC
	Arr1		Forward	CAGTCAGGATGCGAGGGATGC
			Reverse	CCCAGGGCTCCCAAGAAAAG
	CG3699		Forward	TCTGCCTGCGTGCCCTTCA
			Reverse	CCGCCATCGCCCAAGTTCT
	CG3902		Forward	CACGGTGGCGATCTGATGCT
			Reverse	GCGCAAGCAGTTCGGTGATG
	CG3999		Forward	CCATCGACAATGGGCGTGTTC
			Reverse	CTGGGCATTCATGTTGGCTCC
	CG9914		Forward	GGGACCCAGGAAGGCGTAGC
			Reverse	GCCGGCATCCTGAATGTCAAG
	CG11089		Forward	CCCGCAGGATCCACCAATGA
			Reverse	GGGCCATGATGATACCGTGCTC
	CG15369		Forward	CGGTGCACCAAAAGTCCTCG
			Reverse	GTCCTTCGCCAGCAGCCAAT
	CG16884		Forward	GCGATCGCGGGACCACTGT
			Reverse	GGCCACGGAAGCTACGGACAT
	CG30360		Forward	CGATCAGCGGAGAGTGGGTAGT
			Reverse	ACGCCGGGCAGGAACATCT
	CG31233		Forward	CCAGCACGCAGACCAACATAGC
			Reverse	GCCACCAGATCACCAAACCACA
	Cpr62Bc		Forward	CGTCTCCGGTGTGAGAGTCAGC
			Reverse	GGTCACCACGACGAGGGAATC
	Cpr72Ec		Forward	CGCATCCTCATCGGTCAGACTC
			Reverse	GCGTGAGGAGGCGGACAGA
	Cpr100A		Forward	TCCAGCCAGCACTATCACCAGG
			Reverse	AGCTCCGAACTTTCCATCTCCG

	Gal	Forward	CCAGACGCTTAGCGGGATTCA
		Reverse	CCGGTGGCGTCACCACTAAGTA
	Gasp	Forward	CTCGCCGTTCCAGCAGTTCC
		Reverse	CTCGCCTGTACGGCATCTTCC
	GstD4	Forward	TCCCCAGCACACCATTCCC
		Reverse	CCTTGCCGTACTTTTCCACCAG
	Lsp1beta	Forward	CCCGCCCACGAGCAGTTCT
		Reverse	CGCACGGTCGAAGGGATAGC
	Lsp2	Forward	TGCCCAACCGAATGATGCTG
		Reverse	CGGGCTGGTGGTACGGGTAG
	LvpH	Forward	CGACTTGAATATGGGCGACAGC
		Reverse	ACGGCATTGGCGACCTGAAC
	Mgstl	Forward	GATGTCCCCCAAGCTGAAGGTC
		Reverse	GGCGAAGAAGGGCAGGATGTT
	mus209	Forward	ACATCGACAGCTGCACTTGGGT
		Reverse	GCCGGTGACGCTGACATTTG
	Obp44a	Forward	TGCTCGCTCGGAGGAAACTGT
		Reverse	TGCGACATACCCACATTGAGCG
	Obp56a	Forward	CGCCTCCAAGTTGTACGATTGC
		Reverse	CCGAATCACAATTTGCCAAGCA
	Obp56e	Forward	CCGCCCTTGCAGCTCTATCTTT
		Reverse	TTGCCTCAGCCTTTTGGGAATC
	Obp99b	Forward	CTCCTCGCTGGCGTGAACCT
		Reverse	TCACCATCACCATCACCACGAC
	obst-A	Forward	CATCCCACCGACTGCCAGAAG
		Reverse	ATCGTTGTAGACCTCGCCCAGC
	pro-PO-A1	Forward	GGCGGTCCACGTCCCTCAG
		Reverse	CCAGCACGAATAACCGCACCTA
	Sucb	Forward	TTGGCTGATCTGCGGTGGTAAC
		Reverse	CGGCGATTTTCGGTTGTGTTT

[a] For cloning, cutting sites for indicated restriction enzymes were added to 5`end of the designed primers.

All primers were designed using Lasergene Software.

File S1. Supplemental Experimental Procedures

SILAC labeling and MS/MS Analysis

Heavy amino acid-labeled (Lys-8, Lys-13C615N2, Cambridge Isotope Laboratories, Inc.) yeast and flies were cultivated as published (SURY *et al.* 2010). Lysine auxotrophic *S. cerevisiae* strain SUB62 (kindly provided by Matthias Selbach) was precultured 1:1000 for 24 hours and then inoculated for 1:100 and incubated for another 24 hours in defined, labeling medium before harvesting. Prior to feeding of *Drosophila*, incorporation of Lys-8 to yeast cells was measured by mass spectrometry and almost complete incorporation (>95%) was achieved. We used w^{1118} stock as the control strain. Control flies were grown with light-labeled (Lys-0, Lys-12C614N2, Sigma) and *mir-310s* mutant (*KT40/KT40*) flies with heavy-labeled yeast (Lys-8). In parallel, as a replicate experiment the reverse labeling was done, where control flies were fed with heavy and *mir-310s* mutant flies were fed with light-labeled yeast. Hatched flies were kept on the same medium with labeled yeast pellet for 3 days before harvesting. For sample preparation, 10 female flies were snap frozen in liquid nitrogen and homogenized in 100µl RIPA buffer (SURY *et al.* 2010) supplemented with 1X Protease inhibitor cocktail (Thermo). Total protein amounts were quantified using Bradford Reagent (Sigma). Samples containing 25µg of total protein from each labeling-genotype experiment were used for the analysis.

Proteins were separated by one-dimensional SDS-PAGE (4%–12% NuPAGE Bis-Tris Gel, Invitrogen) and stained with Coomassie Blue G-250 (Fluka). The complete gel lanes were cut into 23 equally sized slices. Proteins were digested as described previously (SHEVCHENKO *et al.* 2006). Briefly, proteins were reduced with 10 mM DTT for 50 min at 50°C, afterwards alkylated with 55

mM iodoacetamide for 20 min at 26°C. In-gel digestion was performed with Lys-C (Roche Applied Science) overnight. Extracted peptides from gel slices were loaded onto the in-house packed C18 trap column (ReproSil-Pur 120 C18-AQ, 5 µm, Dr. Maisch GmbH; 20 x 0.100 mm) at a flow rate of 5 µl/min loading buffer (2% acetonitrile, 0.1% formic acid). Peptides were separated on the analytical column (ReproSil-Pur 120 C18-AQ, 3 µm, Dr. Maisch GmbH; 200 x 0.050 mm, packed in-house into a PF360-75-15-N picofrit capillary, New Objective) with a 90 min linear gradient from 5% to 40% acetonitrile containing 0.1% formic acid at a flow rate of 300 nl/min using nanoflow liquid chromatography system (EASY n-LC 1000, Thermo Scientific) coupled to hybrid quadrupole-Orbitrap (Q Exactive, Thermo Scientific). The mass spectrometer was operated in data-dependent acquisition mode where survey scans acquired from m/z 350-1600 in the Orbitrap at resolution settings of 70,000 FWHM at m/z 200 at a target value of 1 x 10E6. Up to 15 most abundant precursor ions with charge states 2+ or more were sequentially isolated and fragmented with higher collision-induced dissociation (HCD) with normalized collision energy of 28. Dynamic exclusion was set to 18 s to avoid repeating the sequencing of the peptides.

The generated raw Mass Spectrometry files were analyzed with MaxQuant software (version 1.3.0.5, using Andromeda search engine) (COX AND MANN 2008) against UniProtKB *D. melanogaster* database containing 18826 entries (downloaded in April 2013) and Flybase *D. melanogaster* database (release 6.02) supplemented with common contaminants and concatenated with the reverse sequences of all entries. The following Andromeda search parameters were set: carbamidomethylation of cysteines as a fixed modification, oxidation of methionine and N-terminal

acetylation as a variable modification; and Lys-C specificity with no proline restriction and up to two missed cleavages. The MS survey scan mass tolerance was 7 ppm and for MS/MS 20 ppm. For protein identification minimum of five amino acids per identified peptide and at least one peptide per protein group were required. The false discovery rate was set to 1% at both peptide and protein levels. "Re-quantify" was enabled, and "keep low scoring versions of identified peptides" was disabled. Statistical analysis was performed with Perseus bioinformatics platform which is part of MaxQuant (COX AND MANN 2008).

qRT-PCR

Total RNA was extracted using Trizol (Ambion) followed by isolation using Direct-Zol RNA Miniprep (Zymo Research) following the manufacturers' protocols.

Relative transcript levels were measured using total RNA extracts from 10 females of control (w^{1118}) and *mir-310s* mutant (*KT40/KT40*) genotypes kept under well-fed or starved condition for 10 days using 3 biological replicates. To synthesize total cDNA, High-Capacity reverse transcription kit (Applied Biosystems) and random primers were used. Quantitative PCR (qPCR) was performed using SYBR green master mix (Applied Biosystems) using a StepOne Plus thermocycler (Applied Biosystems) according to manufacturer's instructions. The gene *Rpl32* was used as an endogenous control. Primers for qPCR for each gene were designed using Lasergene software (Table S11). The amplicons were selected to be intron spanning. If that was not possible, additional DNAse (Zymo Research) treatment of the RNA samples was performed and reverse transcriptase negative controls were included.

Relative miRNA levels were measured using RNA extracts from 5 ovaries from 7 day well-fed or starved control (*w*^{1118}*/Oregon-R-C*) females in at least 3 biological replicates. TaqMan microRNA assays (Applied Biosystems) and High-Capacity reverse transcription kit were used to synthesize cDNA specific to *mir-310, mir-312,* and *2S rRNA* as an endogenous control. qPCR was performed using the Taqman qPCR master mix (Applied Biosystems) using a StepOne Plus thermocycler.

For the relative quantitative analysis, average C_T values of technical replicates were first normalized by subtraction of the housekeeping gene expression (*Rpl32* for transcript expression and *2S rRNA* for miRNA expression) and then of the gene of interest expression in the well-fed controls. Relative expression levels were obtained with these calculated $\Delta\Delta C_T$ values using the formula $2^{-\Delta\Delta CT}$. Statistical analysis was done using non-paired two-tailed Student's t-test.

Immunohistochemistry

Adult ovaries were dissected in cold 1X PBS and fixed for 10-15 minutes in 4% formaldehyde (Polysciences Inc.) at room temperature. The subsequent staining procedure was performed as described (KONIG AND SHCHERBATA 2013). The following antibodies were used with the indicated dilutions: mouse monoclonal anti-Adducin (1:50), anti-LaminC (1:20), anti-Fasciclin III (1:50), and anti-β-Gal (1:25), rat monoclonal anti-DE-Cadherin (1:25) (Developmental Studies Hybridoma Bank); chicken polyclonal anti-GFP (1:5000, Abcam); guinea pig polyclonal anti-Hh (1:100, gift from Acaimo González-Reyes); rabbit polyclonal anti-PH3 (1:5000, Upstate Biotechnology); goat secondary antibodies Alexa 568 anti-mouse, Alexa 488 anti-rat, Alexa 488 anti-rabbit, Alexa 488 anti-chicken, and Alexa 568 anti-guinea pig (1:500, Invitrogen). To stain cell nuclei, DAPI dye

(Sigma) was used. All samples were mounted on glass slides in 1X PBS with 70% glycerol and 3% n-propyl gallate. Fluorescence images of the stained tissues were taken with confocal laser-scanning microscope (Zeiss LSM 700) and processed with Adobe Photoshop software.

Luciferase Assay

The reporter constructs with a short *3`UTR* fragment of each gene containing the *mir-310s* binding site was cloned downstream of *Renilla* luciferase gene (Table S11). The same vector contained an unmodified *Firefly* luciferase gene, activity of which served as an internal transfection control for each experiment and for the normalization of *Renilla* luciferase signal. *Drosophila* S2 cells were kept in Schneider's *Drosophila* medium (Gibco) supplemented with 10% heat inactivated fetal bovine serum (GE healthcare), 100 units/ml penicillin, and 100 µg/ml streptomycin (Gibco). The cells were split 1:6 the day before transfection and seeded into 96 well plates. All wells were transfected with 5ng actin Gal4, 20ng of *UAS-mir-310s* (gifts from Eric Lai), and 10ng psiCHECK™-2 vectors (Promega) with or without the *3`UTR* fragment of the respective gene using Effectene® Transfection Reagent (Qiagen). Experiments were done in triplicates. *Firefly* and *Renilla* luciferase activities were measured 72h after transfection using Dual-Glo® Luciferase Assay System (Promega) by Wallac 1420 luminometer (PerkinElmer). For analysis, the *Renilla* luciferase signal was divided by *Firefly* luciferase signal to normalize the data to the amount of cells transfected in each well. Next, this ratio was normalized to the control, unmodified *Renilla* luciferase signals, for each respective miRNA overexpression experiment.

Coupled Colorimetric Assay (CCA)

Total body fat content of the flies was measured by CCA as described (GALIKOVA *et al.* 2015). Five female flies were homogenized in 1000µl 0.05% TWEEN® 20 (Sigma) and incubated at 70°C for 5 minutes. Samples were cleared by centrifuging at 3000g for 3 minutes and the supernatant was used for subsequent colorimetric analyses. To measure the triglyceride (TAG) equivalent amounts, we used 200µl of prewarmed (37°C) Triglycerides Reagent (Thermo Scientific™) with 50µl of the well-fed and 75µl of the starved samples measuring the absorbance at 540nm after incubation at 37°C for 30 minutes. Absolute TAG equivalent amounts were calculated with help of serial dilutions of Thermo Trace Triglyceride standard (Thermo Scientific™) and calculated standard curve. For normalization, we measured total protein content of the samples using BCA Protein Assay Reagent (Thermo Scientific Pierce), where we used 50µl of the samples with 200µl BCA-mix and measured absorbance at 570nm after an incubation for 30 minutes at 37°C. Absolute protein contents of the samples were calculated with the help of a standard curve obtained using measurements of serial dilutions of bovine serum albumin standard. Both absorbance measurements were done in 96 well microtest plates (Sarstedt) using a Benchmark Microplate Reader (Biorad).

Fat bodies were visualized from non-fixed dorsal carcass preparations using Bodipy493/503 (38 µM; Invitrogen) to label lipid droplets, CellMaskTM Deep Red (5 µg/mL; Invitrogen) to label plasma membrane, and DAPI (3,6 µM; Invitrogen) to label nuclei (GALIKOVA *et al.* 2015).

Co-immunoprecipitation

Whole lysates were prepared from approximately 1-week-old male and female flies, which were kept on nutrient rich food for 2-3 days and harvested by snap freezing in liquid nitrogen. Three biological

replicates of 750mg of both control (w^{1118}) and *Rab23::YFP::4xmyc* flies were homogenized by grinding in 2ml buffer with 20mM Tris (pH 7.4), 150mM NaCl, 5% glycerol, 5mM EDTA, 0.1% Triton™ X-100 (Sigma) and 2X protease inhibitor cocktail (Roche) in a mortar with pestle using liquid nitrogen. Lysates were cleared by three centrifuging steps once for 10 minutes at 15000g and twice at 21000g at 4°C. Next, control and *Rab23::YFP::4xmyc* lysates were diluted with buffer to 5ml and were added 50µl agarose beads coupled with anti-myc antibodies (Sigma) in 15ml tubes and incubated rotating at 4°C for 100 minutes. To collect the beads, lysates were centrifuged at 100g for 2 minutes at 4°C. The beads were washed 10 times with 700µl buffer at 100g for 30 seconds at 4°C and finally eluted with 50µl warm 2X sample buffer (NuPAGE® LDS Sample Buffer, Novex®). The eluates were analyzed by mass spectrometry with the same workflow used in SILAC analysis described above with the exception for trypsin used for in-gel digestion.

Supplemental References

Cox, J., and M. Mann, 2008 MaxQuant enables high peptide identification rates, individualized p.p.b.-range mass accuracies and proteome-wide protein quantification. Nat Biotechnol 26**:** 1367-1372.

Galikova, M., M. Diesner, P. Klepsatel, P. Hehlert, Y. Xu *et al.*, 2015 Energy Homeostasis Control in Drosophila Adipokinetic Hormone Mutants. Genetics 201**:** 665-683.

Konig, A., and H. R. Shcherbata, 2013 Visualization of adult stem cells within their niches using the Drosophila germline as a model system. Methods Mol Biol 1035**:** 25-33.

Shevchenko, A., H. Tomas, J. Havlis, J. V. Olsen and M. Mann, 2006 In-gel digestion for mass spectrometric characterization of proteins and proteomes. Nat Protoc 1**:** 2856-2860.

Sury, M. D., J. X. Chen and M. Selbach, 2010 The SILAC fly allows for accurate protein quantification in vivo. Mol Cell Proteomics 9**:** 2173-2183.

Yatsenko, A. S., A. K. Marrone and H. R. Shcherbata, 2014 miRNA-based buffering of the cobblestone-lissencephaly-associated extracellular matrix receptor dystroglycan via its alternative 3'-UTR. Nat Commun 5**:** 4906.